Artificial Neural Network Based Rotor Flux Estimation and Fuzzy-logic Sensorless Speed Control of an Induction Motor

Rahel Shirge Sinta

A Thesis Submitted to

The Department of Electrical Power and Control Engineering

School of Electrical Engineering and Computing

Presented in Partial Fulfillment of the Requirement for the Master of Science Degree in Electrical Power and Control Engineering (Power Electronics)

Office of Graduate Studies

Adama Science and Technology University

October 2020

Adama, Ethiopia

Artificial Neural Network Based Rotor Flux Estimation and Fuzzy-logic Sensorless Speed Control of an Induction Motor

By: Rahel Shirge Sinta

Advisor: Tefera T. Yetayew (PhD)

A Thesis Submitted to

The Department of Electrical Power and Control Engineering

School of Electrical Engineering and Computing

Presented in Partial Fulfillment of the Requirement for the Master of Science Degree in Electrical Power and Control Engineering (Power Electronics)

Office of Graduate Studies

Adama Science and Technology University

October 2020

Adama, Ethiopia

APPROVAL OF BOARD OF EXAMINERS

We, the undersigned, members of the Board of Examiners of the final open defense by Rahel Shirge have read and evaluated her thesis entitled **"**Artificial Neural Network Based Rotor Flux Estimation and Fuzzy-logic Sensorless Speed Control of an Induction Motor**"** and examined the candidate. This is, therefore, to certify that the thesis has been accepted in partial fulfillment of the requirement of the Degree of Master of Science Electrical Power and Control (Power Electronics).

Name	Signature	Date
______________________	__________________	__________________
Name of student		
______________________	__________________	__________________
Advisor		
______________________	__________________	__________________
External Examiner		
______________________	__________________	__________________
Internal Examiner		
______________________	__________________	__________________
Chair Person		
______________________	__________________	__________________
Head of a department		
______________________	__________________	__________________
School Dean		
______________________	__________________	__________________
Postgraduate Dean		

DECLARATION

I hereby declare that this MSc thesis is my original work and has not been presented for a degree in any other university, and all sources of material used for this thesis have been duly acknowledged.

Name: _________________________

Signature____________

This MSc Thesis has been submitted for examination with my approval as a thesis advisor.

Name: __________________________

Signature____________

Date of submission: ……………….………...

ADVISOR APPROVAL SHEET

To: Electrical Power and Control Engineering Department

This is to certify that the thesis entitled "Artificial Neural Network Based Rotor Flux Estimation and Fuzzy-logic Sensorless Speed Control of an Induction Motor" submitted in partial fulfillment of the requirements of the Masters of Science Degree in Electrical Power and Control (Power Electronics), the Graduate program of the department of Electrical Power and Control, and has been carried out by Rahel Shirge Id. No PGR/18364/11, under my supervision. Therefore, I recommend that the student has fulfilled the requirements and hence hereby she can submit the thesis to the department.

Advisor	Signature	Date
______________________________	_______________	______________

ACKNOWLEDGMENT

At first and most, I would like to thank the almighty of GOD, who gave me strength, patience, and courage to complete the thesis successfully.

I would like to express my truthful gratefulness to my advisor **Dr. Tefera T. Yetayew** for his continuous support of my thesis, for his patience, motivation, interest, and most importantly his guidance helped me in all times of the research and writing of the thesis document.

I am also very grateful to **Dr. Milkias Berhanu** for lots of advice and helping in preparing the thesis documentation, but also for good ideas and discussions regarding everything from implementations of the system in Simulink in general.

Furthermore, I would also like to thank the EPCE department head **Mr. Hinsermu Alemayehu Garbaabaa (MSc.)** and laboratory staff members for encouraging, making open computer labs for discussion when I have a meeting with my advisor, for a very friendly working environment, and for making me feel very welcome during my thesis work.

Finally, I would like to thank my whole family. Especially words cannot express how grateful I am to my mother and friends for their love, encouragement, and all of the sacrifices that they have made on my behalf.

ABSTRACT

*Induction motor is one of the most widely used machines in industrial applications due to its high reliability, relatively low cost, and less maintenance requirements. Variable speed induction motor drives that operate without speed or position sensors have the benefits of reduced drive system's size and overall cost as well as high system reliability. This thesis aims to design rotor flux estimation based on Artificial Neural Network and fuzzy-logic based speed control of indirect field-oriented control for an induction motor drive to achieve high dynamic performance. For implementation purposes, the corresponding model is done using MATLAB software tools. The performance of speed control of the indirect vector control of an induction motor for conventional PI and Fuzzy logic speed control has been compared. Accordingly, the PI speed controller has a settling time 0.2sec, 5.851% overshoot, 0.045sec rise time, and has no steady-state error for 100 rad/s at no-load condition. On the other hand, the fuzzy logic speed controller has a settling time of 0.085sec, 0.505% overshoot, 0.0386sec rise time, and has no steady-state error for 100 rad/s at no-load condition. Thus, values show that the fuzzy-logic based speed control of indirect vector control of induction motor gives a better speed response than that of the conventional PI controller. The performance of PI and fuzzy logic speed controller evaluated under the application of sudden load change for constant setpoint conditions. The settling time, rise time, and peak time values are increased when compared to the system simulated under no-load condition. This shows that when the load is increased, the system performance will be decreased. There is no variation in the case of overshoot but there is a steady-state error in the result with the system simulated under no-load conditio*n. *Generally, the rotor flux angle is estimated by using ANN and the speed estimated by using open-loop speed estimation techniques. The sensorless speed control tracks the actual speed of the motor when the motor run at the constant speed, changing the reference speed, and in the regenerative mode of operation.*

Key Words: *Artificial Neural Network, fuzzy logic, Induction motor drive, indirect field-oriented control, MATLAB software, and PI control.*

TABLE OF CONTENTS

LIST OF FIGURES

LIST OF TABLES

LIST OF ACRONYMS

AC	Alternating Current
ANN	Artificial Neural Network
CSI	Current Source Inverter
DC	Direct Current
DFOC	Direct Field Oriented Control
DSP	Digital Signal Processor
DTC	Direct Torque Control
FLC	Fuzzy Logic Controller
GM	Gain Margin
IFOC	Indirect Field Oriented Control
IGBT	Insulated Gate Bipolar Transistor
IM	Induction Motor
NN	Neural Network
PD	Proportional Derivative
PI	Proportional Integral
PI	Proportional Integral
PID	Proportional Integral Derivative
PM	Phase Margin
PWM	Pulse Width Modulation
SVM	Space Vector Modulation
SCIM	Squirrel Cage Induction Motors
SISO	Single Input Single Output
MOSFET	Metallic Oxide Semiconductor Field Effect Transistor
V_DC	DC Link Voltage
VSI	Voltage Source Inverter

LIST OF SYMBOLS

L_m	Magnetizing inductance
L_{ls}	Stator leakage inductance
L_{lr}	Rotor leakage inductance
L_s	Stator self-inductance
L_r	Rotor self-inductance
X_m	Stator magnetizing reactance
X_{ls}	Stator leakage reactance
X_{lr}	Rotor leakage reactance
X_s	Stator self-reactance
J	The moment of inertia
X_r	Rotor self-reactance
R_S	Stator resistance
R_r	Rotor resistance
$\theta_{\psi r}$	Rotor flux angle
ψ_r	Rotor flux
w_e	Angular synchronous speed
w_r	Angular rotor speed
w_{sl}	Angular slip speed
T_r	Rotor time-constant
T_L	Load Torque
T_{em}	Electromagnetic torque
i_{as}, i_{bs}, i_{cs}	Phase a, Phase b and Phase c of stator current
v_{as}, v_{bs}, v_{cs}	Phase a, Phase b and Phase c of stator voltage
i_{ds}^e	d axis stator current expressed in synchronous frame

i_{qs}^{e}	q axis stator current expressed in a synchronous frame
i_{ds}^{s}	d axis stator current expressed in a stationary frame
i_{qs}^{s}	q axis stator current expressed in a stationary frame
v_{ds}^{e}	d axis stator voltage expressed in a synchronous frame
v_{qs}^{e}	q axis stator voltage expressed in a synchronous frame
v_{ds}^{s}	d axis stator voltage expressed in a stationary frame
v_{qs}^{s}	q axis stator voltage expressed in a stationary frame
ψ_{ds}^{s}	d axis stator flux expressed in a stationary frame
ψ_{qs}^{s}	q axis stator flux expressed in a stationary frame
ψ_{ds}^{e}	d axis stator flux expressed in a synchronous frame
ψ_{qs}^{e}	q axis stator flux expressed in a synchronous frame
θ_{e}	The angle between the synchronous frame and the stationary frame

CHAPTER 1

INTRODUCTION

1.1. Background

Three-phase induction motor has been a reliable electromechanical energy conversion device for over 100 years. Induction motors, particularly the squirrel cage induction motors (SCIM) have been widely used in industrial applications because of their several inherent advantages such as their simple construction, robustness, reliability, low cost, and less maintenance needs [1].

In 1888, Tesla introduced the alternating current (AC) induction motor for the first time. Tesla believed that his invention is more useful and applicable than the DC motor. Without proper controlling, it is virtually impossible to achieve the desired task for any industrial application. However, there are different control schemes for induction motor drives these are scalar control, vector or field-oriented control, direct torque control, and adaptive control, etc. The induction motor control methods are broadly classified into two categories i.e. scalar control and vector control.

Scalar control: one of the primary ways of controlling induction motor was the Volts/Hertz speed control during which the motor was excited with constant voltage to frequency ratio to take care of a constant air gap flux and hence provide maximum torque sensitivity. This method is comparatively simple but doesn't yield satisfactory results for a high- performance application. This is often the fact that within the scalar control, an inherent coupling exists between the torque and air gap flux, which results in a sluggish response of the induction motor [2].

Field oriented control (Vector control), overcome the limitation of the scalar control method, the field-oriented method was developed Blaschke in 1972 has introduced the principle of vector control to understand the dc motor characteristics in an induction motor drive. For an equivalent, he has used decoupled control of torque and flux within the motor and provides the name trans vector control. The induction motor (Ac motor) is often controlled sort of a separately excited dc motor, brought a renaissance within the high-speed performance control of ac drives. the essential principle of vector control is to separate the components of stator current liable for the assembly of flux and torque. To accomplish this, the state variables utilized in the dynamic model of IM are transformed into a coordinate system during which independent control of the machine flux and torque achieved. There are two methods of vector control this is the Direct or feedback method and the Indirect or feed-forward method [3].

The direct method of vector control attempts to directly measure or estimate the machine flux, and use this to find out the transformation angle. Direct vector-controlled drive, the control is dependent on stator resistance. Therefore, for perfect decoupling of flux and torque, estimation and compensation for these parameter variations are necessary. Also, for certain speed Sensorless drives, the estimation technique is dependent on plant parameters. In such cases, compensation for variation of these parameters is an absolute necessity.The major disadvantage of direct vector method is the need of so many sensors. Fixing so many sensors in a machine is a tedious work as well as costlier. Due to this the scheme is prevented from being used. Several other problems like drift because of temperature, poor flux sensing at lower speeds also persists. Due to these disadvantages and some more related ones, indirect vector control is used. In indirect vector control technique, the rotor position is calculated from the speed feedback signal of the motor. This technique eliminates most of the problems, which are associated with the flux sensors as they are absent [3], [4]. This thesis briefly describes the design of the most efficient form of a vector control scheme of the indirect field orientated control method.

In the last several years, an excellent effort has been made on the elimination of speed sensor or shaft position for drives. The ongoing research has been concentrated on the elimination of the speed sensor at the machine shaft without reducing the dynamic performance of the drive control system [5], [6]. Generally, high- performance vector control induction motor drives require speed or position information for its operation. However, these Sensors mounted on the machine shaft are not desirable for a variety of reasons. First of all, the cost is substantial. Secondly, their mounting requires a machine with two shaft ends available - one for the sensor and therefore the other one for the load coupling. Thirdly, electrical signals from the shaft sensor need to be taken to the controller and therefore the sensor needs an influence supply these require additional cabling. Finally, the presence of a shaft sensor reduces the mechanical robustness of the machine and its reliability [7]. Due to these reasons, speed Sensorless systems, in which rotor speed measurements are not available, are preferred and find applications in many areas for speed regulation, load torque variation, and speed tracking purposes.

It is for all those reasons that substantial efforts are put in the recent past into possibilities of eliminating the shaft-mounted sensor for rotor speed sensing. However, the information regarding the actual speed and position of the rotor shaft remains to be necessary for closed-loop speed control albeit the shaft sensor is not installed. Hence the speed and rotor flux position has got to be estimated by using different speed and flux estimation techniques from easily measurable electrical quantities (in general, stator voltages, and currents).

1.2. Statement of the Problem

The induction motor speed control methods are conventionally handled by fixed gain PI and PID controllers. However, in the conventional controllers, the unexpected change in load condition produce overshoot, fluctuation of motor speed, an oscillation of the torque, steady-state error, and long settling time causes deterioration of drive performance. To overcome these problems, an intelligent controller based on fuzzy logic speed control employ in the place of the conventional PI controller. In this thesis, a fuzzy-logic based speed control has been applied in the indirect field-oriented control of the induction motor drive. The performance of speed control for the conventional PI and Fuzzy control has been compared for indirect vector control of an induction motor.

In the speed control of the induction motor, it is possible to use a speed sensor for accessing actual speed information. This speed sensor (position sensor which senses the position of rotor continuously and it should be very high precision) has a disadvantage like an extra cost, system configuration, and reducing reliability. For solving this problem, this thesis work has been applied to the sensorless speed control of the vector control of the induction motor drives.

1.3. Objectives of the Study

1.3.1. General Objective

The general objective of the thesis is:

To design the rotor flux estimation based on ANN and fuzzy-logic based speed control of indirect field-oriented control for an induction motor to achieve high dynamic performance

1.3.2. Specific Objectives

The specific objectives of the thesis are:

- To design a rotor flux estimator using an artificial neural network and estimate the speed using open- loop estimator of the induction motor drive.
- To design closed-loop Fuzzy logic and PI-controller for indirect field-oriented speed control of induction motor drive.
- To evaluate the dynamic performance of PI and Fuzzy-logic based controllers of the indirect field-oriented Sensorless speed control of an induction motor drive.
- To simulate PI and Fuzzy-logic indirect field-oriented Sensorless speed control of an induction motor drive in MATLAB/Simulink software.

1.4. Scope of the Study

The thesis focuses on the mathematical modeling and simulation design for indirect vector control of an induction motor. Intending to that flux and speed estimated for sensorless speed control of indirect field-oriented control of an induction motor drive. Design the closed-loop PI and fuzzy logic speed controller for an induction motor. The performance of the fuzzy-logic and PI controller for speed control of an induction motor is discussed and compared. The overall system for vector control of an induction motor realized in MATLAB/Simulink software.

1.5. Limitation of the Study

There are different techniques of speed estimation for induction motor. In this case, open-loop speed estimation is carried out to estimate the rotor speed of the induction motor drive and simulated in MATLAB/SIMULINK. The thesis is implemented using only MATLAB/SIMULINK simulation without practical implementation.

1.6. Motivation of the Study

Induction motors have been used more in the industrial variable speed control of the drive system with the development of the vector control technology. This method requires a speed sensor such as a shaft encoder for speed control of the induction motor. However, a speed sensor cannot be mounted in some cases such as motor drives in a hostile environment and high-speed drives. Besides, it requires careful cabling arrangements to give attention to electrical noise. Moreover, it causes them to become expensive and bulky in motor size. In other words, it has some demerits in both mechanical and economical aspects. The interest in sensorless drives of induction motor (IM) has grown significantly over the past few years due to some of their advantages, such as mechanical robustness, simple construction, and less maintenance. This thesis focused on the sensorless vector control problem, in which rotor speed measurements are not available, to reduce cost and to increase reliability.

1.6. Significance of the Study

The proposed study will contribute to the following advantages. Running an induction motor without a position mechanical sensor has an advantage over an induction motor with a position sensor:

- It minimizes the drive cost.
- It decreases the mechanical size of the machine
- It increases the reliability of the system.
- It improves the noise immunity efficiency of the system.
- It avoids the complex process of embedding the position sensor in the stator.

1.7. Thesis Organization

The thesis has been organized into five chapters.

Chapter 1: Presents background of the study, statement of the problems, objectives of the study, significance**,** scope, motivation, and limitation of the research.

Chapter 2: Discusses, the literature review and explains in detail the theoretical background of the Induction motor, field oriented control of induction motor, fuzzy logic control, and aritificial neural network.

Chapter 3: Describes the methodology followed in this thesis. It brief description induction machine dynamics model, the voltage and current model for flux and speed estimation, ANN for flux estimation, indirect vector control algorithm, fuzz logic and PI speed controller, current control gain and space vector pulse width modulation.

Chapter 4: Presents the proposed results and discussions for sensorless speed control of indirect vector control of an induction motor .

Chapter 5: Discusses the conclusions and recommendations for future work. .

CHAPTER 2

LITERATURE REVIEW AND THEORETICAL BACKGROUND

2.1. Chapter Overview

In this chapter closely related works especially in speed control mechanisms and the flux and speed estimation are reviewed. The introduction to induction motor and varieties of the control techniques, construction, principle of operation are reviewed and discussed. In addition to this, the vector control of the direct torque control method is compared with the field-oriented control method.

2.2. Related Works on the Sensorless Speed Control of Indirect Vector Control of Induction Motor

Scalar controlled drives have been widely used in industry, but the inherent coupling effect of both torque and flux is a function of voltage or current and frequency gives the sluggish response. To make it clearer, if torque is increased by incrementing the slip (the frequency), the flux tends to decrease. It has been noted that the flux variation is also sluggish . Decreases in flux are then compensated by the sluggish flux control loop feeding an additional voltage. This temporary dipping of flux reduces the torque sensitivity with slip and increase the response time [8]. However, to improve the scalar control method different research work on the vector or Field orientated control (FOC) drives areas.

Investigation of ways to estimate the rotor flux and speed control of the induction machine has been extensively studied in the past two decades. Classically, the rotor flux was measured by using a special sensing element, such as Hall-effect sensors placed in the air-gap. An advantage of this method is that additional required parameters, rotor leakage inductance, Magnetizing inductance, and rotor self-inductance are not significantly affected by changes in temperature and flux level. However, the disadvantage of this method is that a flux sensor is expensive, reduces the mechanical robustness of the machine, and decreases its reliability. Therefore, to remove this Hall-effect sensor there are different research work on this area. In industries, mechanical loads should not only be driven at a constant speed but should also be driven at the desired speed by varying the speed of the motor and the need for the speed control methods for the induction motor arises. Therefore, different research work on the speed control for an induction motor.

The authors in [9] proposed an internal model control approach for the PI tuning control within the vector control of induction motor. This paper deals with the design of PI controllers to satisfy the desired torque and speed response of Induction motor drive. design PI controller gains giving a satisfying performance at low as well as high speed but this PI controller induces some problems like high overshoot, the oscillation of speed, and torque due to sudden changes in the load and external disturbances. This behavior of the PI controller causes deterioration of drive performance. The fuzzy controller has the benefits of conventional PI control, so it can get better control performance. To overcome the problem this thesis is applied to a fuzzy controller in the place of the conventional PI controller for desired torque and speed control of the induction motor.

The design of the direct torque controller model of an Induction Motor has been developed and tested by using the MATLAB/Simulink package was discussed in the literature [10]. Simulation results have shown the validity and high accuracy of the proposed model. The independence of the torque and stator flux control of the induction motor has been confirmed. However, a significant starting up stator current is caused due to any small variation within the stator flux. In addition to that during this project, the torque and flux estimated are often directly controlled in a way that keeps them within a hysteresis band. Therefore, further work is desired to limit the starting up stator current to protect the machine and power electronics devices, and on the control method of independent torque and flux control.

The performance comparison between conventional PI and PI-Like fuzzy speed controller for a three-phase induction motor is performed in the literature [11]. This thesis introduced a dynamic model of a three-phase induction motor and speed control of the induction motor for field-oriented vector control. The comparison between Conventional PI and PI-Like fuzzy speed controller for a three-phase induction motor is done in this research work. From the result the performance of IM with the fuzzy logic controller is more stable than with a conventional PI controller, the speed almost has to be constant even though load torque is applied at a specific instant because of the instantaneous response of FLC. Even though the fuzzy controller gives better control performance than the PI controller, it has high overshoot, rise time, and settling time in the speed of the motor. The other drawback of the study is, it does not discuss the application of variable speed and regenerative speed to controlling the speed of the induction motor.

The novel method for speed control of Single-Phase induction motor is based on indirect field-oriented control is presented in the literature [12]. It is shown that using an appropriate transformation matrix (TM) for stator current variables, the unbalanced single-phase induction motor equations can be changed into balanced equations. Simulation results showed the excellent speed and torque responses obtained using the proposed technique. The drawback of the presented method is that the motor speed of a single-phase induction motor must be measured, which needs a speed sensor. To overcome this problem this thesis has applied Sensorless speed control of the indirect FOC method for an induction motor.

Sensorless Control of Induction Motor using Simulink by Direct Synthesis Technique presented in the literature [13]. The sensorless control of induction motor using direct synthesis from the state equations has been presented for starting, steady-state, transient, and speed reversal without using any shaft encoder as in the case of vector control. In the simulation result, the estimated speed has a high steady-state error and works only at high-speed range and also high starting current. Therefore, this thesis work must be improved the direct synthesis technique improved by using an artificial neural network for flux estimation technique.

This thesis focused on the design of sensorless speed control for an induction motor based open-loop speed estimator to estimate the speed and neural network for flux estimation. Control the speed of induction motor by using PI and fuzzy logic speed controller and for independent control of the torque and flux the PI control used for indirect vector control of the induction motor.

2.3. Theoretical Background of Induction Motor

2.3.1. Introduction

Since the invention of the induction motor by Nikola Tesla in 1888, the use of three-phase squirrel cage induction motors have grown extremely in industry. They are widely used in the industries to control the speed of the conveyor system, blower speed, machine tool speed, and other applications that need adjustable speed. An induction or asynchronous motor is an AC motor in which the electric current in the rotor needed to produce torque is obtained by electromagnetic induction from the magnetic flux of the stator winding. Induction refers to the field in the rotor is induced by the stator current and asynchronous refers to the fact that the rotor speed is not equal to the stator speed. No sliding contacts and permanent magnets are needed to make an induction motor work which makes it very simple and cheap to manufacture. nowadays, AC motor is preferred to DC motors, in particular, an induction motor due to its low cost, less maintenance, lower weight, high efficiency, improved ruggedness, and reliability. All these features make wide use of induction motor in many areas of the industrial application [7].

The synchronous speed Ns of an ac motor is related to supply frequency f and poles P by the equation

$$N_s = \frac{120 f}{p} \tag{2.1}$$

Where Ns is the speed in rpm, *f* is the frequency of the applied excitation in Hz, and *P* is a number of the poles. The rotor attempts to turn at this speed, also known as the synchronous speed, but never quite reaches this speed, rotating instead at a speed Nr due to slip. The difference between the source angular frequency (ω_s) and the angular frequency of the rotor electrical speed (ω_r) is termed the angular slip frequency (ω_{sl}) while the ratio of the slip speed to the stator speed is the actual slip (S) [1].

$$S = \frac{N_s - N_r}{N_s} = \frac{\omega_s - \omega_r}{\omega_s} = \frac{\omega_{sl}}{\omega_s} \tag{2.2}$$

Note that slip can also be defined in terms of N_r and N_s as shown in Equation 2.2 where N_r is the rotor speed in *rpm*. There must always exist some non-zero slip to running unload will often be running at very nearly zero slip.

2.3.2. Construction of the Three Phase Induction Motor

Three-phase AC induction motors are mainly used in industrial applications. This induction motor has three main parts; rotor, stator, and enclosure. The stator and the rotor do the work and the enclosure protects the stator and rotor. Most induction motors are the rotary type with basically a stationary stator and a rotating rotor. The stationary stator has a cylindrical magnetic core that is housed inside a metal frame. The stator magnetic core is formed by stacking thin electrical steel laminations with uniformly spaced slots stamped in the inner circumference to accommodate the three distributed stator windings. The stator windings are formed by connecting coils of copper or aluminum conductors that are insulated from the slot walls. The rotor consists of a cylindrical laminated iron core with uniformly spaced peripheral slots to accommodate the rotor windings [1].

There are two different types of induction motor depend on the rotor; the Wound rotor induction motor has a three-phase winding in the rotor, similar to the stator winding. The rotor winding terminals are connected to the three slip rings which turn with the rotor. The slip rings/brushes have external resistors to be connected in series with the winding. The external resistors are mainly used during start-up under normal running conditions the windings are short-circuited externally. The second type of induction motor rotor is the squirrel cage rotor. It consists of a series of conducting bars laid into slots carved in the face of the rotor and shorted at either end by the big shorting rings. The construction of the slip ring motor is complicated because it consists of a slip ring and brushes whereas the construction of the squirrel cage induction motor is simple [3].

The maintenance cost of the slip ring motor is high as compared to the squirrel cage motor because the slip ring motor consists of brushes and rings. The slip ring motor has a brush transferring the power whereas the squirrel cage motor is brushless. The copper loss in the wound motor is high as compared to a squirrel cage motor. The starting current of the wound rotor motor is low because it is controlled by a resistance circuit whereas it is high in squirrel cage motor. The wound rotor motor is mostly used in the place where high starting torque is required like a hoist, crane, etc. the squirrel cage motor is used in drilling machines, lath machines, etc. In general, because of the above reviewed- literature merit, this thesis work focuses on the speed control of three-phase squirrel cage motor in closed-loop drives system control. The squirrel Cage induction motor is shown in Figure 2.1.

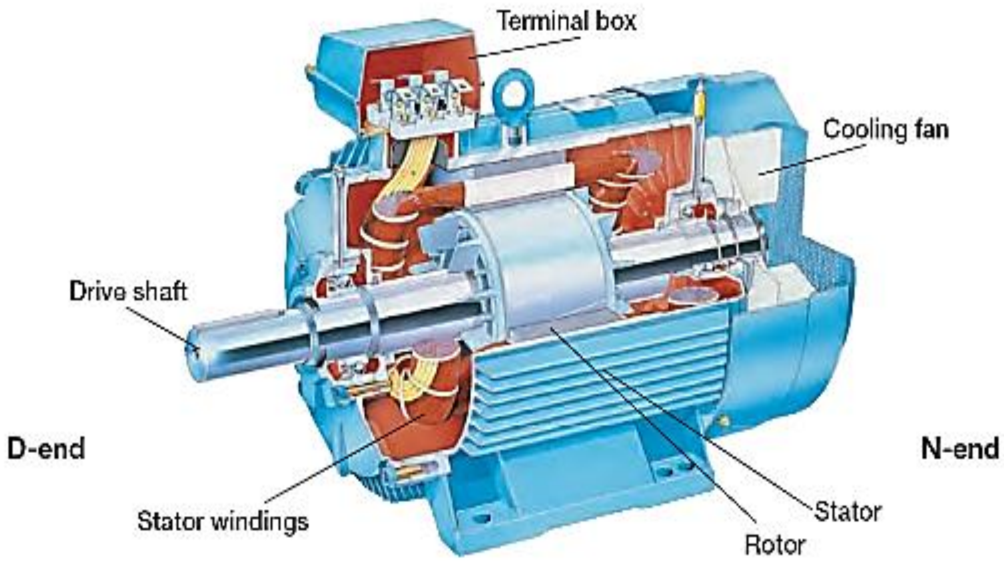

Figure 2.1: Squirrel Cage Induction Motor [14]

2.3.3. Principle of Operation

The principle of operation of the induction motor is based on generating a rotating magnetic field. When a three-phase induction motor is connected to the appropriate AC voltage source it produces stator current and each of the three coils for each phase is fed with an alternating current. The current induced in each phase generate magnetic field intensity and this causes a flow of magnetic flux. The rotating magnetic field interacts with a set of conductors arranged on the rotor and short-circuited at the ends with two rings. This interaction between the magnetic field and the conductor induces a current in the bars. Current flow in the conductors of the rotor through the short-circuiting rings at the end. This current, in turn, produces a magnetic field. There is a difference between revolving field speed and rotor speed then the revolving field induces a voltage in the rotor winding. The difference between the rotor speed and the revolving field speeds is called the slip speed. The induced voltage present in a rotor current that generates flux in the counter direction by the stator windings. The interaction between the rotor magnetic field and the squirrel cage bars induces torque and causes rotation [1].

2.4. Induction Machine Control Techniques

Induction motors are the most widely used electrical motors because of their reliability, low cost, and robustness. However, induction motors do not inherently have the potential of variable speed operation. Due to this reason, earlier dc motors were used in most of the electrical drives but in the recent developments in speed control methods of the induction motor lead to their large-scale use in most electrical drives. There is a different method of speed control of the induction motor. From those methods, the general classification of the induction motor control methods presented in Figure 2.2 [15]. These methods can be classified into two groups: scalar and vector.

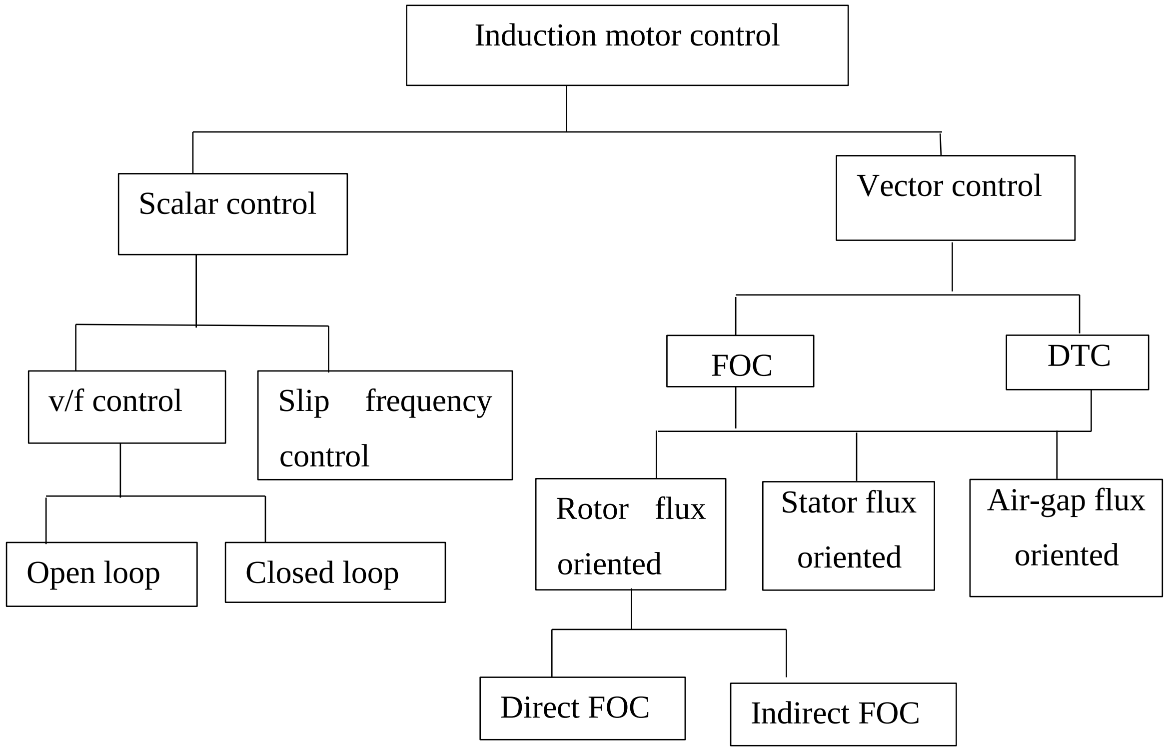

Figure 2.2: Classification of induction motor control methods

Scalar control involves controlling the magnitude of voltage or frequency of supply fed to the induction motor. The V/f control method is a control method based on the principle of keeping air gap flux constant by controlling stator voltage and frequency so that the V/f ratio is kept constant. When V/f is constant, air-gap flux remains constant. Along with V/f, another control technique is the slip frequency control. In this control method to keep the slip frequency constant and control the speed by controlling the current and hence the magnitude flux of the motor. In this scheme, the torque command is given to the drive as either a current command or a slip command. The current/slip relationship is then utilized to calculate the slip or current command.

The scalar control is somewhat simple to implement, but the inherent coupling effect (i.e. both torque and flux are functions of voltage or current and frequency) gives a sluggish response, and the system is prone to instability because of a high-order (fifth-order) system effect. To make it clearer, for example, if the torque is increased by increasing the slip (i.e. the frequency), the flux tends to decrease. The flux variation in such a system is always sluggish. The decrease in flux is compensated by the sluggish flux control loop feeding in the additional voltage. This temporary dipping of flux reduces the torque sensitivity with slip and lengthens response time. The foregoing problems can be solved by vector or field-oriented control. The invention of vector control at the beginning of the 1970s, and the demonstration that an induction motor can be controlled like a separately excited dc motor, brought a renaissance in the high-performance control of ac drives. Because of dc machine-like performance, vector control is also known as decoupling, orthogonal, or transvector control. Vector control is a very widely used control method for high- performance induction motor drive applications. Vector control is applicable to both induction and synchronous motors. The goal of the FOC (also called vector control) on synchronous and the asynchronous machine is to be able to separately control the torque producing and magnetizing flux components. It implies independent decoupled control of flux and torque components of stator current through a coordinated change in supply voltage amplitude, phase, and frequency [16]. .

This concept is copied from the dc machine for field-oriented control that has three requirements

- an independently controlled armature current to overcome the effects of armature winding resistance, leakage inductance, and induced voltage
- an independently controlled constant value of flux
- an independently controlled orthogonal spatial angle between the flux axis and magnetomotive force (MMF) axis to avoid interaction of MMF and flux.

Therefore, high- performance induction motor drives use vector control (field-oriented control (FOC) or direct torque and flux control (DTFC)).

2.4.1. Comparison of Direct Torque Control and Field Oriented Control

Table 2.1: Comparison between DTC and FOC [17]

Parameters for comparison	DTC	FOC
Dynamic response for torque	Quicker	Slower
Steady-state behavior for torque, stator flux, and currents	High ripple and distortion	Low ripple and distortion
Parameter sensitivity	Sensitive to stator resistance	Sensitive to rotor time constant
Current control	No	Yes
PWM modulator	No	Yes
Coordinate transformation	No	Yes
Audible noise	Spread spectrum, high noise especially at low speed	Low noise at a fixed frequency
Switching frequency	Variable, depending on the operating point and during transient	Constant
Controllers	Hysteresis controllers for Torque and Stator flux	PI regulators for Torque and Stator flux

Table 2.1: presents the comparison between DTC and FOC regarding the performance and the control structure of both systems. Both field-oriented control and direct torque control schemes aim at controlling separately the motor torque and flux over a wide speed range. The major drawbacks of direct torque control are high torque, flux ripples, and No modulator. Instead of that, FOC has low torque ripple, has Modulator, Constant switching frequency it overcomes the disadvantage of DTC.

2.5. Concept of Intelligent Control

Intelligence is defined as the ability to comprehend, reason, and learn. An intelligent control system has the ability to comprehend, reason, and learn about processes, disturbances and operating conditions in order to optimize the performance of the process under consideration. Intelligent control techniques are generally classified as expert system control, fuzzy logic control, neural network control, and genetic algorithm.

2.5.1. Fuzzy Logic Controller

The term fuzzy logic was introduced with the 1965 proposed by Lotfi Zadeh which is based on the fuzzy set theory. Fuzzy logic is one form of artificial intelligence. It is argued that human thinking does not always follow crisp 'yes no' logic, but is often vague, uncertain, indecisive, or fuzzy. The main characteristic of the fuzzy logic technique is to use the fuzzy rule sets and the linguistic representation of a human's knowledge to describe the controlled plant or to construct the fuzzy controller.

A fuzzy logic controller consists of fuzzification, fuzzy inference with rulebase and database, and defuzzification. The basic structure of a fuzzy inference System consists of three conceptual components: a rule base, which contains a selection of fuzzy rules; a database, which defines the membership functions used in the fuzzy rules; and a reasoning mechanism, which performs the inference procedure upon the rules and given facts to derive a reasonable output or conclusion. Fuzzy IF–THEN rules and fuzzy reasoning are the backbone of fuzzy inference systems, which are the most important modelling tool based on fuzzy set theory. Hence fuzzy control does not require any mathematical model of the system and so it can be applied to nonlinear systems [18].

2.5.2. Artificial Neural Network

Artificial neural networks(ANN) began with Warren McCulloch and Walter pitts in 1943 who created a computational model for neural networks. ANN usually simply called neural networks (NNs), are computing systems vaguely inspired by the biological neural networks that constitute animal brains. ANNs are composed of artificial neurons which are conceptually derived from biological neurons. Each artificial neuron has inputs and produce a single output which can be sent to multiple other neurons [19].

In squirrel cage induction motor it is difficult to measure the flux inside the rotor bars. Hence for control purposes the flux has to be estimated by different methods. One of such method is artificial neural networks. Neural networks have the function approximation capabilities. Using this capability the functional relationship between input and output can be established. By using this property the rotor flux can be estimated using neural networks.

CHAPTER 3

METHODOLOGY

3.1. Introduction

This chapter deals with the methodology that has been followed in this thesis work. The materials and methods used are explained. In addition to that, PI and Fuzzy logic controller techniques for speed control of the motor, the voltage and current model for flux estimation, open-loop speed estimation, Artificial neural network for flux estimation, field-oriented control algorithm, clark and park transformation, and space vector modulation are presented.

3.2. Materials

In this research work, software such as MATLAB/2016a, Microsoft office 2016, and MathType 6.0 equation are used. MATLAB is the computing software which consists of technical toolboxes and Simulink. Microsoft office is used for writing the thesis documentation. MathType 6.0 is used for writing mathematical formulas and equations in Microsoft offices word and PowerPoint presentation tools.

3.3. Methods

For the accomplishment of sensorless speed control of indirect vector control of IM the following methodologies have been followed:

- Gathering & survey related works from various techniques which are literature, reading books, journals, publications, and documents on related areas.
- Design the Clark and park transformation and space vector modulation
- Design an appropriate estimator and Controller for the system
- Performance evaluation and discussed the result
- Analyze the design with MATLAB/Simulink simulation. In general, the method followed throughout the research study can be summarized in the following flow chart of Figure 3.1.

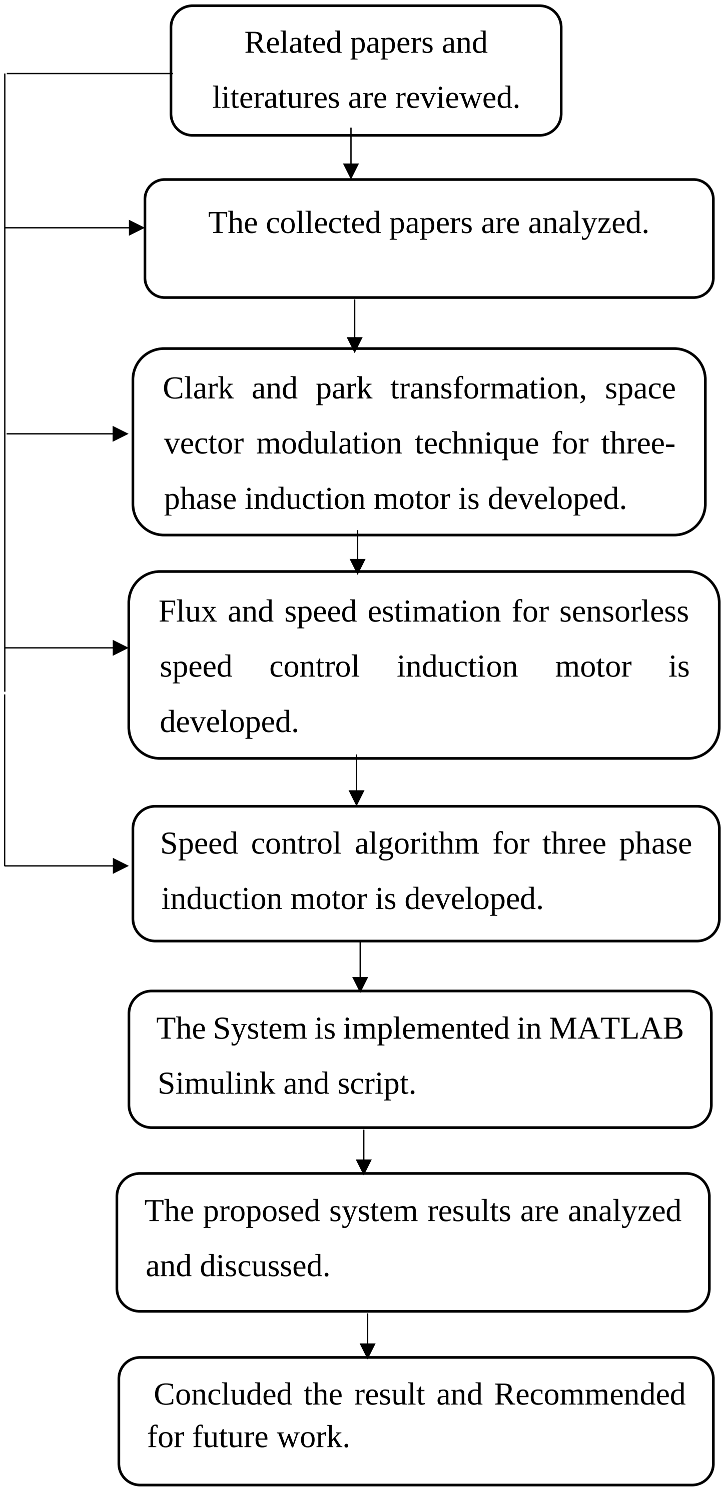

Figure 3.1: Block diagram of the research methodology

3.4. The General Block Diagram of Sensorless Speed Control of IM

The design of sensorless speed control of induction motor based on neural network flux estimation and fuzzy logic speed control is shown in Figure 3.2.

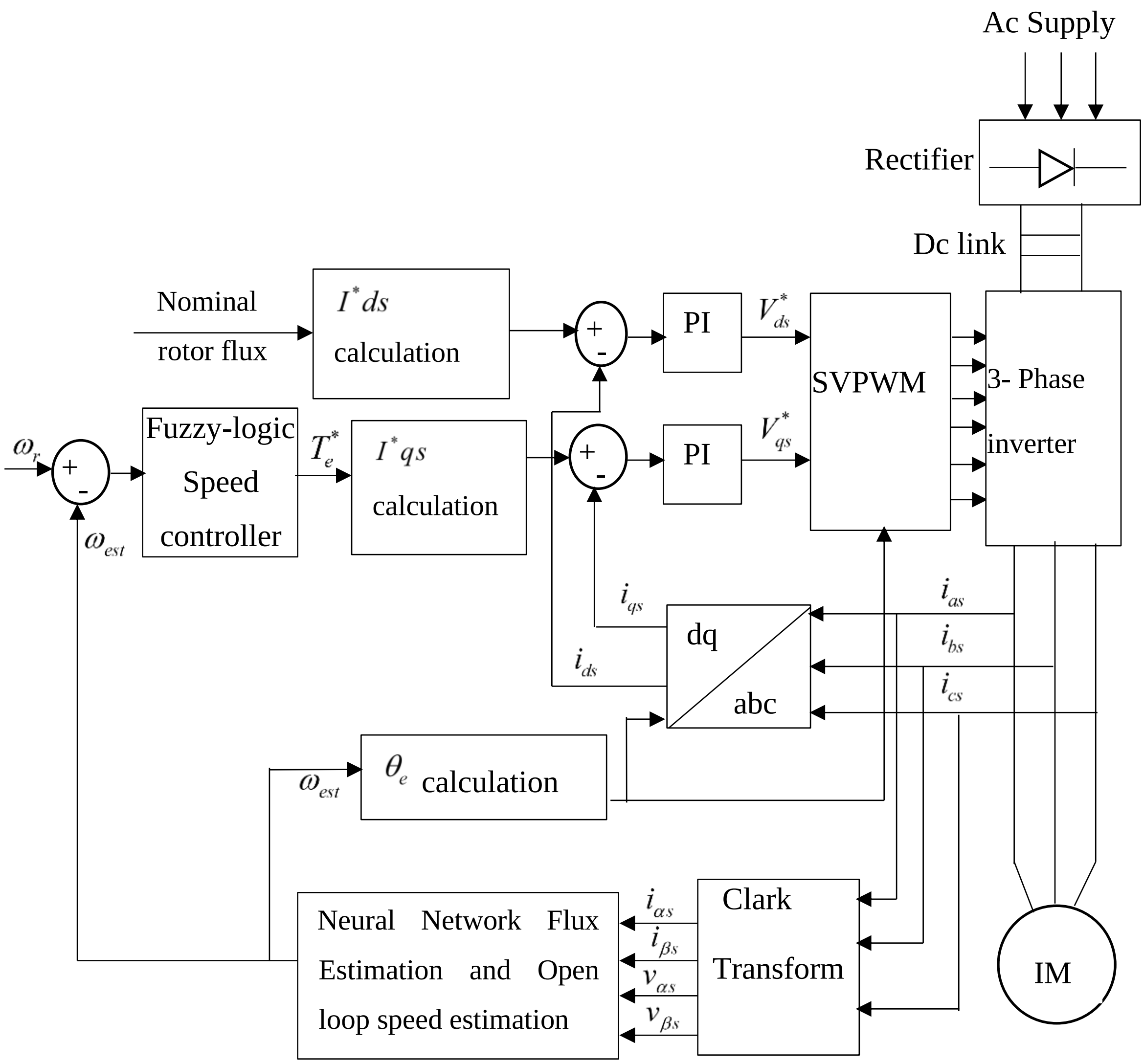

Figure 3.2:Block diagram of the proposed drive control system

Induction motor drives require variable voltage/current input at variable frequency to deliver variable speed operation. As the utility power source has constant frequency and voltage, it cannot be directly used in these machines. As a result there must be a power conversion process to obtain a variable voltage/current, variable frequency power supply from a fixed frequency, and voltage ac power source. The power conversion process involves first a utility AC to variable or fixed DC conversion (rectification) and then a DC to variable voltage/current, variable frequency AC conversion (inversion).

Voltage Source Inverters are devices that convert a DC voltage to AC voltage of variable frequency and magnitude. The inverter requires a dc voltage input, which, in a majority of the cases, is obtained from an AC supply by rectification with a diode bridge.

The output voltage could be fixed or variable at a fixed or variable frequency. A variable output voltage can be obtained by varying the input DC voltage and maintaining the gain of the inverter constant. On the other hand, if the DC input voltage is fixed and is not controllable, a variable output voltage can be obtained by varying the gain of the inverter, which is normally accomplished by pulse width modulation (PWM) control within the inverter.

The vector control of the induction machine is separately excited in which the torque and flux are controlled independently by using a PI controller. The torque and flux commands are regulated by using the PI controller into consideration of the current commands to develop the required voltage commands. These voltages are transformed into a stationary reference frame by using inverse park transformation and fed to SVPWM. The space vector pulse width modulation generates a gate signal to feed into the three-phase inverter.

Its main emphasis that to design the sensorless speed control for induction motor the simulation is done in MATLAB/Simulink. The overall completed indirect vector control of the induction motor drive, such a way that the rotor flux position is estimated by using a neural network. The speed of the induction motor is controlled by using a fuzzy logic controller and PI controller by comparing the estimated speed of the motor to the set value or reference generator.

3.5. Induction Machine Dynamic Model

The control of an induction motor can be made similar to that of a DC machine with a vector control technique, where it is possible to have independent control of flux and torque. To achieve this, the mathematical model of the motor in a rotating reference frame has to be synchronized either to the stator, air gap, or rotor flux vector.

3.5.1. General Equation of AC Motor

AC induction motor is represented by a stator and a concentric rotor and a narrow air gap between the smooth surfaces of the rotor and the stator. The connection between the stator and the rotor is formed by the flux, which implies there is no mechanical connection between them aside from the bearings. For deducing the general equations of the AC induction motor (with "squirrel cage" rotor), let us make the following assumptions:

- Neglect the coper losses and the slots in the machine;
- Spatial distribution of fluxes and amper turns wave are considered sinusoidal
- All the losses due to wiring, saturation, and slot effects can be neglected
- Stator and rotor permeability is assumed to be infinite.

Model of an induction machine in the synchronous frame [20, 21, 8];

Stator dq0 voltage equations:

$$v_{ds}^{e} = R_s i_{ds}^{e} - \omega_e \varphi_{ds}^{e} + \frac{d\varphi_{ds}^{e}}{dt} \tag{3.1}$$

$$v_{qs}^{e} = R_s i_{qs}^{e} - \omega_e \varphi_{qs}^{e} + \frac{d\varphi_{qs}^{e}}{dt} \tag{3.2}$$

Where v_{ds}^{e}, v_{qs}^{e} is stator voltages along d,q-axis respectively

Rotor dq0 voltage equations:

$$v_{dr}^{e} = R_r i_{dr}^{e} - (\omega_e - \omega_r)\varphi_{dr}^{e} + \frac{d\varphi_{dr}^{e}}{dt} \tag{3.3}$$

$$v_{qr}^{e} = R_r i_{qr}^{e} + (\omega_e - \omega_r)\varphi_{qr}^{e} + \frac{d\varphi_{qr}^{e}}{dt} \tag{3.4}$$

Where v_{dr}^{e}, v_{qr}^{e} is rotor voltages along d,q-axis respectively

Stator and rotor linkage flux in the synchronous reference frame in Matrics form is given as follow.

$$\begin{bmatrix} \varphi_{ds}^{e} \\ \varphi_{qs}^{e} \\ \varphi_{dr}^{e} \\ \varphi_{qr}^{e} \end{bmatrix} = \begin{bmatrix} L_s & 0 & L_m & 0 \\ 0 & L_s & 0 & L_m \\ L_m & 0 & L_r & 0 \\ 0 & L_m & 0 & L_r \end{bmatrix} \begin{bmatrix} i_{ds}^{e} \\ i_{qs}^{e} \\ i_{dr}^{e} \\ i_{qr}^{e} \end{bmatrix} \tag{3.5}$$

The torque developed by the motor in terms of q-axis current and flux linkage, using 'rms' convention [22] is

$$T_e = \frac{3}{2}\frac{P}{2}\frac{L_m}{L_r}\left(\varphi_{rd} i_{sq} - \varphi_{rq} i_{sd}\right) \tag{3.6}$$

The electromagnetic torque of the mechanical system is given by;

$$T_e = J\frac{dw_r}{dt} + fw_r + T_L \tag{3.7}$$

Where, w_r is rotor speed in RPM and J-is moment of inertia and f-friction coefficient.

Model of an induction machine in the Stationary reference frame: Let us choose first a standstill co-ordinate system $\omega_e = 0$ (where ω_e is synchronous speed), which means that the common coordinate system is a stationary one. Replacing the value $\omega_e = 0$ in the general Equations of the motor given by (3.1), (3.2), (3.3), and (3.4), the following vector voltage equations conclude:

Stator voltage equations in a stationary reference frame:

$$v_{ds}^s = R_s i_{ds}^s + \frac{d\varphi_{ds}^s}{dt} \tag{3.8}$$

$$v_{qs}^s = R_s i_{qs}^s + \frac{d\varphi_{qs}^s}{dt} \tag{3.9}$$

Rotor voltage equations in a stationary reference frame;

$$v_{dr}^s = R_s i_{dr}^s + \frac{d\varphi_{dr}^s}{dt} + w_r \varphi_{qr}^s = 0 \tag{3.10}$$

$$v_{qr}^s = R_s i_{qr}^s + \frac{d\varphi_{qr}^s}{dt} - w_r \varphi_{dr}^s = 0 \tag{3.11}$$

The stator and rotor voltage equations and the electromagnetic torque equations can be represented in matrix form as given below separately;

$$\begin{bmatrix}\varphi_{ds}\\ \varphi_{qs}\end{bmatrix}=\begin{bmatrix}L_s & 0\\ 0 & L_s\end{bmatrix}\begin{bmatrix}i_{ds}\\ i_{qs}\end{bmatrix}+\begin{bmatrix}L_m & 0\\ 0 & L_m\end{bmatrix}\begin{bmatrix}i_{dr}\\ i_{qr}\end{bmatrix} \tag{3.12}$$

$$\begin{bmatrix}\varphi_{dr}\\ \varphi_{qr}\end{bmatrix}=\begin{bmatrix}L_r & 0\\ 0 & L_r\end{bmatrix}\begin{bmatrix}i_{dr}\\ i_{qr}\end{bmatrix}+\begin{bmatrix}L_m & 0\\ 0 & L_m\end{bmatrix}\begin{bmatrix}i_{ds}\\ i_{qs}\end{bmatrix} \tag{3.13}$$

So, neglecting the magnetic saturation of the circuit and iron losses, the flux linkage Equations (3.1) and (3.2) of the circuit can be represented in matrix form as given below separately: -

$$\begin{bmatrix}v_{ds}\\ v_{qs}\end{bmatrix}=\begin{bmatrix}R_s & 0\\ 0 & R_s\end{bmatrix}\begin{bmatrix}i_{ds}\\ i_{qs}\end{bmatrix}+\frac{d}{dt}\begin{bmatrix}\varphi_{ds}\\ \varphi_{qs}\end{bmatrix}+\begin{bmatrix}0 & -w_e\\ w_e & 0\end{bmatrix}\begin{bmatrix}\varphi_{ds}\\ \varphi_{qs}\end{bmatrix} \tag{3.14}$$

$$\begin{bmatrix}v_{dr}\\ v_{qr}\end{bmatrix}=\begin{bmatrix}R_r & 0\\ 0 & R_r\end{bmatrix}\begin{bmatrix}i_{dr}\\ i_{qr}\end{bmatrix}+\frac{d}{dt}\begin{bmatrix}\varphi_{dr}\\ \varphi_{qr}\end{bmatrix}+\begin{bmatrix}0 & -(w_e-w_r)\\ (w_e-w_r) & 0\end{bmatrix}\begin{bmatrix}\varphi_{dr}\\ \varphi_{qr}\end{bmatrix} \tag{3.15}$$

$$T_e=\frac{3}{2}\frac{P}{2}\frac{L_m}{L_r}\begin{bmatrix}\varphi_{dr} & \varphi_{qr}\end{bmatrix}\begin{bmatrix}i_{ds}\\ -i_{qs}\end{bmatrix} \tag{3.16}$$

Solving Equation (3.13) for the rotor currents i_{dr}^{s} and i_{qr}^{s} putting these values in Equation (3.12), as follows;

$$\begin{bmatrix}\varphi_{ds}\\ \varphi_{qs}\end{bmatrix}=\begin{bmatrix}\sigma L_s & 0\\ 0 & \sigma L_s\end{bmatrix}\begin{bmatrix}i_{ds}\\ i_{qs}\end{bmatrix}+\begin{bmatrix}\frac{L_m}{L_r} & 0\\ 0 & \frac{L_m}{L_r}\end{bmatrix}\begin{bmatrix}\varphi_{dr}\\ \varphi_{qr}\end{bmatrix} \tag{3.17}$$

Where the total leakage factor σ is defined as $\sigma=1-\frac{L_m^2}{L_sL_r}$

Putting the values of rotor d- and q-axis voltage as zero and the values of rotor d- and q-axis currents from Equation (3.13) in (3.14), as follows;

$$\frac{d}{dt}\begin{bmatrix}\varphi_{dr}\\ \varphi_{qr}\end{bmatrix}=\frac{L_m}{T_r}\begin{bmatrix}1 & 0\\ 0 & 1\end{bmatrix}\begin{bmatrix}i_{ds}\\ i_{qs}\end{bmatrix}-\frac{1}{T_r}\begin{bmatrix}1 & 0\\ 0 & 1\end{bmatrix}\begin{bmatrix}\varphi_{dr}\\ \varphi_{qr}\end{bmatrix}+\left(w_e-w_r\right)\begin{bmatrix}0 & 1\\ -1 & 0\end{bmatrix}\begin{bmatrix}\varphi_{dr}\\ \varphi_{qr}\end{bmatrix} \tag{3.18}$$

Again, substituting, the values of stator fluxes from Equation (3.17) in (3.14), as follows;

$$\frac{d}{dt}\begin{bmatrix} i_{ds} \\ i_{qs} \end{bmatrix} = \begin{bmatrix} -R_1 & w_e \\ w_e & -R_1 \end{bmatrix}\begin{bmatrix} i_{ds} \\ i_{qs} \end{bmatrix} + \begin{bmatrix} R_2 & R_3 w_r \\ -R_3 w_r & R_2 \end{bmatrix}\begin{bmatrix} \varphi_{dr} \\ \varphi_{qr} \end{bmatrix} + \begin{bmatrix} \frac{1}{\sigma L_s} & 0 \\ 0 & \frac{1}{\sigma L_s} \end{bmatrix}\begin{bmatrix} v_{ds} \\ v_{qs} \end{bmatrix} \quad (3.19)$$

So, the state-space model of the induction motor in terms of stator currents and rotor flux linkages as the state variables are obtained by combining Equation (3.18) and (3.19), as follows;

$$\frac{d}{dt}\begin{bmatrix} i_{ds} \\ i_{qs} \\ \varphi_{dr} \\ \varphi_{qr} \end{bmatrix} = \begin{bmatrix} -R_1 & w_e & R_2 & R_3 w_r \\ -w_e & -R_1 & R_3 w_r & R_2 \\ R_5 & 0 & -R_4 & w_{sl} \\ 0 & R_5 & -w_{sl} & -R_4 \end{bmatrix}\begin{bmatrix} i_{ds} \\ i_{qs} \\ \varphi_{dr} \\ \varphi_{qr} \end{bmatrix} \begin{bmatrix} \frac{1}{\sigma L_s} & 0 \\ 0 & \frac{1}{\sigma L_s} \\ 0 & 0 \\ 0 & 0 \end{bmatrix}\begin{bmatrix} v_{ds} \\ v_{qs} \end{bmatrix} \quad (3.20)$$

$$Where,\ R_1 = \frac{1}{\sigma L_s}\left(R_s + R_r \frac{L_m^2}{L_r^2}\right), \quad R_2 = \frac{1}{\sigma L_s}\frac{R_r L_m}{L_r^2}, \quad R_3 = \frac{1}{\sigma L_s}\frac{L_m}{L_r}, \quad R_4 = \frac{1}{T_r}$$

$R_5 = \frac{R_r L_m}{L_r}$, $w_{sl} = w_e - w_r$ = slip speed.

3.6. Field Oriented Control of Induction Motor

The field orientated control consists of controlling the stator currents represented by a vector. This control is based on projections that transform a three-phase time and speed-dependent system into a two co-ordinate (d and q co-ordinates) time-invariant system. These projections lead to a structure similar to that of a DC machine control. Field orientated controlled machines need two constants as input references: the torque component and the flux component [23]. There are two approaches to obtain the flux vector, one direct measurement, and the other is indirect. According to the field-oriented control can be classified as direct field orientation control (DFOC) and indirect field orientation control (IFOC).

3.6.1. Direct Field Oriented Control

In the case of direct vector control, the motor flux is measured by directly measure the air gap fluxes using Hall Effect sensors [4]. In the direct field-oriented control, the slip frequency of the drive is not controlled. The motor is self-controlled by using the unit vector to control the frequency and phase. The transient response to be fast because torque control does not affect flux. As shown in Figure 3.3 the direct vector control method depends on the generation of unit vector signals from the stator or air-gap flux signals. The air-gap signals can be measured directly or estimated from the stator voltage and current signals. The stator flux components can be directly computed from stator quantities. In these systems, the rotor speed is not required for obtaining rotor field angle information [24, 25].

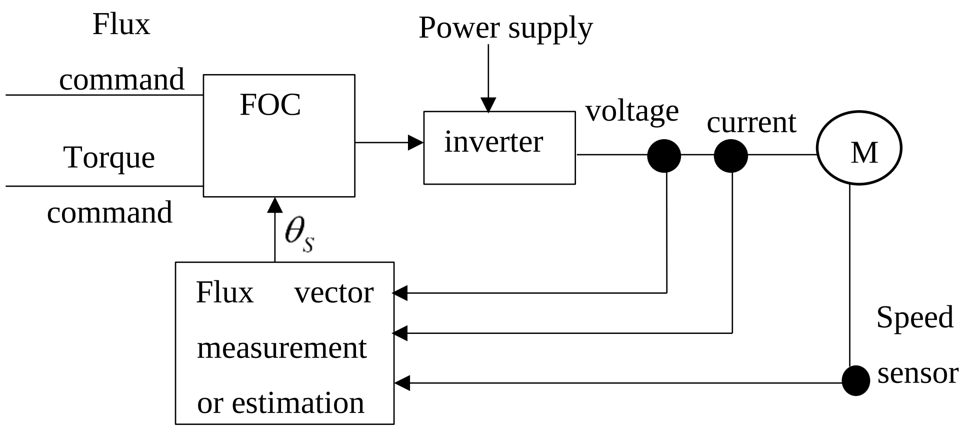

Figure 3.3: Direct FOC method [26]

3.6.2. Indirect Field Oriented Control

From Figure 3.4 in the indirect field-oriented control the rotor flux angle is being measured indirectly, instead of using air-gap flux sensors. IFOC estimates the rotor flux by computing the slip speed (ω_{sl}). In this method, the rotor field angle and thus the unit vectors are indirectly obtained by summation of the rotor speed and slip frequency. In this thesis the indirect field oriented control method applied for an induction motor.

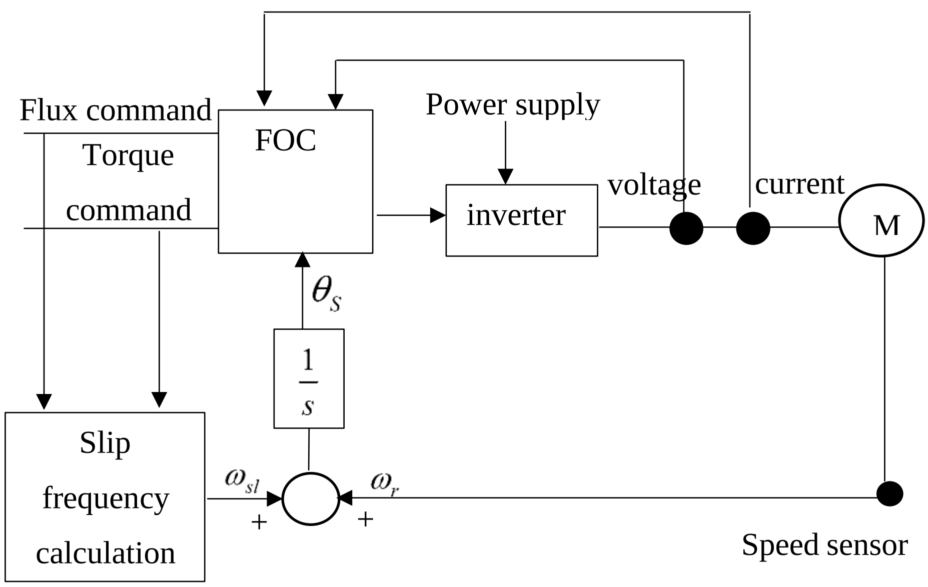

Figure 3.4:Indirect FOC [26]

Indirect field orientation (IFO) is the difference from the direct flux orientation based on the calculation of the slip speed ω_{sl} [4]. The angular position, ϴe, of the rotor flux vector is expressed as

$$\theta_e = \int \omega_e = \int (\omega_r + \omega_{sl}) \tag{3.21}$$

Where, ω_r is the rotor speed, which is easy to measure using a shaft position sensor, and ω_{sl} is the slip frequency speed.

The stator and rotor voltage equations of induction motor in the field orientation synchronous the reference frame can be written as in [27]

$$V_{ds} = R_s i_{ds} - \omega_e \sigma i_{qs} + \frac{d}{dt}(\sigma i_{ds} L_s) - \frac{L_m}{L_r}\frac{d}{dt}\left[\omega_e \varphi_{qr} - \frac{d}{dt}(\varphi_{dr})\right] \tag{3.22}$$

$$V_{qs} = R_s i_{qs} + \omega_e \sigma i_{ds} + \frac{d}{dt}(\sigma i_{qs} L_s) + \frac{L_m}{L_r}\frac{d}{dt}\left[\omega_e \varphi_{dr} - \frac{d}{dt}(\varphi_{qr})\right] \tag{3.23}$$

$$V_{dr} = R_r i_{dr} + \frac{d}{dt}(\varphi_{dr}) - [\omega_e - \omega_r]\varphi_{qr} = 0 \tag{3.24}$$

$$V_{qr} = R_r i_{qr} + \frac{d}{dt}(\varphi_{qr}) + [\omega_e - \omega_r]\varphi_{dr} = 0 \tag{3.25}$$

Where, $\omega_{sl} = \omega_e - \omega_r$

The rotor flux linkage equations can be written as:

$$\varphi_{dr} = L_r i_{dr} + L_m i_{ds} \tag{3.26}$$

$$\varphi_{qr} = L_r i_{qr} + L_m i_{qs} \tag{3.27}$$

These equations may be rewritten as:

$$i_{dr} = \frac{1}{L_r}\varphi_{dr} - \frac{L_m}{L_r} i_{ds} \tag{3.28}$$

$$i_{qr} = \frac{1}{L_r}\varphi_{qr} - \frac{L_m}{L_r} i_{qs} \tag{3.29}$$

For perfect decoupling control, the total rotor flux needs to be aligned with the d-axis so that the q-axis rotor flux is set zero and d-axis rotor flux is maintained constant then equations written as: $\varphi_{qr} = 0$, this implies $\frac{d}{dt}(\varphi_{qr}) = 0$ and $\varphi_{dr} = \varphi_r$ Substitute into the previous equations to implement the indirect vector control strategy[4]:

$$\theta_e = \theta_{sl} + \theta_r \tag{3.30}$$

$$\varphi_r = L_m i_{ds} \tag{3.31}$$

$$\frac{R_r}{L_r}\varphi_{qr} - \frac{R_r L_m}{L_r} i_{qs} + \frac{d}{dt}(\varphi_{qr}) + \omega_{sl}\varphi_{dr} = 0 \tag{3.32}$$

The required value of slip speed can be calculated by the following equation

$$\omega_{sl} = \frac{L_m R_r}{\varphi_r L_r} i_{qs} \quad \text{or} \quad \omega_{sl} = \frac{L_m i_{qs}}{\tau_r \varphi_r} \tag{3.33}$$

Where, τ_r is the rotor time constant calculated by: $\tau_r = \frac{L_r}{R_r}$

3.6.3. Indirect Field Oriented Control Algorithm

The algorithm of indirect vector control is as follows [28]:

1. Measure the stator phase currents Ia, Ib, and Ic. These currents are feed to the Park transformation module that gives two components, Ids and Iqs, in the stationary reference frame.
2. The rotor angle, Ɵe, required for coordinate transformation is computed by Equation (3.21).
3. The motor speed, ω_{est}, is compared with the reference speed ω_{ref}, and the error produced is fed to the speed controller. The output of the speed controller is electromagnetic torque T_e^*.
4. The quadrature stator current component reference I_{qs}^* is calculated by

$$I_{qs}^* = \left(\frac{2}{3}\right)\left(\frac{2}{P}\right)\left(\frac{L_r}{L_m}\right)\left(\frac{T_e^*}{\varphi_r}\right) \tag{3.34}$$

5. The direct stator current component reference I_{ds}^* is obtained from reference rotor flux input λ_r^* .

$$I_{ds}^* = \frac{\lambda_r^*}{L_m} \tag{3.35}$$

Where, λ_r^* is reference nominal flux linkage.

6. I_{ds}^* and I_{qs}^* are references for the current controller. The output of the current controller is the voltage. V_{ds}^* and V_{qs}^* voltage references are converted to $V_{\alpha s}^*$ and $V_{\beta s}^*$ using inverse park transformation and feed to SVPWM inverter to produce the inverter gating signals.

3.7. The Generalized Concept of Reference Frame Transformation

The Reference frame is very much like observer platforms, in that each of the platforms gives a unique view of the system at hand as well as a dramatic simplification of the system equation. The inductances of all alternating current (AC) machines vary according to the rotor position. Because of that, the voltage equations of an alternating current machine are expressed as time-varying differential equations as long as the rotor of the machine rotates. The transformation of the physical variables of an AC machine using reference frame theory could make the analysis easy by transforming the time-varying differential equations to the time-invariant differential equations [29].

The electrical variables such as voltage, current, and flux in a, b, and c phases of a three-phase system can be transformed to the variables in d, q, and n or 0 (direct, quadrature, and neutral) orthogonal axes, where the magnetic couplings between axes are zero. Usually, the d axis, which means the direct axis, is the axis where the main flux directs and the q axis, which means the quadrature axis, lies 90° ahead of the d axis spatially concerning the positive rotational direction of a rotating MMF**.** Also, the n or 0 axes, which means the neutral axis and sometimes called a zero**-s**equenc**e** axis. This kind of transformation from the a, b, and c phases to the orthogonal axes can be done by complex vector algebra or matrix algebra. For theoretical analysis and physical understanding, the transformation based on the complex vector would be easier compared to that on the matrix algebra but for the computer simulation and programming of the real-time control software of the electric machine, the transformation with the matrix algebra is more convenient [30]. In this thesis transformation based on matrix algebra is used.

Based on the speed of the reference frame there are four main reference frames of motion. These are arbitrary reference frame, stationary reference frame, rotor reference frame, and the synchronous reference frame. The two commonly employed coordinate transformations with an induction machine are the stationary and the synchronous reference frame [28]

i. **Stationary reference frame***:* In this case, the dq axis does not rotate. So, the reference frame speed is zero (ω =0). It is best suited for studying stator variables only. The stator d axis variables are identical to the stator phase A variable.

ii. **Rotor reference frame***:* The reference frame speed is equal to the rotor speed (ω =ωr). Since in this reference frame the d axis of the reference frame is moving at the same relative speed as the rotor phase A winding and coincident with its axis, it is best suited when the analysis is confined to rotor variables as the rotor d axis variable is identical to phase-rotor variables.

iii. **Synchronous reference frame***:* When the reference frame is rotating at synchronous speed, both the stator and rotor are rotating at different speeds. The reference frame speed is equal to synchronous speed (ω =ωe). Synchronously rotating reference frame is suitable when an analog computer is employed because both stator and rotor dq quantities become steady DC quantities.

iv. **Arbitrary reference frame**: In this reference frame speed is unspecified ω and the dq axis can rotate at an arbitrary speed, there is no relative speed between the four coils ds, qs, dr, qr.

3.8. Clark and Park Transformations

The Clarke and Park transformation is a transformation of coordinates that designed to transform a multiphase stationary coordinate system into two axes stationary and rotating coordinate system respectively. This transformation is used to reduce the complexity of the system and easier the control method. The stationary two-phase variables of Clarke’s transformation are denoted as α and β [31]. As shown in Figure 3.5 the α axis coincides the phase a-axis and the β axis lags the α axis by 90°.

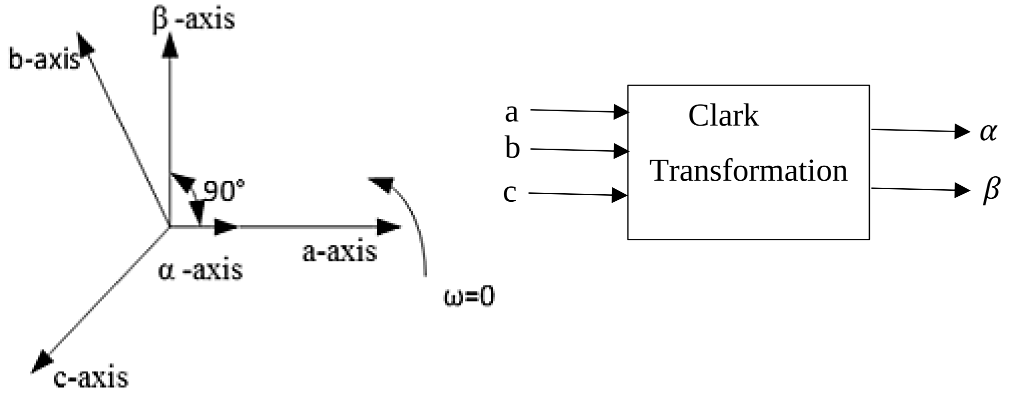

Figure 3.5: Clark transformation

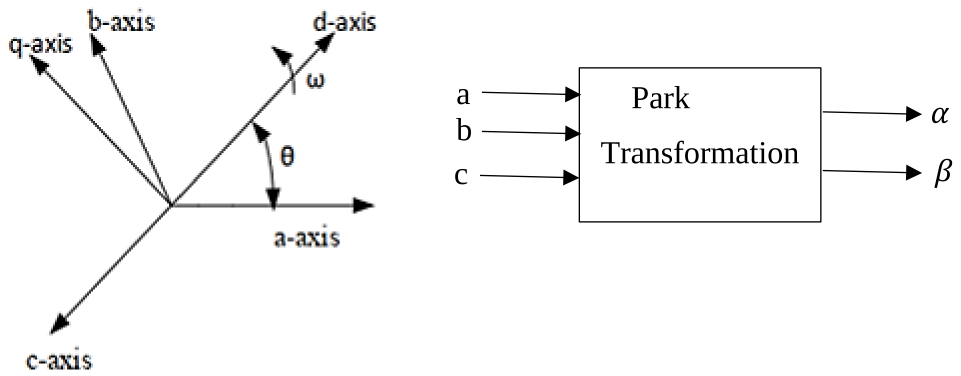

Figure 3.6: Park transformation

The three-phase stator voltages of an induction machine underbalanced condition can be expressed as,

$$V_a = \sqrt{2}V_{rms}\sin(\omega t) \tag{3.36}$$

$$V_b = \sqrt{2}V_{rms}\sin(\omega t - \frac{2\pi}{3}) \tag{3.37}$$

$$V_c = \sqrt{2}V_{rms}\sin(\omega t + \frac{2\pi}{3}) \tag{3.38}$$

Here Va, Vb and Vc is the three-line voltage. The relationship between α_β and abc is as follows

$$\begin{bmatrix} V_\alpha \\ V_\beta \end{bmatrix} = \frac{2}{3}\begin{bmatrix} 1 & -\frac{1}{2} & -\frac{1}{2} \\ 0 & \frac{\sqrt{3}}{2} & -\frac{\sqrt{3}}{2} \end{bmatrix}\begin{bmatrix} V_a \\ V_b \\ V_c \end{bmatrix} \tag{3.39}$$

Then, the direct and quadrature axes voltages are:

$$\begin{bmatrix} V_d \\ V_q \end{bmatrix} = \begin{bmatrix} \cos(\theta) & \sin(\theta) \\ -\sin(\theta) & \cos(\theta) \end{bmatrix} \begin{bmatrix} V_\alpha \\ V_\beta \end{bmatrix} \tag{3.40}$$

The instantaneous values of the stator and rotor currents in the three-phase system are ultimately calculated using the following transformation [32].

$$\begin{bmatrix} i_\alpha \\ i_\beta \end{bmatrix} = \begin{bmatrix} \cos(\theta) & -\sin(\theta) \\ \sin(\theta) & \cos(\theta) \end{bmatrix} \begin{bmatrix} i_d \\ i_q \end{bmatrix} \tag{3.41}$$

$$\begin{bmatrix} i_a \\ i_b \\ i_c \end{bmatrix} = \begin{bmatrix} 1 & 0 \\ -\frac{1}{2} & -\frac{\sqrt{3}}{2} \\ -\frac{1}{2} & -\frac{\sqrt{3}}{2} \end{bmatrix} \begin{bmatrix} i_\alpha \\ i_\beta \end{bmatrix} \tag{3.42}$$

Where ϴ is, the angle between the synchronously rotating reference frame d axis and the stationary frame α axis. The angular velocity ω and the angular displacement θ of arbitrary reference frame are related as:

$$\omega = \frac{d\theta}{dt} \tag{3.43}$$

Thus,

$$\theta = \int \omega dt \tag{3.44}$$

The relationship between abc and dq is as follows

$$\begin{bmatrix} i_d \\ i_q \end{bmatrix} = \frac{2}{3} \begin{bmatrix} \cos(\theta) & \cos(\theta - \frac{2\pi}{3}) & \cos(\theta + \frac{2\pi}{3}) \\ -\sin(\theta) & -\sin(\theta - \frac{2\pi}{3}) & -\sin(\theta + \frac{2\pi}{3}) \end{bmatrix} \begin{bmatrix} i_a \\ i_b \\ i_c \end{bmatrix} \tag{3.45}$$

$$\begin{bmatrix} i_a \\ i_b \\ i_c \end{bmatrix} = \begin{bmatrix} \cos(\theta) & -\sin(\theta) \\ \cos(\theta - \frac{2\pi}{3}) & -\sin(\theta - \frac{2\pi}{3}) \\ \cos(\theta + \frac{2\pi}{3}) & -\sin(\theta + \frac{2\pi}{3}) \end{bmatrix} \begin{bmatrix} i_d \\ i_q \end{bmatrix} \tag{3.46}$$

Note that the transform matrices and multiplying factors are the same for both voltages and currents. The induction motor considered in this thesis is the balanced three-phase. Therefore; the zero-sequence component is null. Rotating transformation from abc to dq coordinates, also called 3/2 rotating transformation, projects balanced three-phase quantities (voltages or currents) to rotating two-axis coordinates at a given angular velocity [33].

3.9. Space Vector Pulse Width Modulation

3.9.1. Voltage Source Inverter (VSI)

Three-phase inverters, supplying voltages and currents of adjustable frequency and magnitude to the stator, are an important element of adjustable speed drive systems employing IM. Inverters with semiconductor power switches are DC to AC power converters. Depending on the type of DC source supplying the inverter, they can be classified as voltage source inverters (VSI) or current source inverters (CSI). Typically, of the three-phase bridge configuration, with DC-link connected between the rectifier and the inverter. The DC link is a simple inductive, capacitive, or inductive-capacitive low-pass filter since neither the voltage across a capacitor nor the current through an inductor can change instantaneously. A capacitive-output DC link is used for a VSI and an inductive output link is employed in CSI [4].

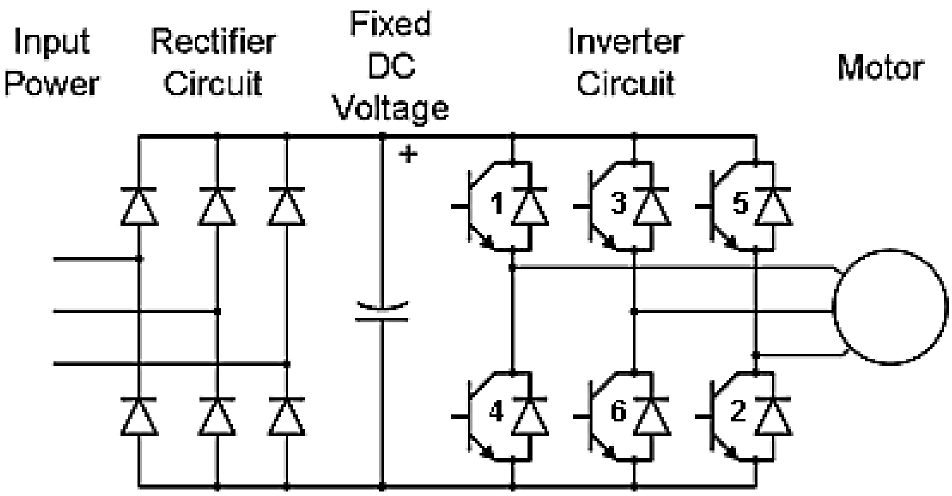

Figure 3.7: Basic three-phase voltage-source converter circuit [34].

A diagram of the power circuit of a three-phase VSI is shown in Figure 3.7. The circuit has bridge topology with three phases, each consisting of two power switches and two freewheeling diodes. In the case illustrated, the inverter is supplied from an uncontrolled, diode-based rectifier, via a DC link which contains an LC filter in the inverted configuration. While this circuit represents only positive power flow from the supply system to the load via a typically three-phase power line. Negative power flow, which occurs when the load feeds the recovered power back to the supply, is not possible since the resulting negative DC component of the current in the DC link cannot pass through the rectifier diodes.

3.9.2. Space Vector Modulation for VSI

Space vector pulse width modulation is an advanced, computation-intensive PWM method that has become a popular PWM technique for three-phase voltage source inverters in applications of AC machine drives [27]. The advantages of SVM, when compared to Sine PWM, are as follows:

- Line-to-line voltage amplitude can be as high as dc-link voltage (VDC). Thus, 100% VDC utilization is possible.
- With the increased output voltage, the user can design the motor control system with a reduced current rating, keeping the power rating the same. The reduced current helps to reduce the conduction loss of the VSI.
- Produce a more efficient output voltage with less Total Harmonic Distortion (THD) and switching loss.
- As the reference space vector is a two-dimensional quantity, it is feasible to implement advanced vector control using SVM.

3.9.3. Principle of Space Vector PWM

The circuit in Figure 3.8 demonstrates the foundation of a two-level voltage source converter. It has six switches (1- 6) and each of these is represented with an IGBT switching device. A, B, and C represents the output for the phase-shifted sinusoidal signals. Depending on the switching combination the inverter produces different outputs, creating the two-level signal. The biggest difference from other pulse width modulation methods is that the SVPWM uses a vector as a reference. This gives the advantage of a better overview of the system.

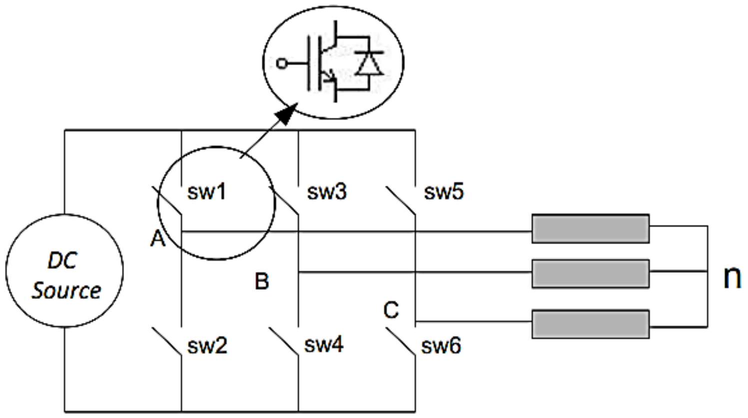

Figure 3.8: Three-phase inverter, with a load and neutral point [35].

Principle of space vector PWM

- Treats the sinusoidal voltage (reference voltage) as a constant amplitude vector rotating at a constant frequency.
- This PWM technique approximates the reference voltage $Vref$ by a combination of the eight switching patterns (V0 to V7).
- Coordinate transformation (dq reference frame to the stationary α-β frame).
- The vectors (V1 to V6) divide the plane into six sectors (each sector: 60 degrees).
- $Vref$ is generated by two adjacent non-zero vectors and two zero vectors.

Table 3.1 shows that the switches can be ON or OFF, meaning 1 or 0. switching state '1' denotes that the upper switch in an inverter leg is on and the inverter terminal voltage (Van, Vbn, Vcn) is positive ($+VDC$) while '0' indicates that the inverter terminal voltage is zero due to the conduction of the lower switch in the inverter leg [36].

Table 3.1: Switching states for each phase leg

Switching States	A			B			C		
	S_1	S_2	V_{an}	S_3	S_4	V_{bn}	S_5	S_6	V_{cn}
1	ON	OFF	V_{DC}	ON	OFF	V_{DC}	ON	OFF	V_{DC}
0	OFF	ON	0	OFF	ON	0	OFF	ON	0

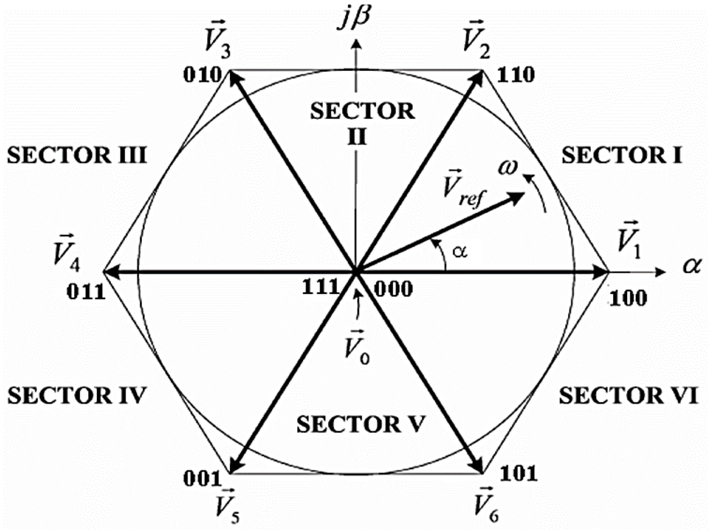

Figure 3. 9: Space voltage vectors in different sectors [37].

The lower switches are complementary to the upper switches, so the only possible combinations are the switching states: 000, 001, 010, 011, 100, 110, 110, 111. This means that there are eight possible switching states, among the eight switching states, for which two of them are zero switching states and six of them are active switching states. These are represented by active ($V1- V6$) and zero ($V0$) vectors. The zero vectors are placed in the axis origin in Figure 3.9.

There are eight possible combinations of switching states in the two-level inverter as listed in Table 3.2. The switching state of [100] corresponds to the conduction of S1, S6, and S2 in the inverter legs A, B, and C, respectively. Among the eight switching states, [111] and [000] are active states and the others are zero state

Table 3. 2: Space vectors, switching states, and on-state switches [38].

Space Vector		Switching state (Three Phases)	On-State Switch	Vector Definition
Zero vector	V_0	[1 1 1]	S1, S3, S5	0
		[0 0 0]	S4, S6, S2	
Active vector	V_1	[1 0 0]	S1, S6, S2	$V_1 = \frac{2}{3} V_d e^{j0}$
	V_2	[1 1 0]	S1, S3, S2	$V_1 = \frac{2}{3} V_d e^{j\frac{\pi}{3}}$
	V_3	[0 1 0]	S4, S3, S2	$V_1 = \frac{2}{3} V_d e^{j\frac{2\pi}{3}}$
	V_4	[0 1 1]	S4, S3, S5	$V_1 = \frac{2}{3} V_d e^{j\frac{3\pi}{3}}$
	V_5	[0 0 1]	S4, S6, S5	$V_1 = \frac{2}{3} V_d e^{j\frac{4\pi}{3}}$
	V_6	[1 0 1]	S1, S6, S5	$V_1 = \frac{2}{3} V_d e^{j\frac{5\pi}{3}}$

Complex vector expression for these eight vectors can be given as:

$$V_k = \begin{cases} \frac{2}{3} V_{dc} e^{\frac{j(k-1)\pi}{3}} & if\ K = 1,2,3,4,5,6 \\ 0 & if\ K = 0,7 \end{cases} \tag{3.47}$$

Since inverter output has eight switching states hence to represent it in binary code it needs three bits ($2^3 = 8$). Let 1“ represents ON state and 0“ OFF state of the switch. Following Figure 3.10 displays the eight states.

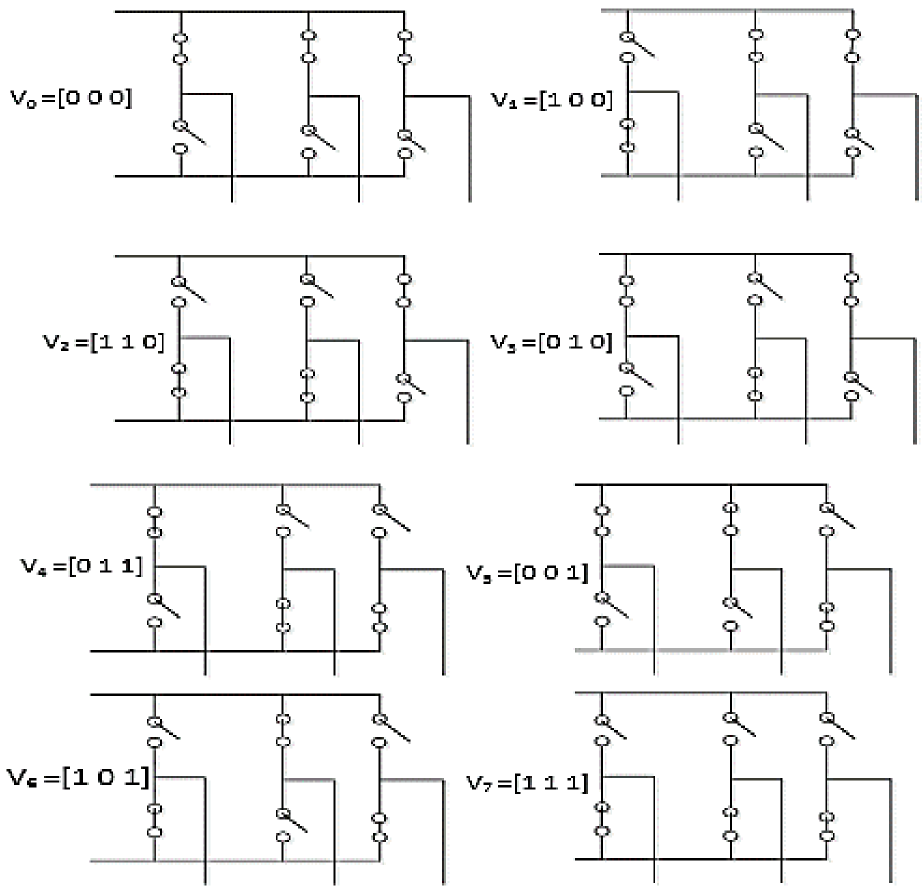

Figure 3. 10: Eight switching states of inverter switches

The space vector pulse width modulation is realized based on the following steps:

Step1. Determine V_α, V_β, V_{ref} and angle (α).

Step2. Determine time duration T1, T2, T0.

Step3. Determine the switching time of each transistor.

3.9.4. Determination of V_α, V_β, V_{ref}, and Angle (α)

From the relationship between the clark and park transformation in Section 3.8. The V_d and V_q transformed into the V_α and V_β by using inverse park transformation. The V_d, V_q, V_{ref} and angle (α) can be determined as follows:

$$V_\alpha = V_d \cos(\theta) - V_q \sin(\theta) \tag{3.48}$$

$$V_\beta = V_d \sin(\theta) + V_q \cos(\theta) \tag{3.49}$$

The magnitude and angle (determining in which sector the reference vector is in) of the reference vector is:

$$\left|V_{ref}\right| = \sqrt{V_\alpha^2 + V_\beta^2} \tag{3.50}$$

$$\alpha = \tan^{-1}\left(\frac{V_\beta}{V_\alpha}\right) \tag{3.51}$$

Having calculated V_α , V_β , V_{ref} and the reference angle in this step is taken. The next step is to calculate the duration time for each vector $V_1 - V_6$.

3.9.5. Calculation of Time Durations

V_{ref} can be found with two active and one zero vector. For sector 1 (0 to $\frac{\pi}{3}$): V_{ref} can be located with V_0, V_1 and V_2. V_{ref} in terms of the duration time can be considered as [39]

$$V_{ref} * T_C = V_1 * \frac{T_1}{T_C} + V_2 * \frac{T_2}{T_C} + V_0 * \frac{T_0}{T_C} \tag{3.52}$$

$$V_{ref} = V_1 T_1 + V_2 T_2 + V_0 T_0 \tag{3.53}$$

The total cycle is given by:

$$T_C = T_1 + T_2 + T_0 \tag{3.54}$$

The position of V_{ref} , V_1, V_2 and V_0 can be described with its magnitude and angle:

$$V_{ref} = V_{ref} e^{j\theta} \tag{3.55}$$

$$V_1 = \frac{2}{3} * V_{DC} * e^{j\frac{\pi}{3}} \tag{3.56}$$

$$V_0 = 0 \tag{3.57}$$

$$T_C * V_{ref} * \begin{pmatrix} \cos\theta \\ \sin\theta \end{pmatrix} = T_1 * \frac{2}{3} * V_{DC} * \begin{pmatrix} 1 \\ 0 \end{pmatrix} + T_2 * \frac{2}{3} * V_{DC} * \begin{pmatrix} \cos\left(\frac{\pi}{3}\right) \\ \sin\left(\frac{\pi}{3}\right) \end{pmatrix} \tag{3.58}$$

Dividing these into real and imaginary parts simplifies the calculation for each duration time:

Real part: $T_C * V_{ref} * \cos(\theta) = T_1 * \frac{2}{3} * V_{DC} + T_2 * \frac{1}{3} * V_{DC}$

Imaginary part: $T_C * V_{ref} * \sin(\theta) = T_2 * {}^{1}\!/\!_{\sqrt{3}} * V_{DC}$

T_1 and T_2 is then given by:

$$T_1 = T_C * \frac{\sqrt{3} * V_{ref}}{V_{DC}} * \sin\left(\frac{\pi}{3} - \theta\right) = T_C * \alpha * \sin\left(\frac{\pi}{3} - \theta\right) \tag{3.59}$$

$$T_2 = T_C * \frac{\sqrt{3} * V_{ref}}{V_{DC}} * \sin(\theta) = T_C * \alpha * \sin(\theta) \tag{3.60}$$

$$T_0 = T_C - T_1 - T_2 \tag{3.61}$$

Where, $\alpha = \frac{\sqrt{3} * V_{ref}}{V_{DC}}$ is the modulation index. T_1, T_2 are the switching time durations of vectors V_1 and V_2 respectively, T_0 is the time duration of the zero vector and T_C is the time which applied for one sector is shown in Figure 3.11.

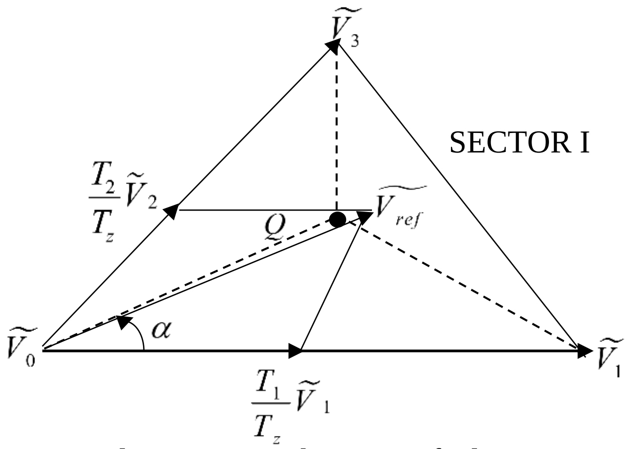

Figure 3. 11: Reference voltage as a combination of adjacent vectors in the sector I [40]

3.9.5.1 Description of Duration Times for All Sectors

The general calculation to receive the duty times in the rest of the sectors is given by

$$T_1 = T_C * \alpha * sin\left(\frac{\pi}{3} - \theta + \frac{n-1}{3} * \pi\right) = T_C * \alpha * \left[sin\left(\frac{n}{3}\pi\right) cos(\theta) - \cos(\frac{n}{3}\pi)\sin(\theta)\right] \tag{3.62}$$

$$T_2 = T_C * \alpha * sin\left(\theta - \frac{n-1}{3} * \pi\right) = T_C * \alpha * \left[-cos(\theta) sin\left(\frac{n-1}{3}\pi\right) + \sin(\theta)\cos\left(\frac{n-1}{3}\pi\right)\right] \quad (3.63)$$

$$T_0 = T_C - T_1 - T_2 \quad (3.64)$$

Choosing n as the number of the sector (n =1, 2, 3, 4, 5, 6) the calculations for the time duration in each sector can be calculated in Table 3.3.

Table 3.3: Duration time for each sector [36]

Sector	Duration times		
	T_1	T_2	T_0
1	$T_C * \alpha * \sin\left(\frac{\pi}{3} - \theta\right)$	$T_C * \alpha * \sin(\theta)$	$T_C - T_1 - T_2$
2	$T_C * \alpha * \sin\left(\frac{2\pi}{3} - \theta\right)$	$T_C * \alpha * \sin\left(\theta - \frac{\pi}{3}\right)$	$T_C - T_1 - T_2$
3	$T_C * \alpha * \sin(\pi - \theta)$	$T_C * \alpha * \sin\left(\theta - \frac{2\pi}{3}\right)$	$T_C - T_1 - T_2$
4	$T_C * \alpha * \sin\left(\frac{4\pi}{3} - \theta\right)$	$T_C * \alpha * \sin(\theta - \pi)$	$T_C - T_1 - T_2$
5	$T_C * \alpha * \sin\left(\frac{5\pi}{3} - \theta\right)$	$T_C * \alpha * \sin\left(\theta - \frac{4\pi}{3}\right)$	$T_C - T_1 - T_2$
6	$T_C * \alpha * \sin(2\pi - \theta)$	$T_C * \alpha * \sin\left(\theta - \frac{5\pi}{3}\right)$	$T_C - T_1 - T_2$

3.9.6. Description of Switching Time

The SVPWM switching patterns for sector 1 and 2 are shown in Figure 3.12:

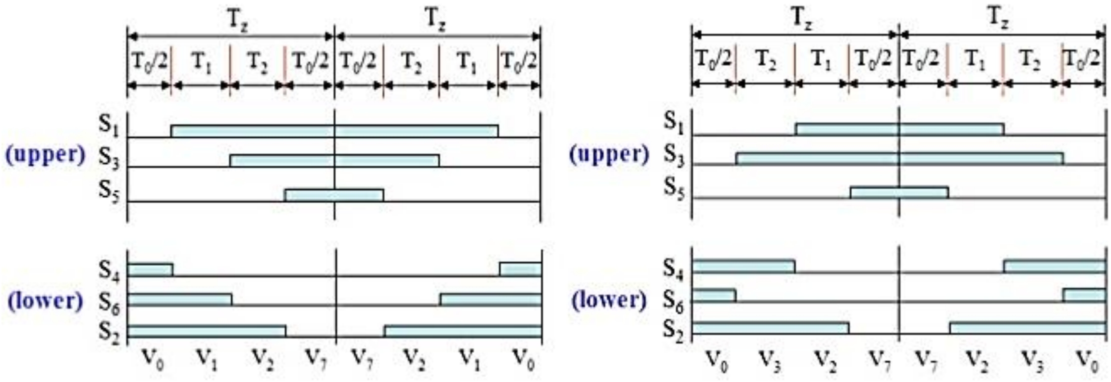

Sector 1.　　　　Sector 2.

Figure 3. 12: Space vector PWM switching patterns for the first two sectors [41]

Based on Figure 3.12, the switching time in each sector is summarized in Table 3.4

Table 3. 4: Duty time for each sector [42]

Sector	Upper Switches (S1, S3.S5)	Lower Switches (S4, S6.S2)
1	S1=T1+T2+T0/2	S4=T0/2
	S3=T2+T0/2	S6=T1+T0/2
	S5=T0/2	S2=T1+T2+T0/2
2	S1=T1+T0/2	S4=T2+T0/2
	S3=T1+T2+T0/2	S6=T0/2
	S5=T0/2	S2=T1+T2+T0/2
3	S1=T0/2	S4=T1+T2+T0/2
	S3=T1+T2+T0/2	S6=T0/2
	S5=T2+T0/2	S2=T1+T0/2
4	S1=T0/2	S4=T1+T2+T0/2
	S3=T1+T0/2	S6=T2+T0/2
	S5=T1+T2+T0/2	S2=T0/2
5	S1=T2+T0/2	S4=T1+T0/2
	S3=T0/2	S6=T1+T2+T0/2
	S5=T1+T2+T0/2	S2=T0/2
6	S1=T1+T2+T0/2	S4=T0/2
	S3=T0/2	S6=T1+T2+T0/2
	S5=T1+T0/2	S2=T2+T0/2

3.10. Flux and Speed Estimation for Sensor-less IFOC of IM

3.10.1. Flux Estimation of the Three-phase Induction Motor

Most of the sensorless control schemes rely directly or indirectly on the estimation of the stator flux linkage vector being defined;

$$\frac{d\psi^{s,v}}{dt} = u_s - R_s i_s + u_{off}, \psi_s(0) = \psi_{s0} \tag{3.65}$$

where, uoff represents all disturbances such as offsets, unbalances, and other errors present in the estimated induced emf. A major source of error in the emf is due to the changes in the model parameter Rs.

The flux estimator used can be computed both the synchronous speed and the rotor speed. The logic underlying this flux observer is an advanced voltage model approach in which integration of the back-emf is calculated and compensated for the errors associated with pure integrator and stator resistance Rs measurement at low speeds. At high speeds, the voltage model provides an accurate stator flux estimate because the machine back emf dominates the measured terminal voltage. However, at low speeds, the stator IR drop becomes significant, causing the accuracy of the flux estimate to be sensitive to the estimated stator resistance. Due to this effect, at low excitation frequencies, flux estimation based upon the voltage model is generally not capable of achieving high dynamic performance at low speeds.

Consequences of these problems are compensated with the addition of a closed-loop in the flux observer. The fluxes obtained by the current model are compared with those obtained by the voltage model regarding the current model, or the current model about the voltage model according to the range in which one of these models is superior to the other [43]. In this flux observer the voltage model is corrected by the current model through a basic PI block. In the end, the stator fluxes are used to obtain rotor fluxes and rotor flux angle. The overall observer structure is given below.

Firstly, the rotor flux linkage dynamics in the synchronously rotating reference frame $w = w_e = w_\varphi$ can be shown as below [44]:

$$\frac{d\varphi_{dr}^{e,i}}{dt} = \frac{L_m}{T_r} i_{ds}^e - \frac{1}{T_r}\varphi_{dr}^{e,i} + \left(w_e - w_r\right)\varphi_{qr}^{e,i} \tag{3.66}$$

$$\frac{d\varphi_{qr}^{e,i}}{dt} = \frac{L_m}{T_r} i_{qs}^e - \frac{1}{T_r}\varphi_{qr}^{e,i} + \left(w_e - w_r\right)\varphi_{dr}^{e,i} \tag{3.67}$$

where L_m is the magnetizing inductance (H), $T_r = \frac{L_r}{R_r}$ is the rotor time-constant (sec), and w_r is the electrical angular velocity of the rotor (rad/sec). In the current model, the total rotor flux-linkage is aligned with the d-axis component, and hence;

$$\varphi_r^{e,i} = \varphi_{dr}^{e,i} \quad \text{and} \quad \varphi_{qr}^{e,i} = 0$$

Substitution of $\varphi_{qr}^{e,i} = 0$ into Equations (3.66) and (3.67) yields the oriented rotor flux dynamics as;

$$\frac{d\varphi_{dr}^{e,i}}{dt} = \frac{L_m}{T_r} i_{ds}^e - \frac{1}{T_r}\varphi_{dr}^{e,i} \tag{3.68}$$

$$\varphi_{qr}^{e,i} = 0 \tag{3.69}$$

Note that Equations (3.68) and (3.69) are the commonly recognized forms of the rotor flux vector equations. When the rotor flux linkages in Equations (3.68) and (3.69) undergoes the inverse park transformation in the stationary reference frame the result becomes [45].

$$\varphi_{dr}^{s,i} = \varphi_{dr}^{e,i}\cos\left(\theta_{\varphi r}\right) - \varphi_{qr}^{e,i}\sin\left(\theta_{\varphi r}\right) = \varphi_{dr}^{e,i}\cos\left(\theta_{\varphi r}\right) \tag{3.70}$$

$$\varphi_{qr}^{s,i} = \varphi_{qr}^{e,i}\cos\left(\theta_{\varphi r}\right) + \varphi_{dr}^{e,i}\sin\left(\theta_{\varphi r}\right) = \varphi_{dr}^{e,i}\sin\left(\theta_{\varphi r}\right) \tag{3.71}$$

Where, $\theta_{\varphi r}$ is the rotor flux angle (rad). The stator flux linkages in the stationary reference frame are then computed using Equations (3.72) and (3.73) as;

$$\varphi_{ds}^{s,i} = L_s i_{ds}^s + L_m i_{dr}^s \tag{3.72}$$

$$\varphi_{qs}^{s,i} = L_s i_{qs}^s + L_m i_{qr}^s \tag{3.73}$$

$$\varphi_{dr}^{s,i} = L_r i_{dr}^s + L_m i_{ds}^s \tag{3.72a}$$

$$\varphi_{qr}^{s,i} = L_r i_{qr}^s + L_m i_{qs}^s \tag{3.73a}$$

$$\text{Where, } i_{dr}^{s} = \frac{\varphi_{dr}^{s,i} - L_m i_{ds}^{s}}{L_r} \text{ and } i_{qr}^{s} = \frac{\varphi_{qr}^{s,i} - L_m i_{qs}^{s}}{L_r} \tag{3.74}$$

By substituting Equation (3.74) into Equations (3.72 & 3.73), the stator flux linkage in stationary reference frame becomes;

$$\varphi_{ds}^{s,i} = L_s i_{ds}^{s} + L_m i_{dr}^{s} = \left(\frac{L_s L_r - L_m^2}{L_r} \right) i_{ds}^{s} + \frac{L_m}{L_r} \varphi_{dr}^{s,i} \tag{3.75}$$

$$\varphi_{qs}^{s,i} = L_s i_{qs}^{s} + L_m i_{qr}^{s} = \left(\frac{L_s L_r - L_m^2}{L_r} \right) i_{qs}^{s} + \frac{L_m}{L_r} \varphi_{qr}^{s,i} \tag{3.76}$$

Where L_s and L_r are the stator and rotor self-inductance (H), respectively.

The stator flux linkage in the voltage model has computed through back emf's integration with compensated voltages.

$$\varphi_{ds}^{s,v} = \int \left(u_{ds}^{s} - i_{ds}^{s} R_s - u_{comp,ds} \right) dt \tag{3.77}$$

$$\varphi_{qs}^{s,v} = \int \left(u_{qs}^{s} - i_{qs}^{s} R_s - u_{comp,qs} \right) dt \tag{3.78}$$

The compensated voltages, on the other hand, are computed by the PI control law as follows [45]:

$$u_{comp,ds} = K_p \left(\varphi_{ds}^{s,v} - \varphi_{ds}^{s,i} \right) + \frac{K_p}{T_i} \int \left(\varphi_{ds}^{s,v} - \varphi_{ds}^{s,i} \right) dt \tag{3.79}$$

$$u_{comp,qs} = K_p \left(\varphi_{qs}^{s,v} - \varphi_{qs}^{s,i} \right) + \frac{K_p}{T_i} \int \left(\varphi_{qs}^{s,v} - \varphi_{qs}^{s,i} \right) dt \tag{3.80}$$

The proportional gain K_p and the reset time T_i are chosen such that the flux linkages computed by the current model becomes dominant at low speed. The reason for that is the back emf computed by the voltage model result to be extremely low at this speed range (even zero for back emf at zero speed). While the motor is running at a high- speed range, the flux linkages computed by the voltage model becomes dominant over the flux linkage components computed through the current model. Once the stator flux linkages in Equations (3.77) and (3.78) are calculated, the rotor flux linkages based on the voltage model are computed once more through Equations (3.83) and (3.84) which are only rearranged forms of Equations (3.75) and (3.76), as in the current model, rotor flux linkage from Equations (3.75) and (3.76) rearranged as:

$$\varphi_{dr}^{s,i} = -\left(\frac{L_s L_r - L_m^2}{L_m}\right) i_{ds}^{s} + \frac{L_r}{L_m}\varphi_{ds}^{s,i} \qquad \text{and} \tag{3.81}$$

$$\varphi_{qr}^{s,i} = -\left(\frac{L_s L_r - L_m^2}{L_m}\right) i_{qs}^{s} + \frac{L_r}{L_m}\varphi_{qs}^{s,i} \tag{3.82}$$

Therefore, the rotor flux linkage in the voltage model is written similarly;

$$\varphi_{dr}^{s,v} = -\left(\frac{L_s L_r - L_m^2}{L_m}\right) i_{ds}^{s} + \frac{L_r}{L_m}\varphi_{ds}^{s,v} \tag{3.83}$$

$$\varphi_{qr}^{s,v} = -\left(\frac{L_s L_r - L_m^2}{L_m}\right) i_{qs}^{s} + \frac{L_r}{L_m}\varphi_{qs}^{s,v} \tag{3.84}$$

It is then a straightforward process to compute the rotor flux angle based on the voltage model as;

$$\theta_{\varphi r} = \tan^{-1}\left(\frac{\varphi_{dr}^{s,v}}{\varphi_{qr}^{s,v}}\right) \tag{3.85}$$

The voltage model has poor performance at very low speed due to the fact of: -

- At low frequency, voltage signals are very low, and ideal integration becomes difficult because dc offset tends to build up at the integrator output.
- The parameter variation effects, especially the stator resistance, tend to reduce the accuracy of the estimated signals. Flux estimation based upon the voltage model is generally not capable of achieving high dynamic performance at low speeds.

These problems are compensated with the addition of a closed-loop in the flux observer. The fluxes obtained by the current model are compared with those obtained by the voltage model by using the PI controller. But, these PI controllers do not give satisfactory output at low speed.

The current model dependent on the rotor time constant. The performance of this system degrades during field weakening, due to the difficulty of determining Tr and Lr with changing flux.

The new technique uses an Artificial Neural Network as a rotor flux estimator to replace the voltage model and current model. This makes the voltage model free of pure integration and less sensitive to stator resistance variations and the current model free from rotor time constant. The data for training the Neural Network is obtained from the current model and voltage model equation.

3.10.2. Speed Estimation of the Three-phase Induction Motor

In this section, a speed estimator for the 3-phase induction motor based upon its mathematical model is investigated. The synchronous speed w_e can be easily calculated from the derivative of the rotor flux angle in Equation (3.85).

$$w_e = \frac{d\theta_{\varphi r}}{dt} = \frac{d\tan^{-1}\left(\frac{\lambda_{qr}^s}{\lambda_{dr}^s}\right)}{dt} = \frac{1}{\left(\varphi_r^s\right)^2}\left(\varphi_{dr}^s \frac{d\varphi_{qr}^s}{dt} - \varphi_{qr}^s \frac{d\varphi_{dr}^s}{dt}\right) \tag{3.86}$$

Substituting Equations (3.66) and (3.67) into Equation (3.86), and a suitable rearrangement of them gives the synchronous speed, w_e as;

$$w_e = \frac{d\theta_{\varphi r}}{dt} = w_r + \frac{L_m}{T_r}\left(\frac{\varphi_{dr}^s i_{qs}^s - \varphi_{qr}^s i_{ds}^s}{\left(\varphi_r^s\right)^2}\right) \tag{3.87}$$

Where, $\frac{L_m}{T_r}\left(\frac{\varphi_{dr}^s i_{qs}^s - \varphi_{qr}^s i_{ds}^s}{\left(\varphi_r^s\right)^2}\right)$

The second term of the right hand in Equation (3.87) is known as the slip that is proportional to the electromagnetic torque when the rotor flux magnitude is maintaining constant. Thus, the rotor speed can be found as

$$\therefore w_r = w_e - \frac{L_m}{T_r}\left(\frac{\varphi_{dr}^s i_{qs}^s - \varphi_{qr}^s i_{ds}^s}{\left(\varphi_r^s\right)^2}\right) \tag{3.88}$$

The typical waveforms of the rotor flux angle $\theta_{\varphi r}$ in both directions can be seen in Figure 3.13. To take the discontinuity of angle from 360° to 0° (CCW) or from 0° to 360° (CW) into account, the differentiator is simply operated only within the differentiable range as seen in the Figure 3.13. This differentiable range does not cause a significant loss of information to compute the estimated speed.

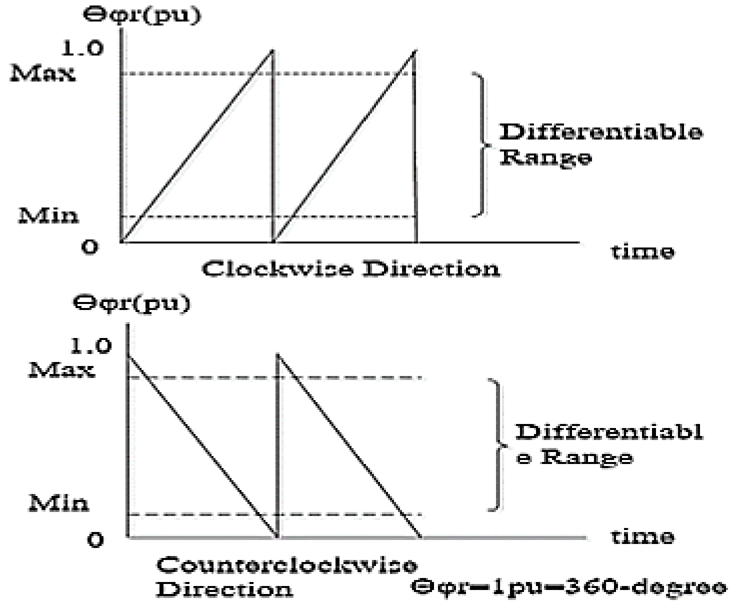

Figure 3.13: The waveforms of rotor flux angle in both directions [46]

3.11. Artificial Neural Network for Flux Estimation

The Artificial Neural Network imitates the behavior of the human brain to perform the faster calculation for complex structures. It establishes its own rules based on experience from training data so the human brain performs this with its real experience**.** ANN needs a learning procedure. In this procedure information is gathered, this information is spared and summed up through weights. These weights are obtained between neurons. To acquire the coveted yield, the learning process incorporates learning calculations, which accomplish this by overhauling the weights [47].

Neurons are essential components of ANN. The most normal neuron model appears in Figure 3.14. A neuron comprises of five sections. These parts are; information sources, weights, summing intersection, initiation capacity, and yields. Inputs take information from different neurons or from outside. Information joins the neuron by weights and these weights decide the impact of the pertinent information [32]. Summing intersection ascertains the net info; net information is the entirety of the augmentation consequences of sources of info and their applicable weights. Initiation work applies the net contribution to a procedure and gives neuron yield.

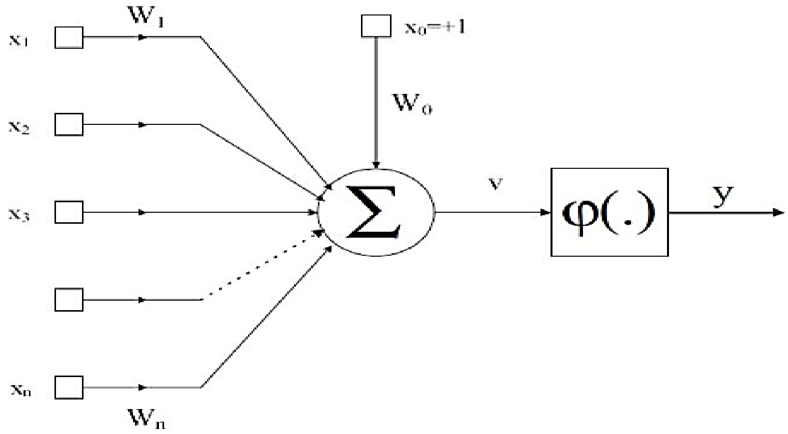

Figure 3.14: Artificial neuron model [48]

Figure 3.14 shows the most basic model for ANN. X0 is constant and called as bias or threshold of the activation function. The mathematical model of neurons is represented as

$$NET_j = \sum_{i=1}^{m} W_{ji} X_i \tag{3.89}$$

In general, ANN neurons are connected and their outputs are also connected to other neurons or themselves by weights with particular delays between them. There are various forms of ANN-based on their activation functions, learning rules, or connection types. The neurons learn by their experiments by applying the learning rules they adjust their weights by using output error generated. Learning in the context of a neural network is the process of adjusting the weights and biases in such a manner that for a given input, the correct response, or outputs are achieved. There are two types of learning. These are the following.

Supervised Learning*:* the network is presented with training data that represents the range of input possibilities, together with the associated desired outputs [28]. The weights are adjusted until the error between the actual and desired outputs meets minimum value. In this thesis Supervised Learning is used since the input and output data for rotor flux is available.

Unsupervised Learning: Also called open-loop adaptation because the technique does not use feedback information to update the network's parameters. Applications for unsupervised learning in speech recognition and image compression [28]. Learning algorithms include backpropagation and hybrid learning Algorithms. A Neural Network consists of a number of these neurons connected to the following network architectures.

3.11.1. Feedforward Networks

ANN is a network of single- neurons joined together by synaptic connections. Figure 3.15 shows a three-layer feedforward neural network. The feedforward network consists of a three-neuron input layer, a two-neuron output layer, and a four-neuron hidden layer [49]. All neurons in a particular layer are connected to all neurons in the subsequent layer. This is generally called a fully connected multilayer network.

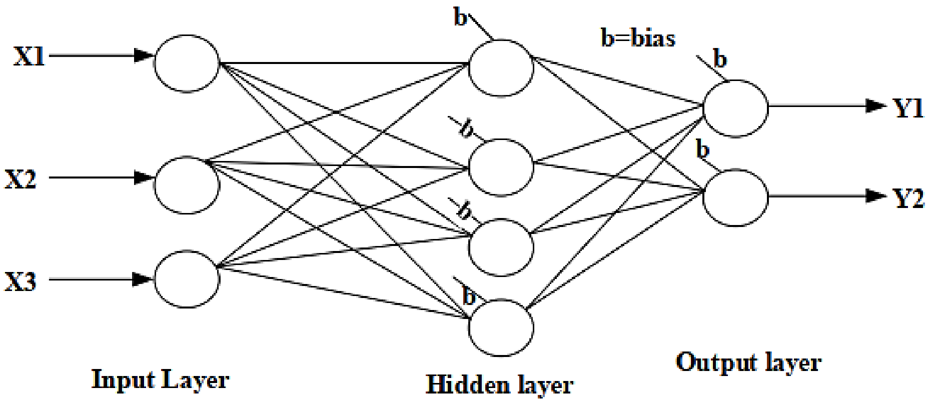

Figure 3.15: Three-layer feedforward neural network [49]

3.11.2. Feedback (Recurrent) Networks

This type of artificial neural network adds feedback connections to the network (the outputs are feedback into the inputs.

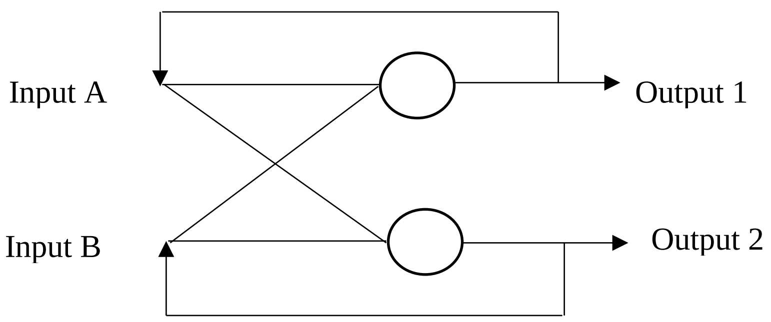

Figure 3.16: Feedback (recurrent) networks [49].

The multilayer feed-forward algorithm is mainly used for supervised learning of ANN because of its good learning capacity. In backpropagation, training data is used to adjust the weight of ANN and by using this corrected weight ANN is checked by testing this data. By performing the check on test data ANN memorized the training data and check for reliability of ANN. The training data needs to be carefully chosen to avoid computational complexity. Therefore, the data which is only capable of giving input-output relation. Training of the neural network continues until;

- The performance index reaches an acceptable low value
- The maximum iteration count (the number of epochs) has been exceeded
- The training time period has been exceeded

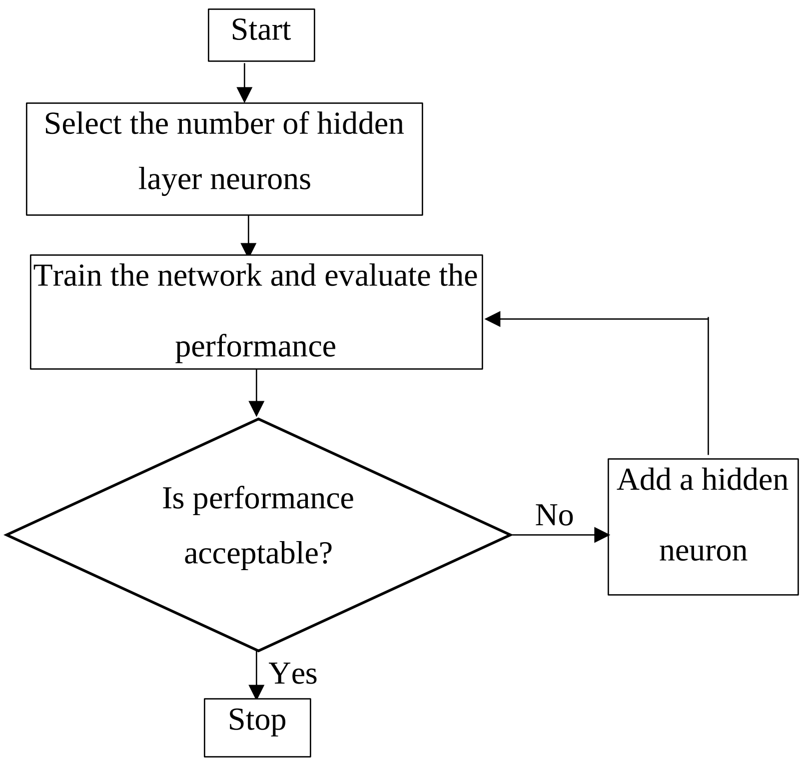

Figure 3.17: Flow chart of the neural network training

Figure 3.17 shows the flowchart of the proposed neural network training for the flux estimation of the induction motor.

To design and establish the network behavior a sigmoid function is used as an activation function. A sigmoid transfer function can introduce nonlinearity in the model and/or make sure that certain signals remain within a specified range. Figure 3.18 shows the final neural network structure used in this thesis work. There are four input and one output for training the neural network. This inputs and output are taken from the voltage model and current model equation.

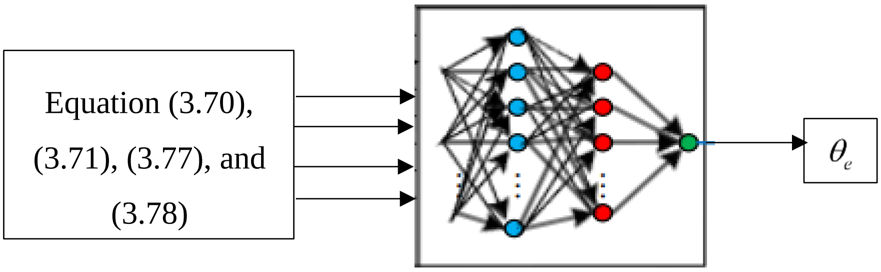

Figure 3.18:Neural network structure used in this thesis

An artificial neural network is composed of simple elements operating in parallel. These systems were inspired by biological nervous systems. Training of a neural network to perform a particular function by adjusting the value of the connections (weight) between elements.

In this system the input layer, which is not neural, has 3 nodes; input layers, hidden layer, and output layer. The activation functions used in the hidden layer and output layer are tan sigmoid and pure linear respectively. Levenberg-Marquardt backpropagation is used to train the network by MATLAB function Trainlm, which updates the ANN weight and bias values. The network is trained by supervised learning using flux from the voltage model and current from the current model equation as a teacher. The MATLAB code was written in Appendix c for training the network . when the training is finished, the SIMULINK model of the ANN controller is generated using the MATLAB genism command.

The procedure to create and train a network using the toolbox is as follows:

1. Inputs and target outputs are generated and loaded to the workspace in MATLAB.
2. A four layer back propagation network created in the MATLAB/script
3. Trainlim and Tansig were chosen as training and transfer function, respectively.
4. Input and target vectors were introduced to the created network.
5. Training parameters such as the epochs and error goal were adjusted.
6. The specified network was trained gradually. This process is finished when the defined error was reached. During the training, weights and biases of the network were iteratively adjusted to minimize the network performance function.

7. Finally, after training the network, the Simulink block is generated.

After executing the MATLAB code, several performance measurements of the trained network are available. Figure 3.19 shows the validation of the mean squared error and its value. At the training epoch of 1000 the mean squared error is 0.00061617.

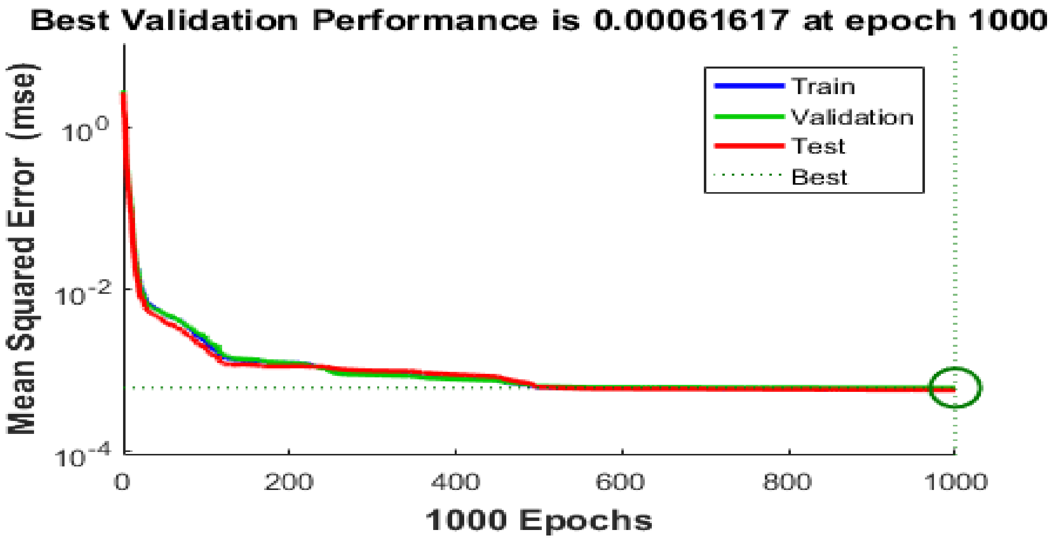

Figure 3.19:Validation of the mean squared error

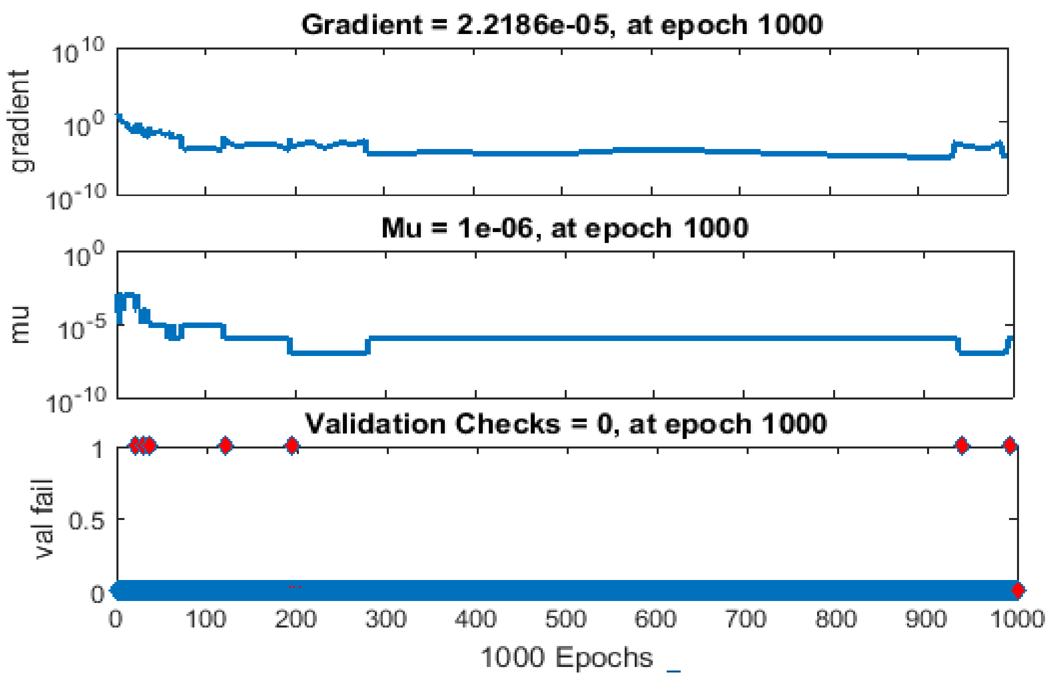

Figure 3.20: Gradient and validation vs epochs result

The regression plots also display the network outputs with respect to targets for training, validation, and test sets as shown below in Figure 3.21. For a perfect fit, the data should fall along a 45-degree line, where the network outputs are adequate to the targets. In this work, the neural network has been retrained many times to have the perfect fit for its output and target. This is done by changing the hidden layers and their neurons. This change updates every time the weights and biases of the network, and it produce an improved network after retraining. For this work, the fit is perfect for all data sets, with R values in each case is 1.

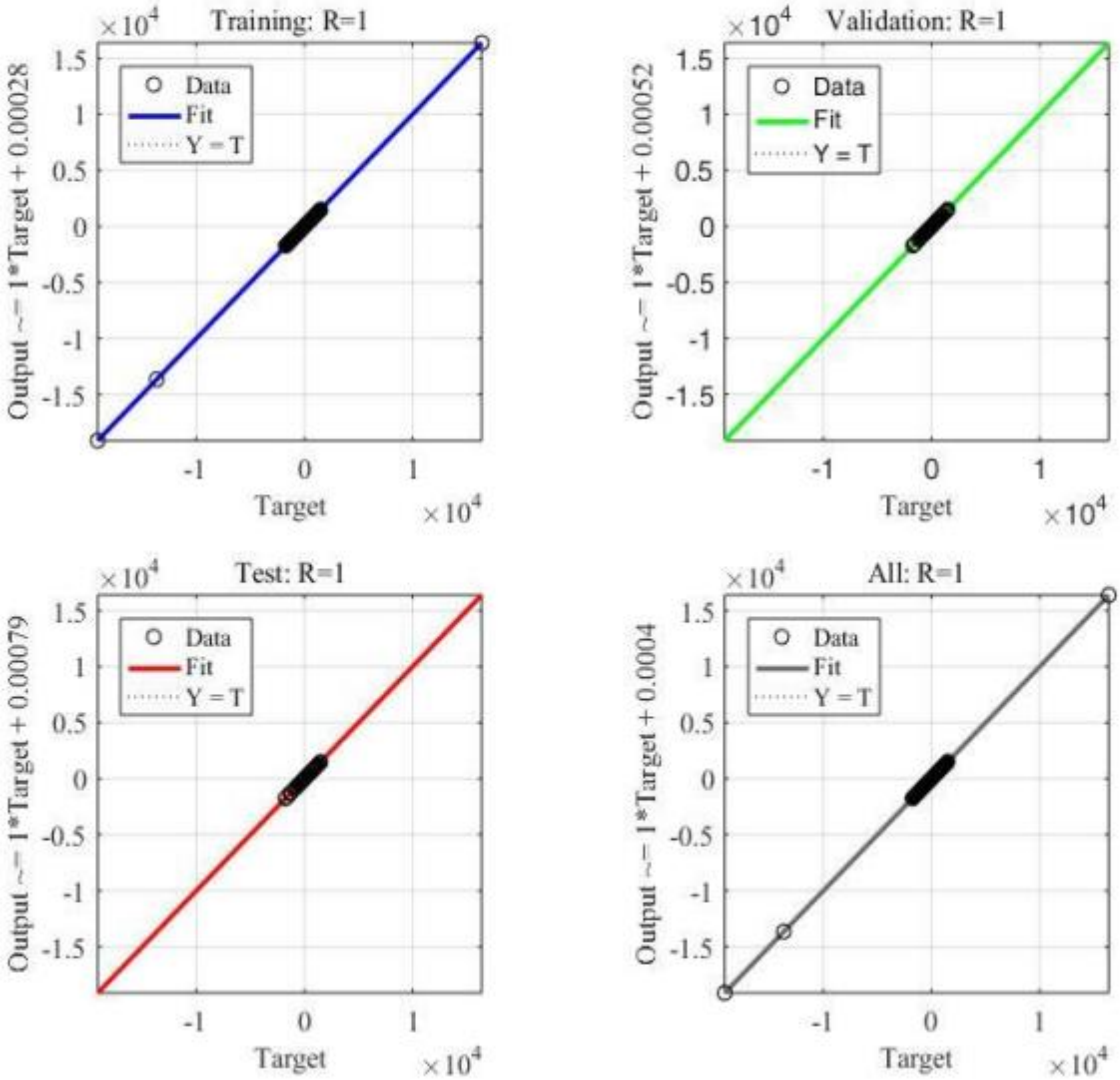

Figure 3.21: Regression plots of the training, validation, and test sets

After training of the network, the following Simulink block in Figure 3.22 is generated. It includes the input and output of trained data, the structure of the network, the weights, and the biases of each layer and neurons.

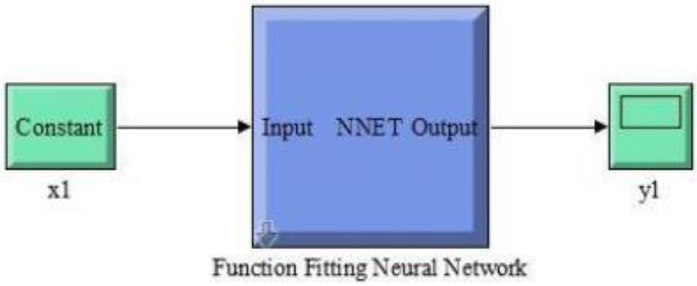

Figure 3.22: The Simulink block of the trained neural network structure

3.12. Design of PI and Fuzzy Logic Speed Controller of Induction Motor

Induction motors do not run at synchronous speed; they are generally fixed-speed motors. In industries, mechanical loads should not only be driven at a constant speed but should also be driven at the desired speed by varying the speed of the motor. Therefore, the need for the speed control methods for the induction motor arises. There is different kind of speed control methods are used for an induction motor, in this thesis the PI and fuzzy logic controllers are used for speed control of indirect vector control of an induction motor.

3.12.1. PI Speed Controller of Induction Motor

The conventional PI controller remains the most popular design approach used in industrial applications due to its simplicity and reliability for the control of first and second-order plants and even high order plants with well-defined conditions. A well-tuned PI controller is capable of achieving an excellent performance [50, 51].

However, it suffers a crucial disadvantage of getting a poor performance whenever the plant is subjected to some kind of disturbance or, the plant has a high order nonlinear structure. Figure 3.23 shows the simplified block diagram of the speed control of induction motor using a PI controller.

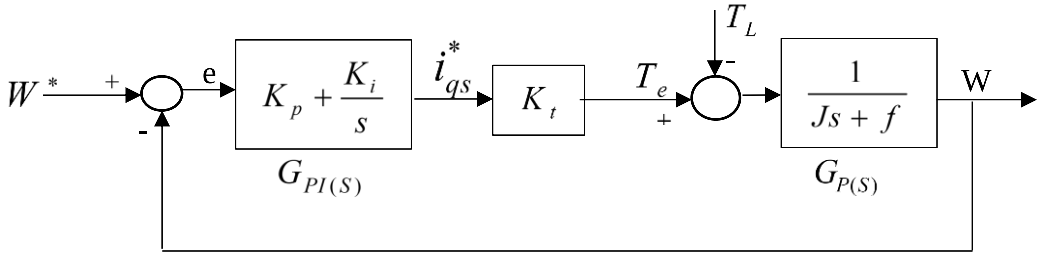

Figure 3.23: Model of Speed PI Controller block diagram

Where W^* is the reference rotor angular speed, W is the rotor angular speed, $e = W^* - W$ is the tracking speed error, K_P is the proportional gain of speed, K_i is the integral gain, f is the total damping coefficient, T_L is load torque, K_t denotes torque constant, T_e denotes the electromagnetic torque. From Figure 3.23.

$$T_e = K_t i_{qs}^* \tag{3.90}$$

$$i_{qs}^* = \frac{2}{3} * \frac{2}{p} * \frac{L_r}{L_m} * \frac{T_e}{\varphi_r} \tag{3.91}$$

$$\phi_r = L_m i_{ds} \tag{3.92}$$

From Equations (3.90-3.92) K_t is given by:

$$K_t = \left(\frac{3pL_m^2}{4L_r} \right) i_{ds}^* \tag{3.93}$$

The parameters K_P and K_i of the continuous controller are obtained by the following steps;
Step 1: calculate the open-loop transfer function of the plant.
Step 2: obtain the controller parameters from the closed-loop transfer function.

1. the open-loop transfer function of the plant as can be seen in Figure 3.23 for zero load torque is given by:

$$Go(s) = G_{PI}(s) \times G_P(s) = K_t \left(\frac{sK_P + K_i}{Js^s + sf} \right) \tag{3.94}$$

2. Now, the closed-loop transfer function for a unity feedback system is given by:

$$G_C(s) = \frac{G_O(s)}{1 + H(s)G_O(s)} = \frac{\frac{K_t}{J}\left(sK_p + K_i\right)}{s^2 + \left(\frac{f + K_t K_p}{J}\right)s + \frac{K_t K_i}{J}} \tag{3.95}$$

Comparing the second-order characteristic equation of the closed-loop transfer function for speed with the standard second-order characteristic equation $S^2 + 2\xi\omega_n s + \omega_n^2$, where ω_n^2 is the un damped natural frequency and ξ is damping ratio, the P-I speed controller gain obtained by.

$$s^2 + \left(\frac{f + K_t K_p}{J}\right)s + \frac{K_t K_i}{J} = s^2 + 2\xi\omega_n s + \omega_n^2 \tag{3.96}$$

So, $\frac{K_t K_i}{J} = \omega_n^2$ or $K_i = \frac{J\omega_n^2}{K_t}$

Also, $\frac{f + K_t K_p}{J} = 2\xi\omega_n$ or $K_p = \frac{2J\xi\omega_n - f}{K_t}$

To obtain a fast response the system should be critically damped and stable, where, $\xi = 1$. The rotor speed and current controller are each controlled by a separate PI module. $K_p(1 + \frac{1}{T_i s})$ is the PI controller; where K_p -proportional gain, $\frac{K_p}{T_i}$ is integral gain, τ= T_i= L/R=time constant-integral action time. Where, $R = R_s + R_r$ and $L = L_s + L_r$

3.12.2 Current Controller Gain Design

As can be given on Equation (3.19), the d-axis and q-axis current for the induction motor model becomes:

$$\frac{di_{ds}}{dt} = -R_1 i_{ds} + w_e i_{qs} + R_2\varphi_{dr} + \frac{v_{ds}}{\sigma L_s} \tag{3.97}$$

$$\frac{di_{qs}}{dt} = -R_1 i_{qs} - w_e i_{ds} + R_3 w_r \varphi_{qr} + \frac{v_{qs}}{\sigma L_s} \tag{3.98}$$

Where $w_e i_{qs} + R_2\varphi_{dr}$ and $-w_e i_{ds} + R_3 w_r \varphi_{qr}$ are the d and q-axis decoupling components. For linearity, these expressions are needed to be eliminated. φ_{qr} = 0. Also, the presence of the coupled terms makes the system nonlinear. So, to make the system linear it to replace these nonlinear coupled terms by $v_d decopule$ and $v_q decopule$ [52]. So, the state-space equations of the induction motor drive for the electrical subsystems, from Equations (3.97) and (3.98) can be represented as:

$$\frac{di_{ds}}{dt} = -R_1 i_{ds} + \frac{v_{ds}}{\sigma L_s} + v_d decopule \tag{3.99}$$

$$\frac{di_{qs}}{dt} = -R_1 i_{qs} + \frac{v_{qs}}{\sigma L_s} + v_q decopule \tag{3.100}$$

To achieve linear control of stator voltage it's necessary to remove the decoupling terms. These terms can be a disturbance and are canceled by using a decoupled method that utilizes nonlinear feedback of the coupling voltage. The transfer function for the d-q current controllers of the vector-controlled induction motor drives after removing the decouple term is given as follows.

$$G(s)_{d\_PI} = \frac{i_{ds}(s)}{v_{ds}(s)} = \frac{\frac{1}{\sigma L_s}}{s + R_1} \tag{3.101}$$

$$G(s)_{q\_PI} = \frac{i_{qs}(s)}{v_{qs}(s)} = \frac{\frac{1}{\sigma L_s}}{s + R_1} \tag{3.102}$$

Figure 3.24 shows the simplified block diagram of the current control of induction motor using a PI current controller.

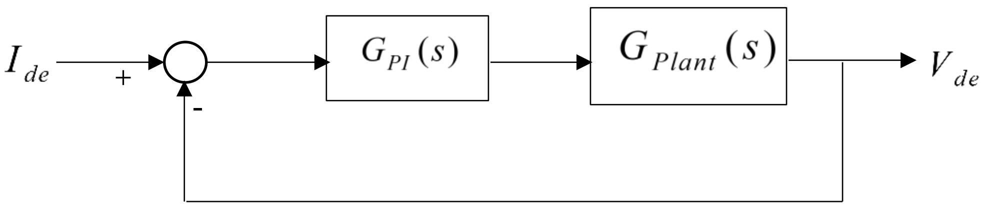

a) d-axis current control

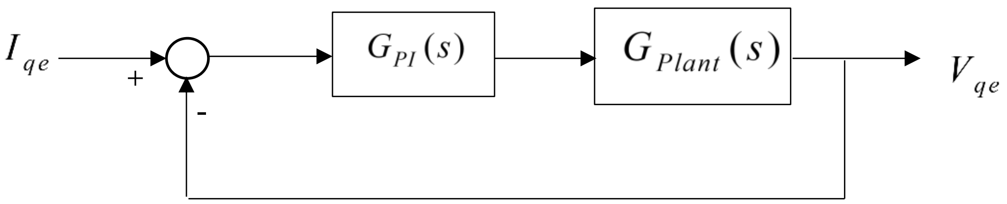

b) q-axis current control

Figure 3.24: closed-loop diagram of dq-axis current control

By using SISO Tools methods of automatic tuning system, proportional and integral constants for current controllers are determined and given in Table 3.5.

```
%.... speed controller by sisotool methods just to determine Kp and Ki...%
a=0.707;
Ls=0.00439
R1=447.19
num=[1/(a*Ls)]; % num=numerator
den = [1 R1]; % den=denominator
current=tf(num,den)
sisotool(current)
```

Parameter determination of the controller gain and the PM and GM values are shown in Figure 3.25. From the control and estimation parameter, the Ki and Kp value is

$$K_i = 265.09 \text{ and } \frac{K_p}{K_i} = 0.00051 \rightarrow K_p = K_i * 0.00051$$

Therefore $K_p = 265.09 * 0.00051 = 0.135$

The speed PI gains are calculated from the Equation (3.96).

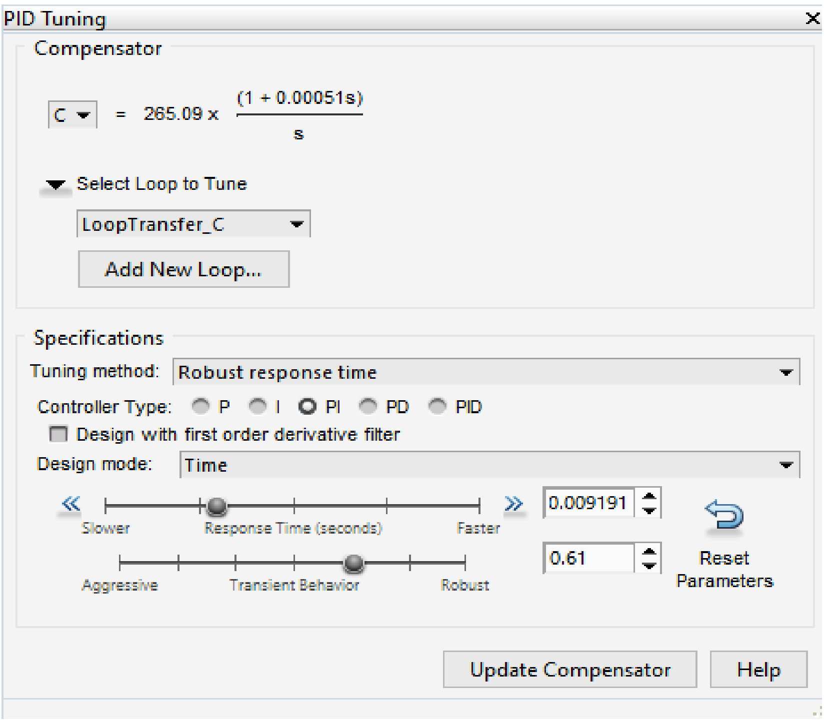

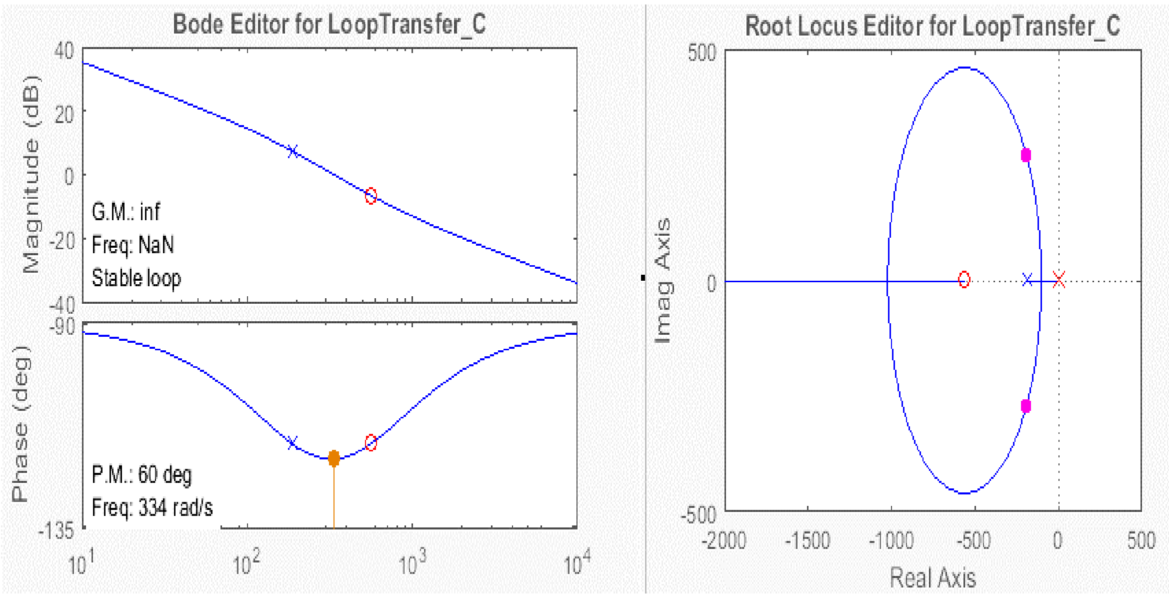

Figure 3.25: Kp and KI value from sisotool and PM and GM values

Table 3.5: Proportional (K_p) and Integral (K_i) Gains for PI Controller

PI controller	K_p	K_i
Speed control loop	2	563
Inner $d_e - q_e$ current loops	0.135	265.09

3.12.3. Fuzzy Logic Speed Controller of Induction Motor

Fuzzy logic, FL, is one class of artificial intelligence. Its goal is to plant human intelligence in a system so that the system can think intelligently like a human being. Fuzzy logic techniques have been recognized in recent years as powerful tools for dealing with the modeling and control of complex systems for which no easy mathematical descriptions can be provided [53].

Fuzzy logic control is considered as a linguistic control strategy based on the use of the If-then statement for the control process. In this statement, several variables that are expressed in words rather than numbers such as positive, zero, and negative could be used either in the antecedent (the if-part of the statement) or in the consequent (the then-part of the statement). As a result, the mathematical model of the system is not desired in fuzzy control so it can be applied to nonlinear systems [54].

3.12.3.1. Membership Functions

A membership function is a curve, often given the designation of μ (degree of membership)**,** which defines how the input space is mapped to a degree of certainty between 0 and 1. The function itself can be an arbitrary curve whose shape is defined as a function of a suitable behavior to assure simplicity, convenience, and efficiency. It is important to notice that the degree of membership plays an important role in designing a fuzzy controller [55]. A fuzzy set is an extension of a classical set. If X is the universe of discourse and its elements are denoted by x, then a fuzzy set A in X is defined as a set of ordered pairs as $A = \{x, \mu A(x)/x \varepsilon X\}$, where $\mu A(x)$ is called the membership function of x in A. The membership function maps each element of X to a membership value between 0 and 1 [56]. Membership functions are built from several basic functions such as;

- Piecewise linear functions
- Gaussian distribution function
- Sigmoid curve
- Quadratic and cubic polynomial curves
- Triangular
- Trapezoidal

In this thesis, the triangular and trapezoidal membership functions are used to define the degree of membership. Each input variable are assigned seven linguistic fuzzy subsets varying from negative large (NL) to positive large (PL) and the output variables are assigned eleven linguistic fuzzy subsets varying from negative large (NL) to positive large (PL).

3.12.3.2. Fuzzy System Structure

The basic structure of the fuzzy logic controller system consists of four main parts as shown in Figure 3.26, which can be illustrated as following [57].

Knowledgebase: The Knowledgebase is composed of a database and a rule base. The database consists of input and output membership functions that provide information for appropriate fuzzification and defuzzification operations. The rule base contains a set of linguistic rules that provide information for the inference engine.

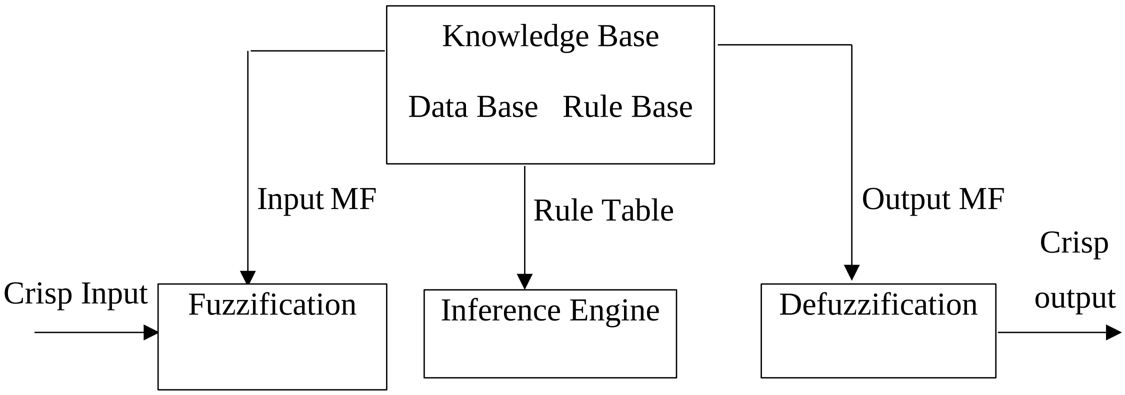

Figure 3.26: Basic structure of the fuzzy logic controller.

Fuzzification: Fuzzification is the process in which the crisp input value is converted into a fuzzy number by using the input membership function.

Inference Engine: The fuzzy inference engine is the process that relates input fuzzy sets to output fuzzy sets using if-then rules and fuzzy operators to drive a reasonable output fuzzy value. There are several inference systems like Mamdani, Lusing Larson, and Sugeno.

Defuzzification: Defuzzification converts the fuzzified output value to a crisp control value using the output membership function. The most famous defuzzification methods are the center of the area, Height, Mean of maxima, and Sugeno.

3.12.3.3. Fuzzy Reasoning

Fuzzy Operators: The fuzzy logical reasoning is based on a superset of standard Boolean logic, which involves operators such as the fuzzy intersection or conjunction (AND), fuzzy union, or disjunction (OR), and fuzzy complement (NOT). The classical operators for these functions are: AND = min, OR = max, and NOT = complement. The intersection of two fuzzy sets A and B is represented in general by a binary mapping T, which aggregates two membership functions as follows:

$$\mu_{A\cap B}(x) = T\left(\mu_A(x), \mu_B(x)\right) \tag{3.103}$$

In general, the fuzzy union operator is specified by a binary mapping S:

$$\mu_{A\cap B}(x) = S\left(\mu_A(x), \mu_B(x)\right) \tag{3.104}$$

If-Then Rules: Fuzzy logic is predicated on rules of the form 'IF…. THEN....' that convert an input fuzzy set to an output fuzzy set. A single fuzzy if-then rule assumes the form of, if x is A then y is B, where A and B are linguistic values defined by fuzzy sets on the ranges (universe of discourse) X and Y, respectively. The if-part of the "x is A" is termed the antecedent or premise, while the then-part of the rule "y is B" is called the consequent or conclusion. In general, one rule alone is not effective. Two or more rules may be needed in the inference process. The output fuzzy sets for each rule aggregated into a single output fuzzy set. Finally, the resulting set is defuzzified or resolved to a single number [58].

Fuzzy Inference Systems: Fuzzy inference is the process of mapping from a given input space (*A*, *B*) to an out space (*R*) based on "IF A, THEN B" rules. The techniques used for obtaining the output space are known as fuzzy implication operations they are valid for all values of $x \in X$ and $y \in Y$. The mapping provides a basics form which decision can be made, or pattern discerned. Although several forms of implication operators exit the Mamdani's form is one used most commonly [53]. This operator is equivalent to the fuzzy cross product of fuzzy sets A and B and is expressed as:

$$\mu_R(x,y) = \min\left[\left(\mu_A(x), \mu_B(y)\right)\right] \tag{3.105}$$

3.12.3.4. Fuzzy Logic Principle

The fuzzy controller block diagram is shown in Figure 3.27. There are two input signals to the fuzzy controller, the error signal E, and the derivative of error which represents the change in error signal CE. The controller output is a U signal. The controller observes the loop error signal and correspondingly changes the output U so that the actual output signal matches the reference or commanded signal.

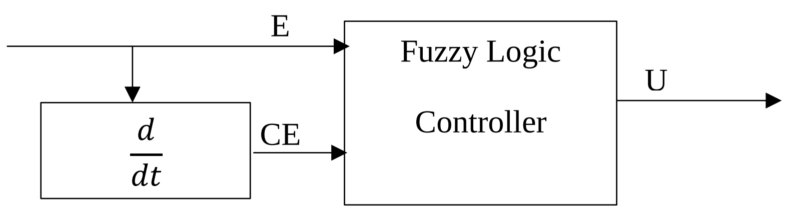

Figure 3.27: Fuzzy control system.

The design of the fuzzy system requires the choice of fuzzy sets and membership functions. The proposed fuzzy sets (linguistic variables) are defined as follow:

NL =	Negative Large	PS =	Positive Small
NML=	Negative Medium Large	PMS=	Positive Medium Small
NM=	Negative Medium	PM=	positive Medium
NMS=	Negative Medium Small	PML=	Positive Medium Large
NS=	Negative Small	PL=	Positive Large
ZE=	Zero		

There are seven membership functions for both error E and change in error CE, and eleven membership functions for output U as shown in Figure 3.28. All membership functions should be chosen such that they cover the whole universe of discourse. To achieve the final control, the inputs membership functions are triangular at the middle and trapezoidal at the end of two regions to the faster response of the system.

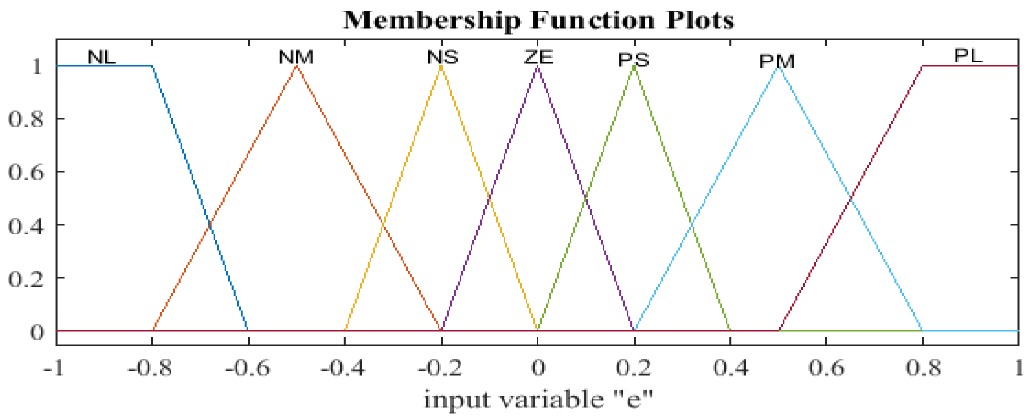

(a)

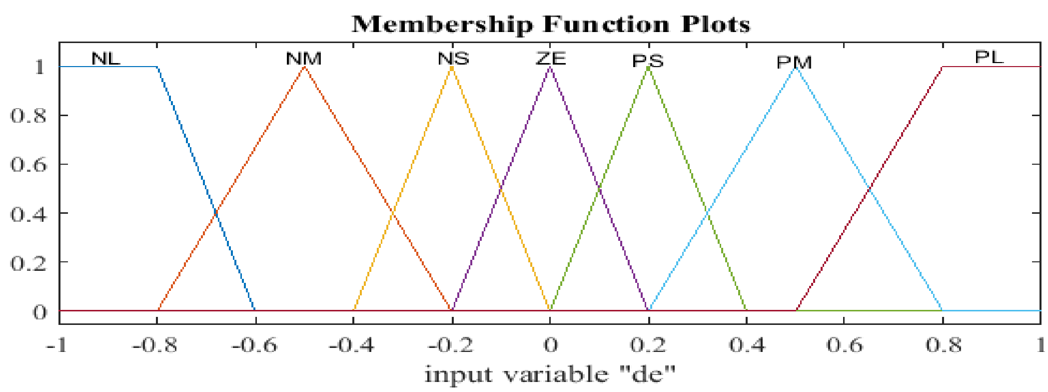

(b)

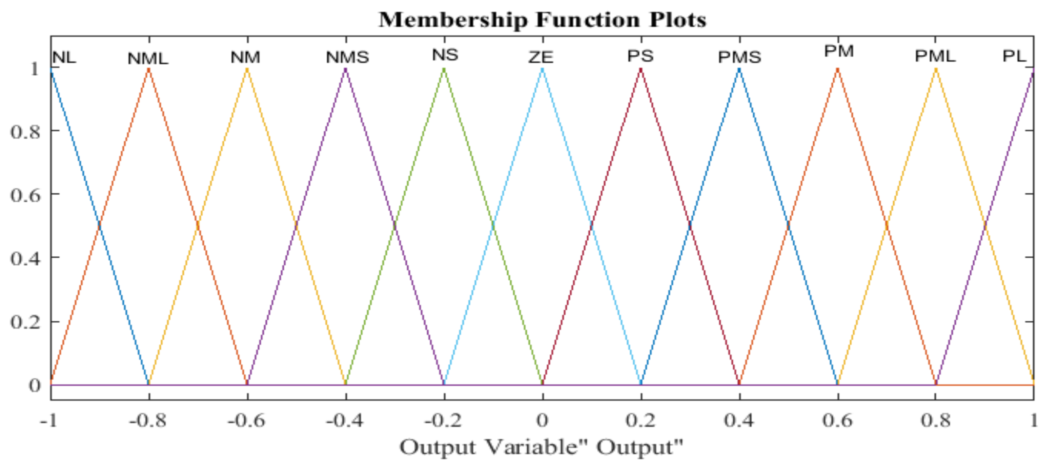

(c)

Figure 3.28: Membership functions for fuzzy speed controller (a) Error, (b) change in error, (c) Output control signal.

The most important step in a fuzzy system is the design of the rule base. It consists of a number of fuzzy IF-THEN rules that define the behavior of the system. Table 3.6 shows the corresponding rule table for the proposed fuzzy control system. The top row of the matrix indicates the fuzzy sets of the error variable E and the left column indicates the change in error variable CE and the output variable U is shown in the body of the matrix.

Table 3.6: Fuzzy rule base table to control the speed of the induction motor.

CE\E	NL	NM	NS	ZE	PS	PM	PL
NL	NL	NL	NML	NM	NMS	NS	ZE
NM	NL	NML	NM	NMS	NS	ZE	PS
NS	NML	NM	NMS	NS	ZE	PS	PMS
ZE	NM	NMS	NS	ZE	PS	PMS	PM
PS	NMS	NS	ZE	PS	PMS	PM	PML
PM	NS	ZE	PS	PMS	PM	PML	PL
PL	ZE	PS	PMS	PM	PML	PL	PL

The controller gives the decision according to rule base for fuzzy logic controller given in Table 3.6. The surface viewer and fuzzy rule output is given in Figure 3.29 and Figure 3.30. respectively.

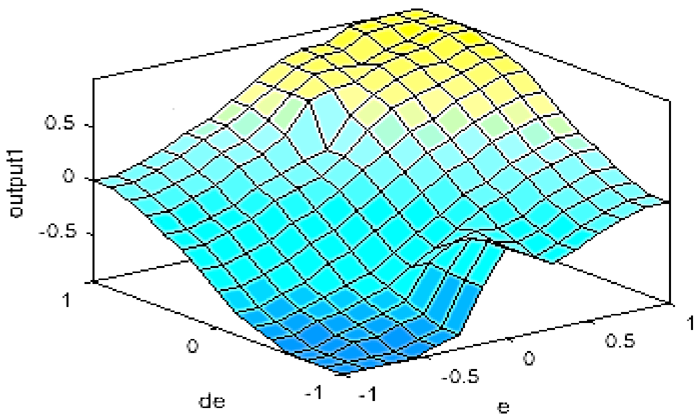

Figure 3.29: Surface viewer of the fuzzy logic design

The surface viewer is used to display the dependency of the output on any one or two of the inputs. It generates and plots an output surface map for the system. The output is presented by a 3D surface model. Upon opening the Surface Viewer, there are a three-dimensional curve that represents the mapping from the error signal e, and the derivative of error which represents the change in error signal de to controller output signal. Because this curve represents a two-input one-output case, it's possible to see the entire mapping in one plot.

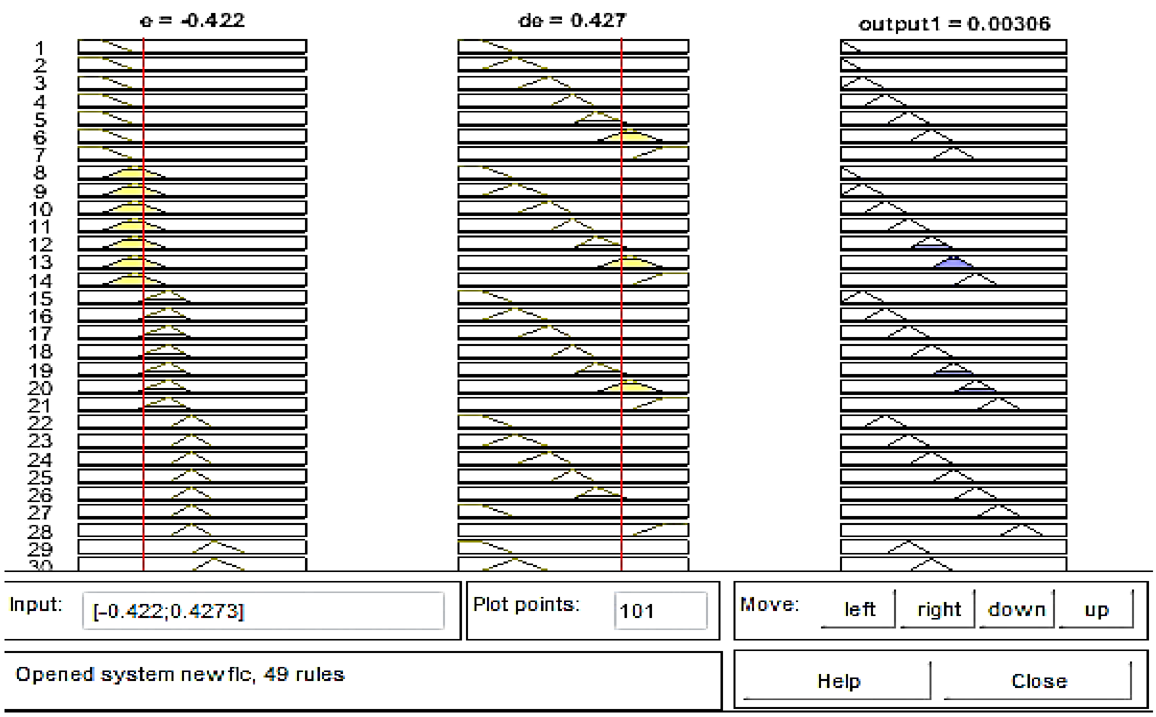

Figure 3.30: Rule Viewer of the fuzzy logic design

The Rule Viewer express the rule written in the Table 3.6 that indicates the fuzzy sets of the error variable E and the change in error variable CE and the output variable U. The rule viewer allows us to express the entire fuzzy inference process at once because it plots every part of every rule. Each rule is a row of plots, and each column presents the input-output signals. So, the first column of plots shows the membership functions references by the antecedent, or if-part, of each rule. The second column of plots shows the membership functions references by the consequent, or then- part of each rule. There is a line across the input signal plots by using those lines it’s possible to move left and right by clicking and dragging with the mouse. This line changes the input value. When the line release, a new calculation is performed. Finally, the aggregation occurs down the third column, and the resultant aggregate plot is shown in the single plot to be found in the lower right corner of the plot field. Due to the large number of rules used in this thesis the figure shows the rule up 30 number of rules only the result of the aggregated plot is not shown.

CHAPTER 4

RESULTS AND DISCUSSIONS

This chapter includes the result and analysis of the proposed sensorless speed control of the three-phase induction motor drive. The simulation results of the proposed system work to fulfill the specific objectives of the research. The MATLAB/Simulink model for the indirect field-oriented control, fuzzy logic controller, space vector modulation, flux and speed estimation, and open-loop speed estimation are shown in Figure.A.1, Figure A.2, Figure A.3, Figure A.4, and Figure A.5 respectively. The MATLAB code for space vector modulation and neural network are shown in Appendix B and Appendix C respectively.

4.1. Simulation Results

The simulation results of the proposed sensorless speed control of indirect field-oriented control of induction motor drive are discussed in terms of:

- Space vector pulse width modulation.
- Setpoint tracking capability.
- Accelerating and decelerating speed reference for ramp input induction motor.
- Step response of drive with speed reversal for step input induction motor.
- Comparison between voltage and current model flux estimation with an Artificial Neural Network flux estimation effect on the speed response.
- Compression between PI and fuzzy logic speed controller with no load and under load condition.

4.1.1. MATLAB Simulation Result of SVPWM

4.1.1.1 Switching Pattern of SVPWM

Figure 4.1 shows the equivalent switching pattern of space-vector modulation. The waveforms of Ta, Tb, and Tc are 120° apart from each other. The waveforms show that Tb lags to the waveform of Ta by 120° and Tc leads to the waveform of Ta by 120°. The SVPWM based on a carrier with reduced switching ratio is the better implementation of SVPWM because, when the switching ratio has reduced the heat generated in switches is also reduced at the same time which improves the lifetime of switches and the efficiency of the inverter. This pattern is compared with high- frequency carrier signal to produce a gating signal to switch on and off all six switches in the inverter in an appropriate sequence.

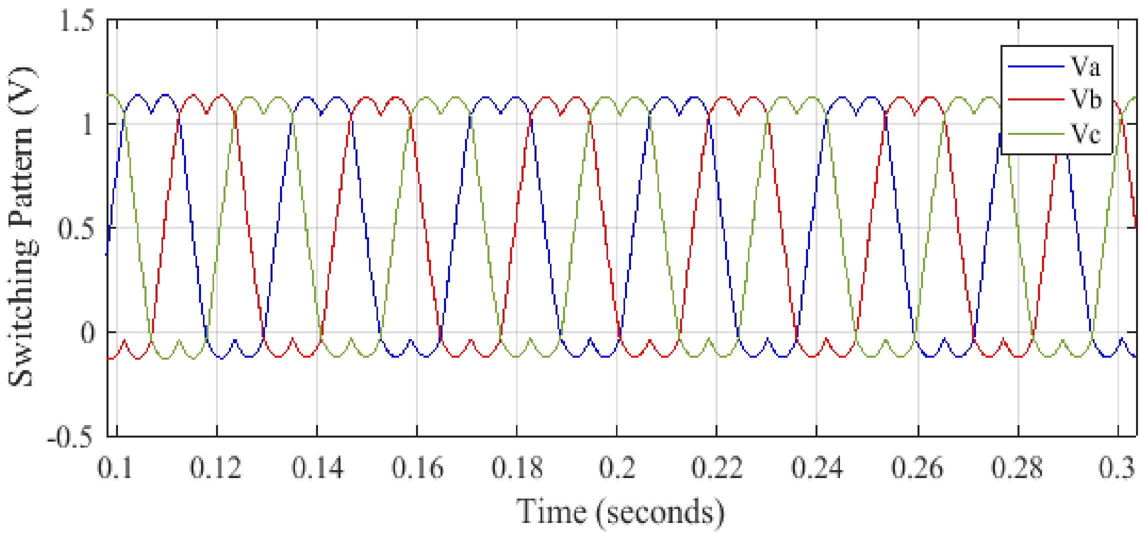

Figure 4.1: Voltage for three phases (PWM Duty cycles)

4.1.1.2. Generated Gate Signal

The generated output get signal based on the SVPWM techniques in order to switch the IGBT of the inverter to generate the required three-phase AC voltage to drive the induction motor is shown in the below Figure 4.2 to Figure 4.4 the signal that generated from the driver circuit is out of phase in one leg as shown in Figure 4.2, Figure 4.3, and Figure 4.4 in different color those pulses is out of phase in on leg because to prevent short circuit which is the cause for damage of the inverter. Therefore, the switches are on and off sequentially based on the pattern of sector vectors to generate three-phase sinusoidal waves.

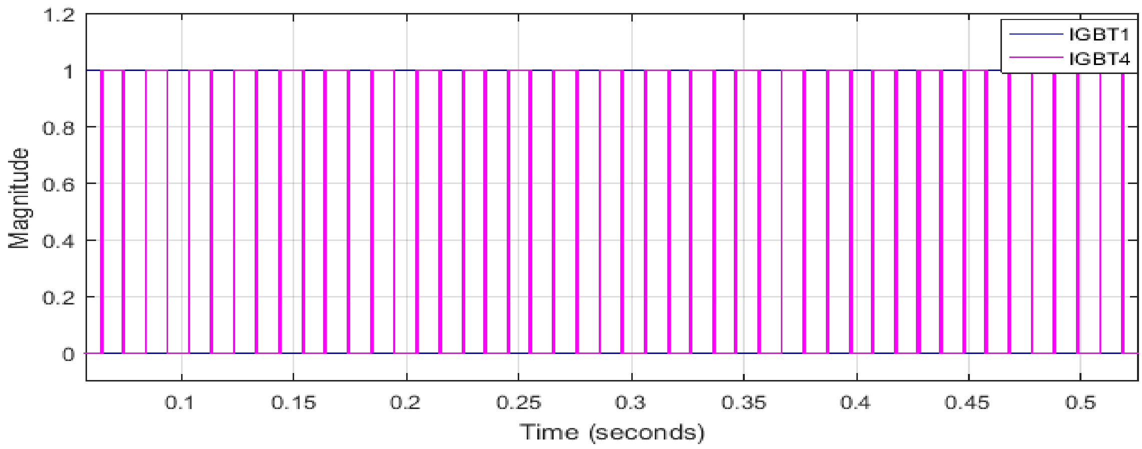

Figure 4.2: Gate signal for IGBT 1 and IGBT 4

As shown in Figure 4.2 the IGBT in the first leg is on and off at different time intervals to prevent short circuit damage.

Figure 4.3 shows the pulse generated from the driver circuit based on SVPWM for IGBT 3 and IGBT 6 of the second leg.

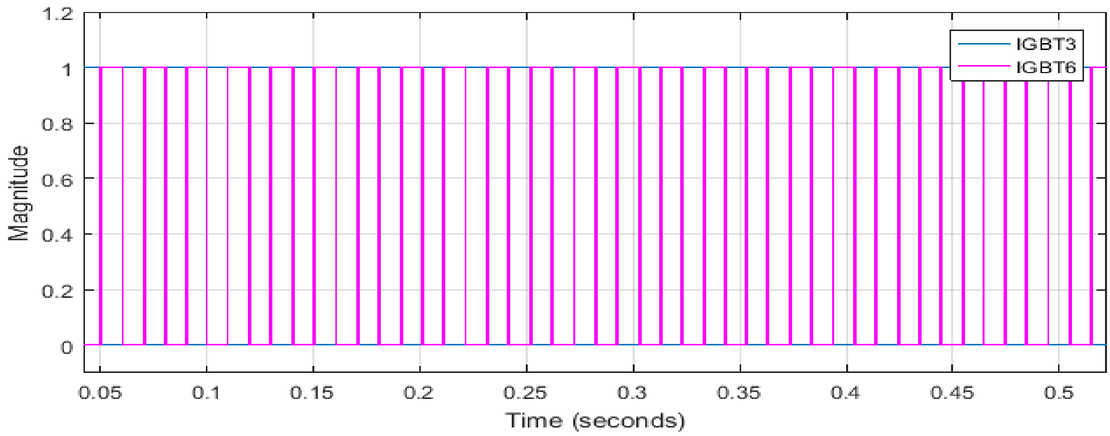

Figure 4. 3: Gate signal for IGBT 3 and IGBT 6.

Figure 4.4 shows the pulse generated from the driver circuit based on SVPWM for IGBT 5 and IGBT 2 of the third leg.

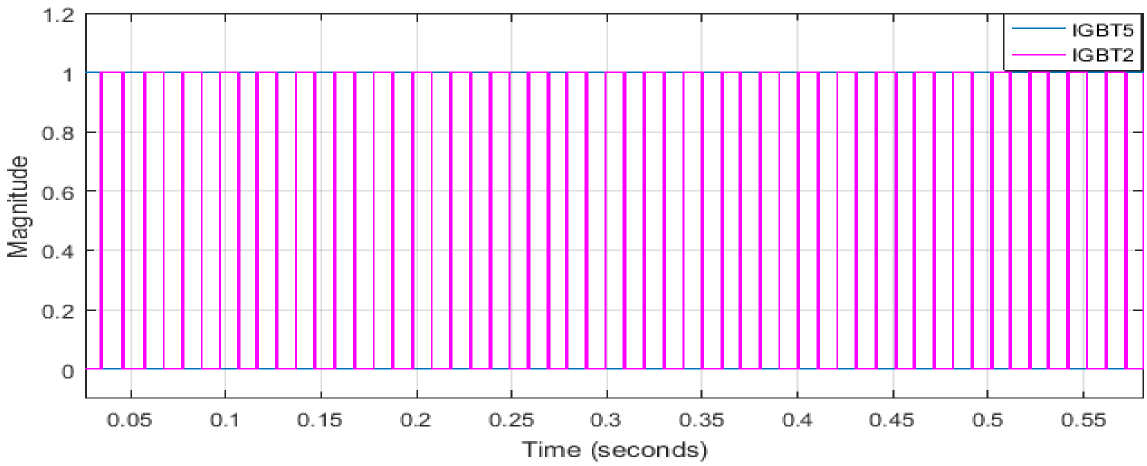

Figure 4. 4: Gate signal for IGBT 5 and IGBT 2

4.1.2. Set Point Tracking Capability

Figures 4.5 to 4-14 shows the simulation results of the sensorless speed control by IFOC that was developed using MATLAB/Simulink with the initial zero load torque condition.

4.1.2.1. Estimated Speed and Actual Fuzzy logic Speed Control for Constant Input Reference

It is always crucial to know the performance of an estimator based on the ability of the estimated speed to converge the actual speed value, especially during the transient response. This criterion has been well accepted as a primary indicator that the performance of a sensorless speed estimator that convergence of the estimated rotor speed to the actual speed.

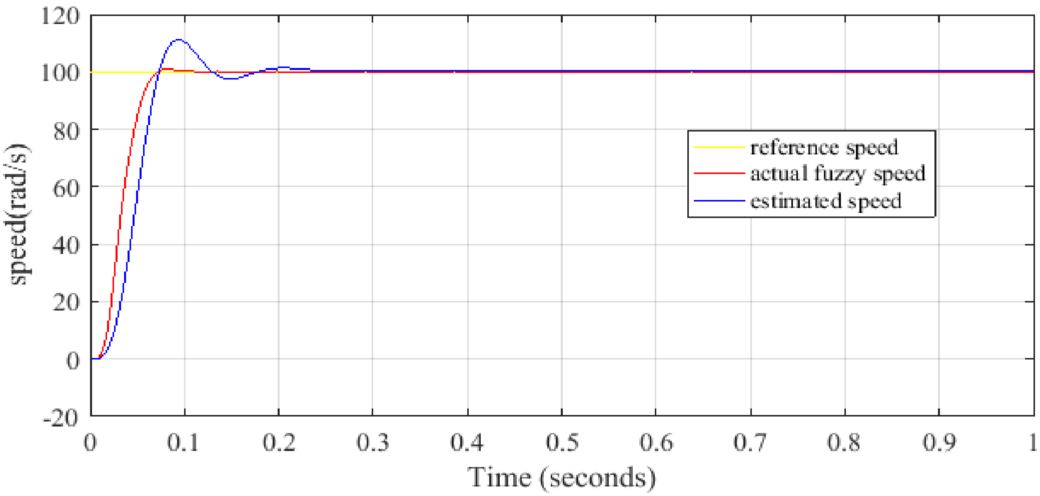

Figure 4. 5: actual speed and estimated speed Vs time.

Figure 4.5 shows the simulation results for an actual fuzzy logic speed controller is used in the outer loop for speed control, the PI controller is used in the inner loop for torque and flux control, and the estimated speed with reference speed at 100rad/sec. The actual fuzzy logic speed controller follows the reference signal and also the sensorless speed track the actual speed of the motor when the motor runs at the constant speed.

4.1.2.2. The Error Signal Between Actual and Estimated Speed

As can be seen from figure 4.6 shown below, the error signal between actual fuzzy Logic speed control and estimated speed is 0.2% which is tolerable. So, the actual speed tracks the reference speed with minimum and acceptable error.

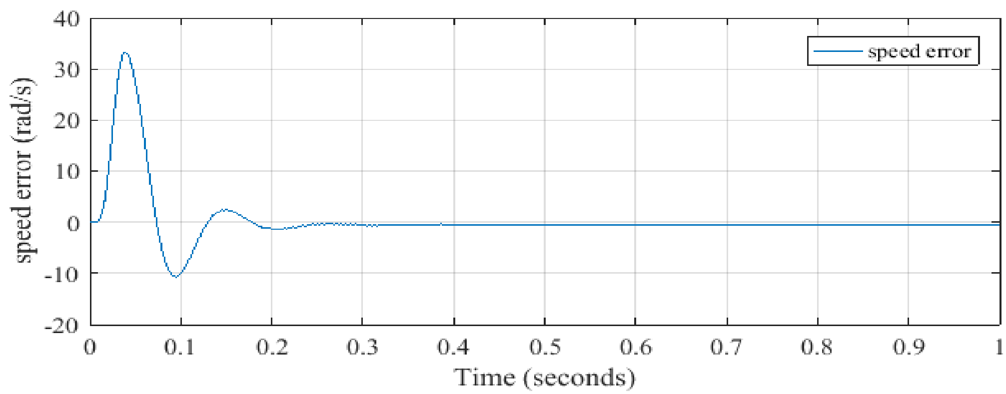

Figure 4. 6: Error signal between the actual and estimated speed in rad/sec vs. time

4.1.2.3. Estimated Rotor Flux

Figure 4.7 shows the estimated rotor flux angle in rad. The angle of rotor flux to the stationary frame d-axis is estimated with the proposed flux linkages in the rotating reference frame are found by using voltage and current flux estimation and then the rotor flux angle improved by using an artificial neural network.

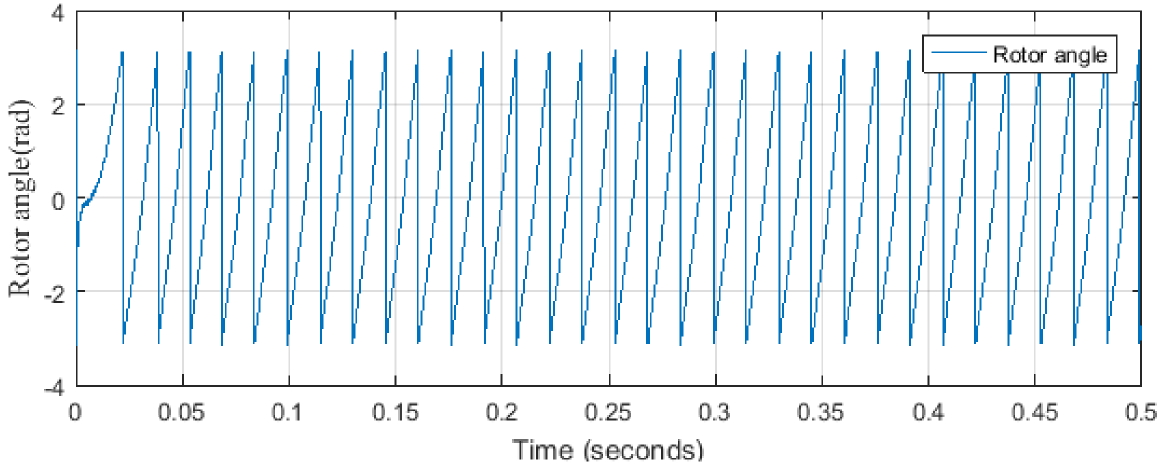

Figure 4. 7: estimated rotor flux angle vs time

The estimated rotor flux with a reference speed of 100 rad/sec is shown as in Figure 4.8. Both the dq-axis fluxes are 90-degree out of phase.

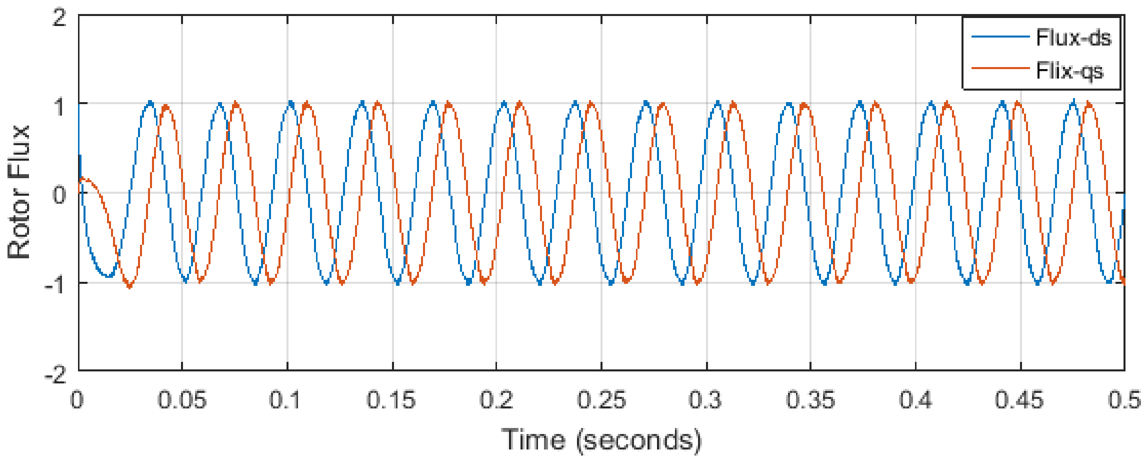

Figure 4. 8: estimated rotor flux in dq-axis reference frame vs time

4.1.2.4. The Three-phases Stator Current Waveform

The three-phase stator currents are generated by the three-phase voltage source inverter shown in Figure 4.9. This three-phase inverter is controlled by space vector pulse width modulation block for appropriate stator current generation. These three-phase currents should be the equal magnitude and 120° phase shift with each other for appropriate rotating flux generation. As shown in Figure 4.9, the appropriate stator phase current value is generated. Hence, the system can feed the appropriate stator voltage to the Induction Motor.

If the voltage applied to the motor is applied with appropriate magnitude and frequency, the speed of the motor is the track to the reference value.

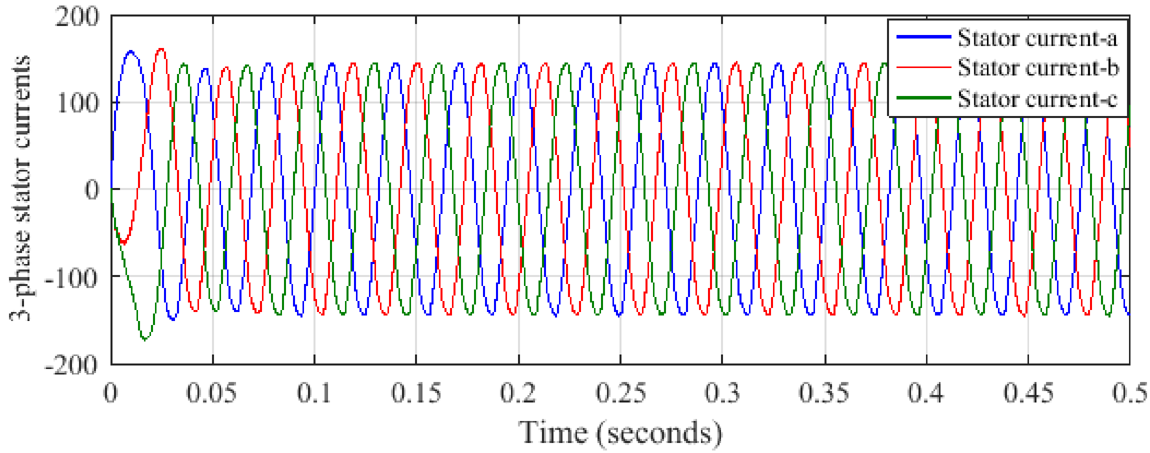

Figure 4. 9: Three-phase stator current vs. time at 100 rad/s.

4.1.2.5. Estimated Speed and Actual Fuzzy Logic Controller for Variable Input Reference

Using the same parameters of the induction motor, the tracking performance of the estimator can be examined by changing the speed of the system. As shown in Figure 4.10 the proposed estimator tracks the pulse with different speed reference inputs. This shows the tracking performance of the estimator and actual speed to the reference speed can be examined by changing the reference of the system.

A reference speed of 20rad/s was initially applied and increased to 60rad/s,100rad/s, and return to zero speed at t = 0.5 sec, t=1 sec, and at t=1.5second respectively. The simulation results are carried out for different reference speeds at no-load condition. As shown in Figure 4.10 the estimated and the actual fuzzy logic speed follow the reference speed with good accuracy.

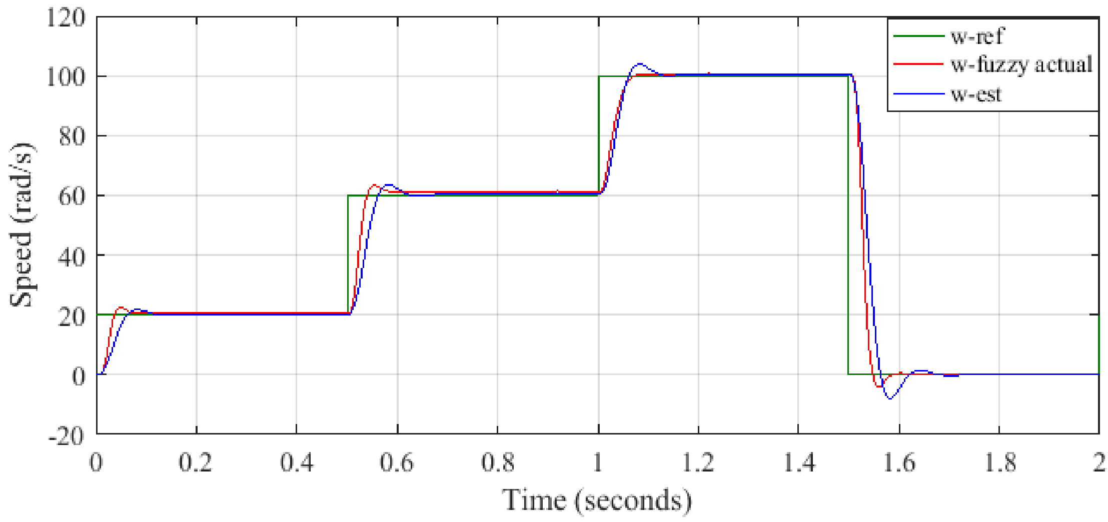

Figure 4. 10: Estimated Speed and actual Fuzzy Logic Controller speed tracking for variable input reference at no load

4.1.2.5. Estimated Rotor Flux Angle for Variable Input Reference

The Estimated rotor flux angle. When the speed is large/minimum the frequency of estimated rotor angle is large/minimum respectively.

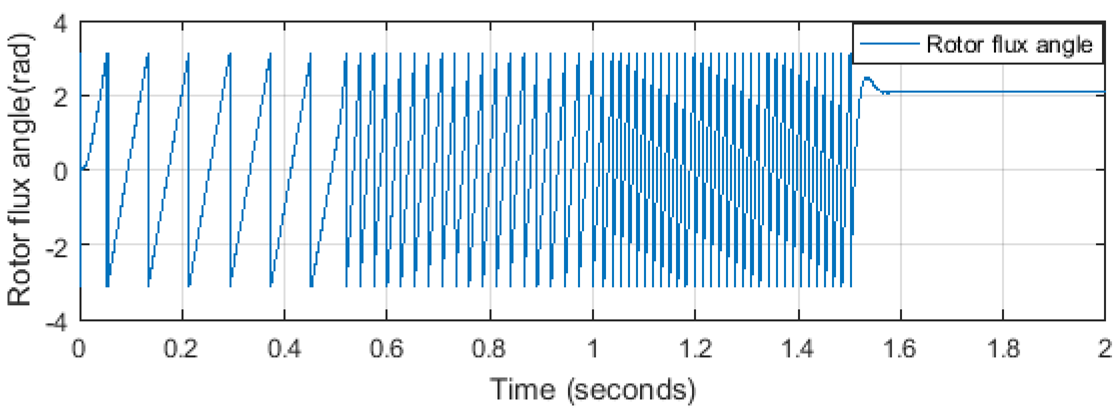

Figure 4. 11: Estimated Rotor flux angle

4.1.3. Decelerating Speed Reference for Induction Motor

Figure 4.12 shows the data reversal of speed response of the induction motor for decelerating the speed. The reference input signal is decelerating torque from 0.6 to 1.2 sec and constant between 0-0.6sec and 1.2-2sec. Data reversal refers to the decelerations of the motor from attained steady speed after a certain time and attained another steady state.

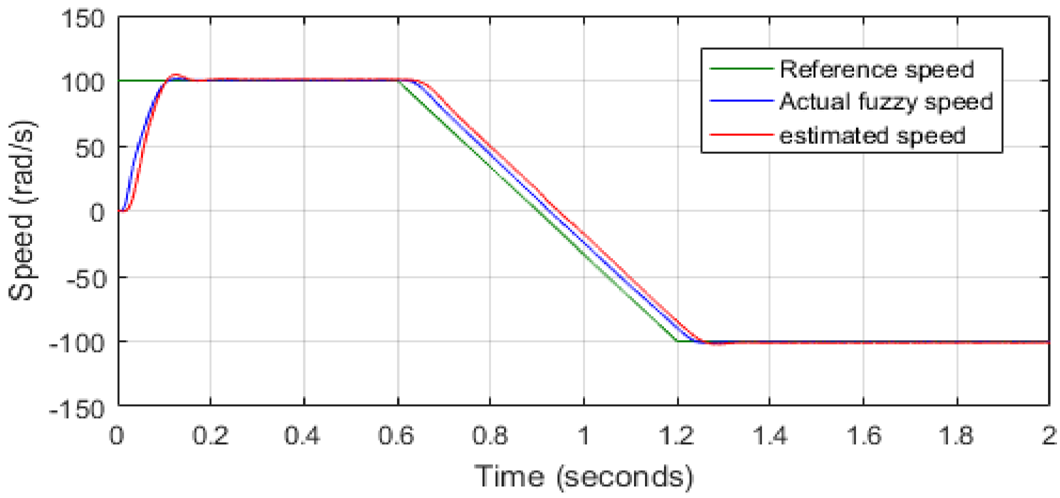

Figure 4. 12 Actual and estimated speed vs time of decelerating speed reference

Figure 4.13 shows 3-ϕ stator current response of the induction motor. When the speed is de-accelerated from 100rad/sec and attained a steady speed of -100rad/sec, the directions of current are changed or the three phases stator currents are reversed for the induction motor.

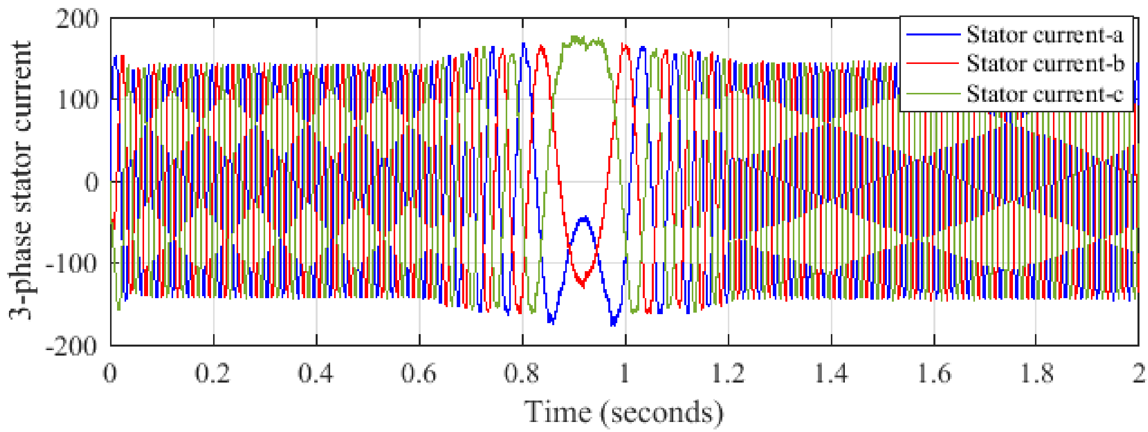

Figure 4.13: The three-phase stator currents for the decelerating reference speed

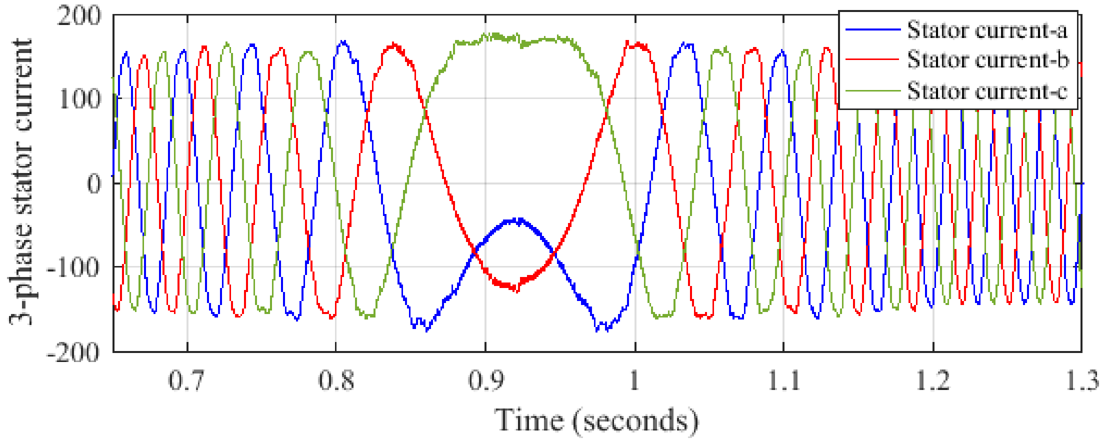

Figure 4. 14: Zoomed out part of 3-phase stator currents

Figure 4.15 shows the generated electromagnetic torque when the speed is decelerated, the torque values are negative at this stage the motor act as a generator.

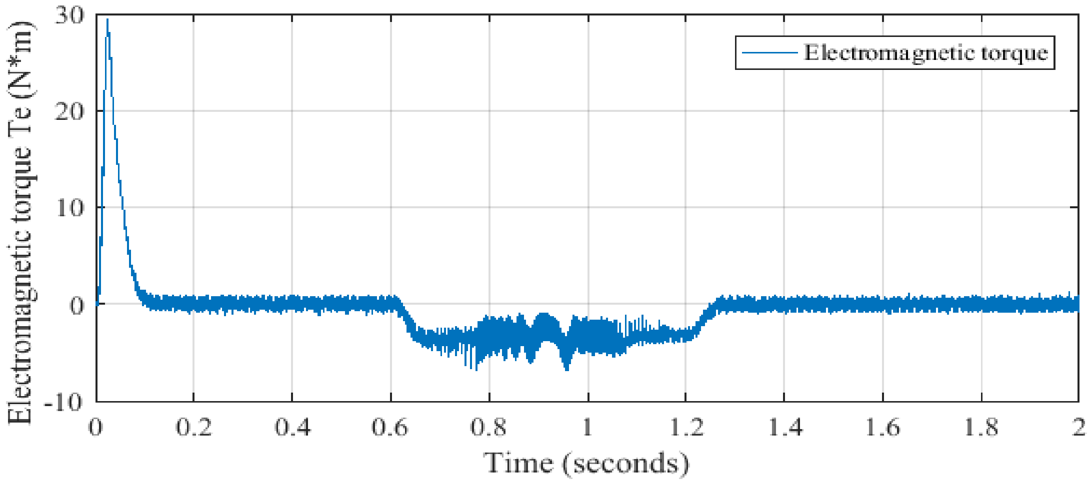

Figure 4. 15: Electromagnetic torque vs time

4.1.4. Step Response of Drive with Speed Reversal

The estimator is also working for a regenerative mode of operation for the step input reference. Motor speed is changed from +100 rad/s to -100rad/s. The drive is operated in motoring mode up to 0.5second. Thereafter, it enters in the regenerating mode of operation for 0.5 seconds (which is the total time of 1 sec) and comes back to the motoring region after 0.5 seconds. As shown in Figure 4.16 the estimate and the actual fuzzy logic controller speed follow the reference speed successfully with a certain transient response in the regenerative mode. When the motor enters the regenerative mode, the direction of the motor is reversed. Fig 4.17 shows 3-ϕ stator current response of the induction motor. the directions of current are changed or the three phases are reversed when the motor is entered into the regenerative mode of operation. Fig 4.19 is shown the estimated rotor flux angle. when the motor enters from motoring to regenerative mode of operation, the direction of the estimated rotor flux angle changes the direction from the clockwise to counter-clockwise direction.

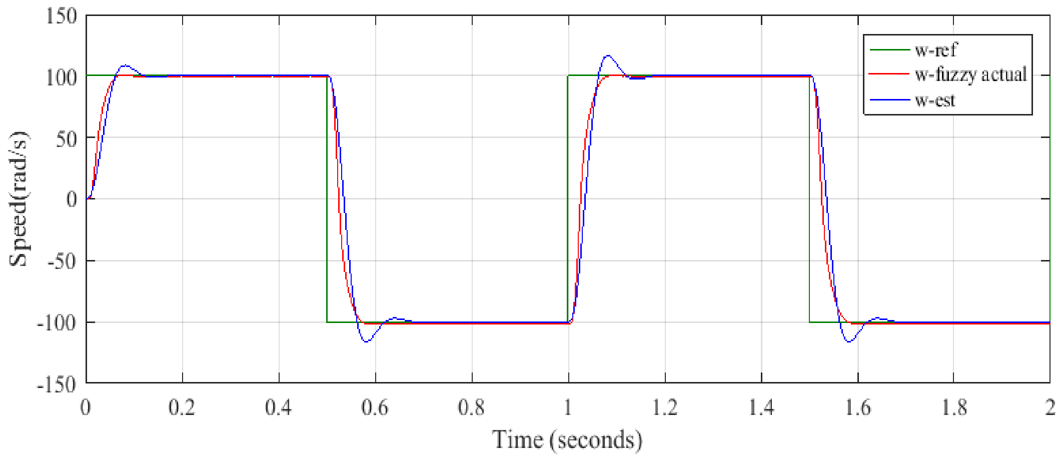

Figure 4. 16:Actual, estimated, and reference speed reversal of drive-in motoring and regenerative mode of operation.

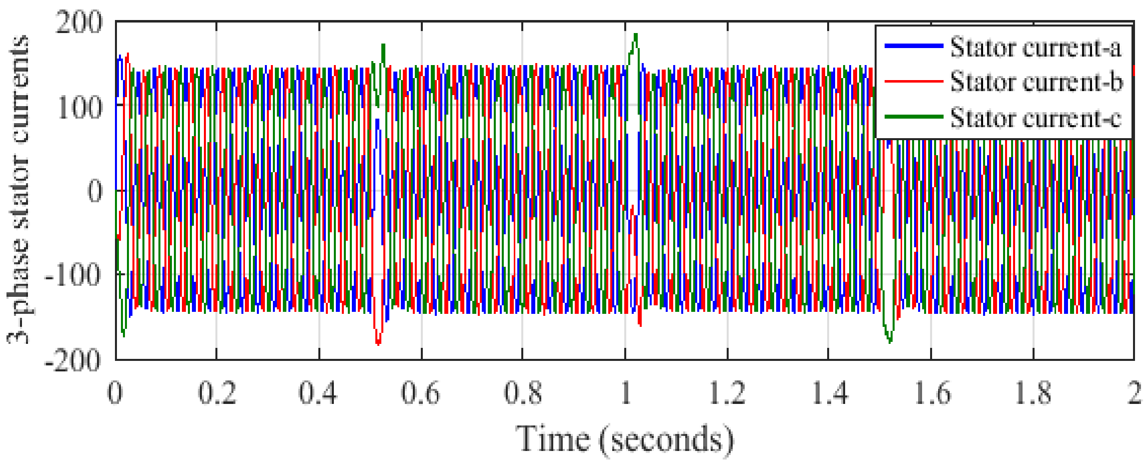

Figure 4.17: 3-phase Stator current of speed reversal of the drive-in motoring and regenerative mode of operation.

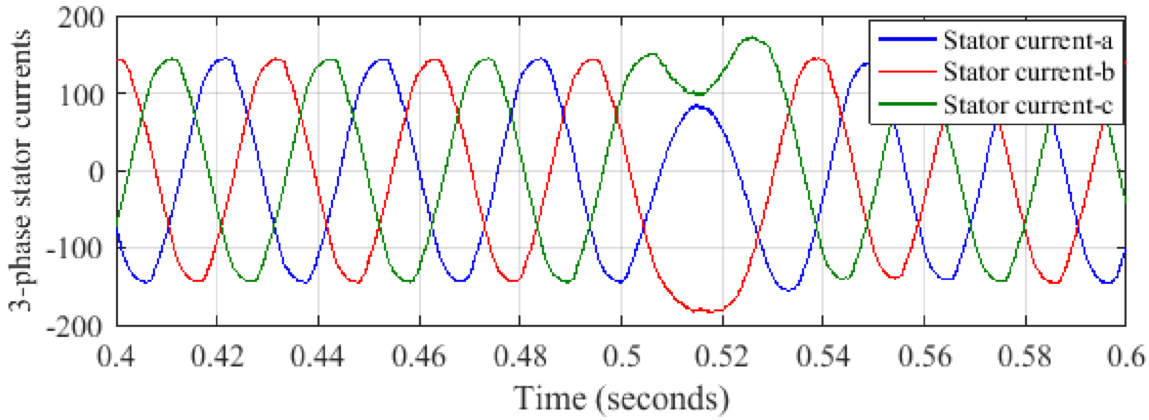

Figure 4. 18: zoomed out part of the three-phase Stator current for speed reversal of the drive-in motoring and regenerative mode of operation.

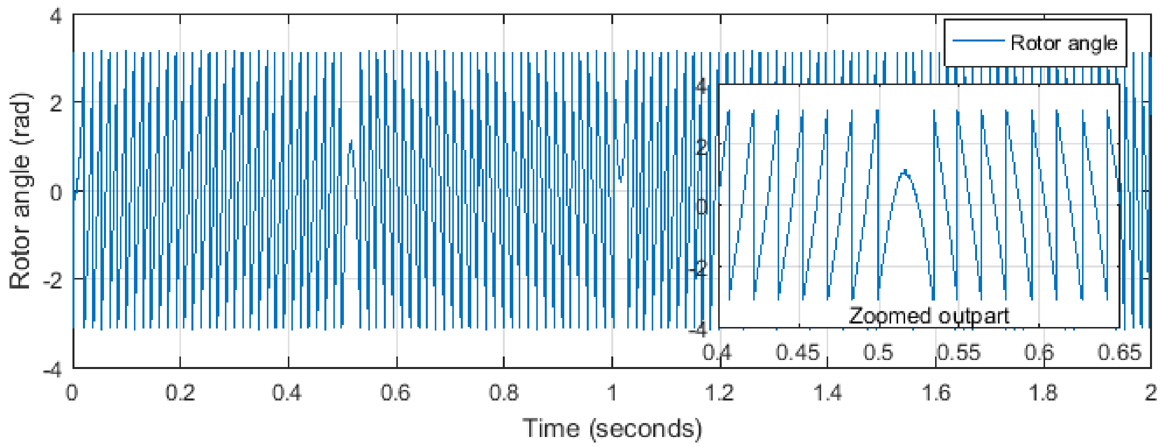

Figure 4.19: estimated rotor angle for speed reversal of drive-in motoring and regenerative mode of operation.

4.1.5 Comparison Between Voltage and Current Model Flux Estimation with Artificial Neural Network Flux Estimation Effect On The Speed Response.

Figure 4.20 shows the PI speed controlled by using voltage and current flux estimation techniques. Flux estimation is based upon the voltage model and the current model is generally not capable of achieving high dynamic performance at low speeds. In Figure 4.20 there is a ripple at the low speed therefore to reduce this ripple it is better to use an artificial neural network for flux estimation. In Figure 4.21 the Artificial neural network reduces the ripple and the motor can run at low speed.

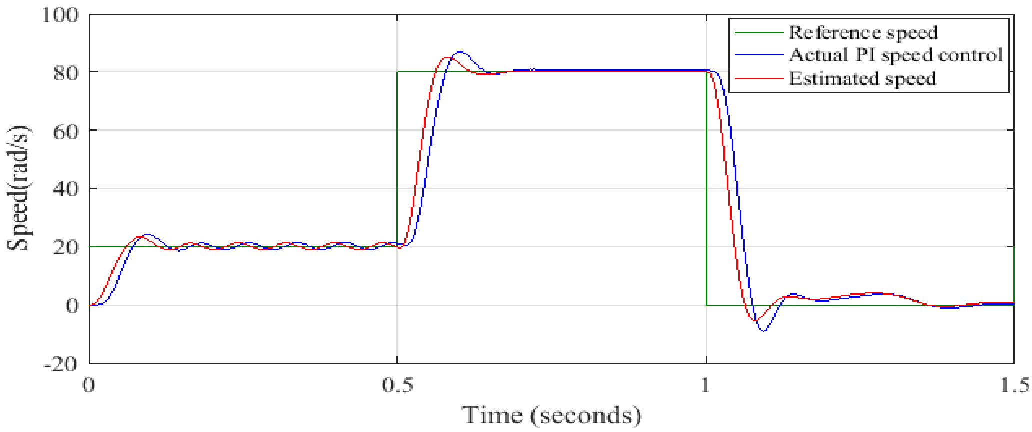

Figure 4.20: Actual speed and estimated speed Vs time-based on current and voltage flux estimation

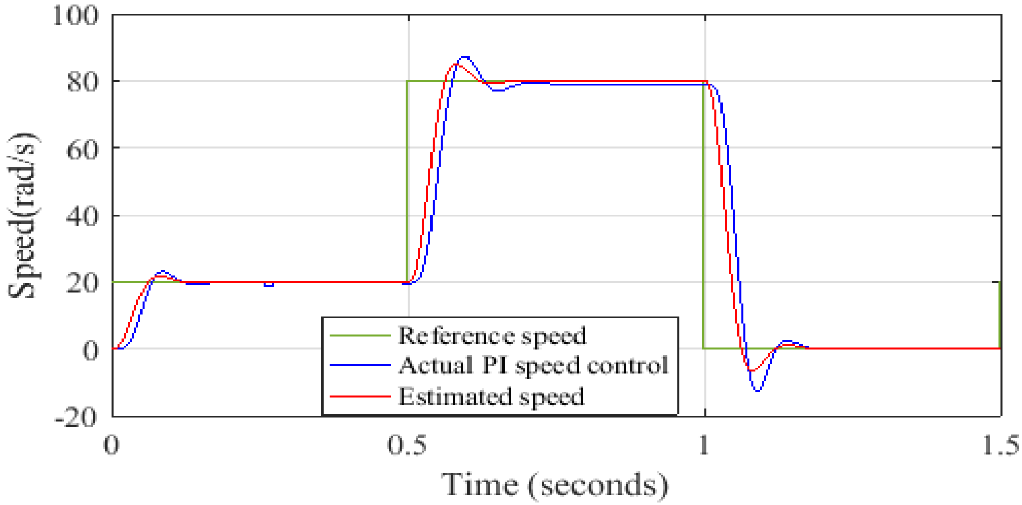

Figure 4.21: Actual speed and estimated speed Vs time- based on neural network flux estimation

4.1.6. The Comparison Between Fuzzy Logic and PI Speed Controller with the Constant Input Reference at No Load Condition.

For the comparison purpose, the simulation is performed in the constant and variable setpoint conditions. Figure 4.22 shows the constant setpoint condition speed result (at 100 rad/s). The reference speed is used to see the performance of the fuzzy and PI speed controller. For both cases, the inner current control loop is controlled by the PI controller. From the control system theory, the system is said to have better dynamic performance if it has a lower rise time, lower percent overshoot, lower settling time, and lower peak time.

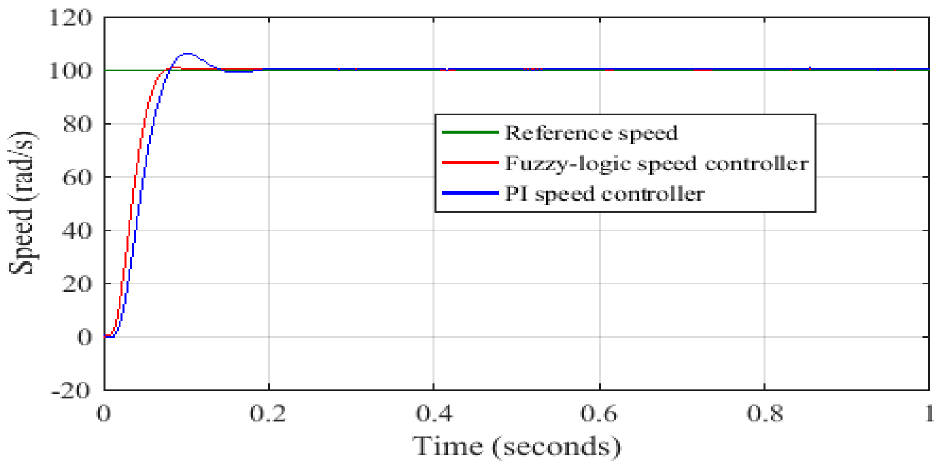

Figure 4.22: PI and fuzzy logic speed controller Vs time for 100 rd/s at no-load condition

Table 4. 1: Shows the detailed speed dynamic performance parameters for the controllers' results at no-load condition.

Performance criteria	Fuzzy logic controller	PI controller
Overshot (%)	0.505%	5.851%
Rise time(sec)	0.0386	0.045
Settling time(sec)	0.085	0.2
Peak time (sec)	0.08	0.1
Steady- state error (%)	0	0

Table 4.1 shows the detailed speed dynamic performance parameters of each controller result. The PI speed controller has poor performance than the fuzzy logic speed controller. It has a 5.851% overshoot and settling time of 0.2sec. The fuzzy logic controller has a better result in the case of overshoot (0.505%) and settling time (0.085sec) than the PI controller. Generally, from the simulation result, the fuzzy logic controller has good dynamic performance than the conventional PI speed controller which has the advantage in reducing the time required for settling and have a low overshot than the conventional PI speed controller.

Figure 4.23 demonstrates the speed dynamic performance parameters (settling, rise, and peak times) graphical results of PI and fuzzy logic speed controller. The graph shows that the fuzzy logic speed controller has better performance parameters than the others.

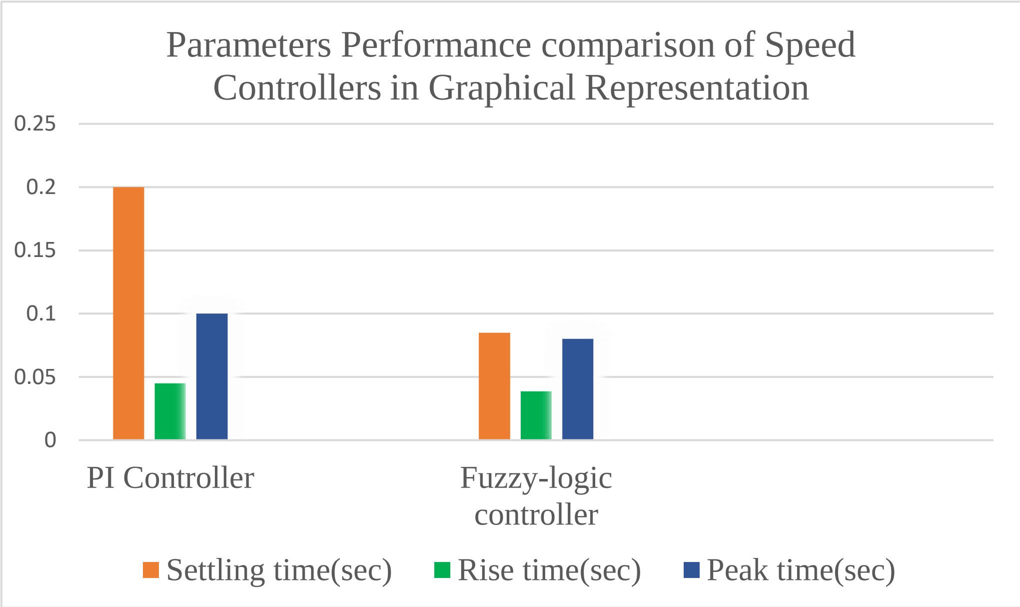

Figure 4. 23: Graphical representation of speed dynamic performance parameters result

4.1.6.1 The Comparison Between Fuzzy Logic and PI Speed Controller with the Variable Input Reference at No Load Condition

For the comparison purpose, the simulation is also performed in variable setpoint conditions. The reference speed initially 20rad/s was applied and increased to 60rad/s,100rad/s, and return to zero speed at t = 0.5 sec, t=1 sec, and at t=1.5second respectively.

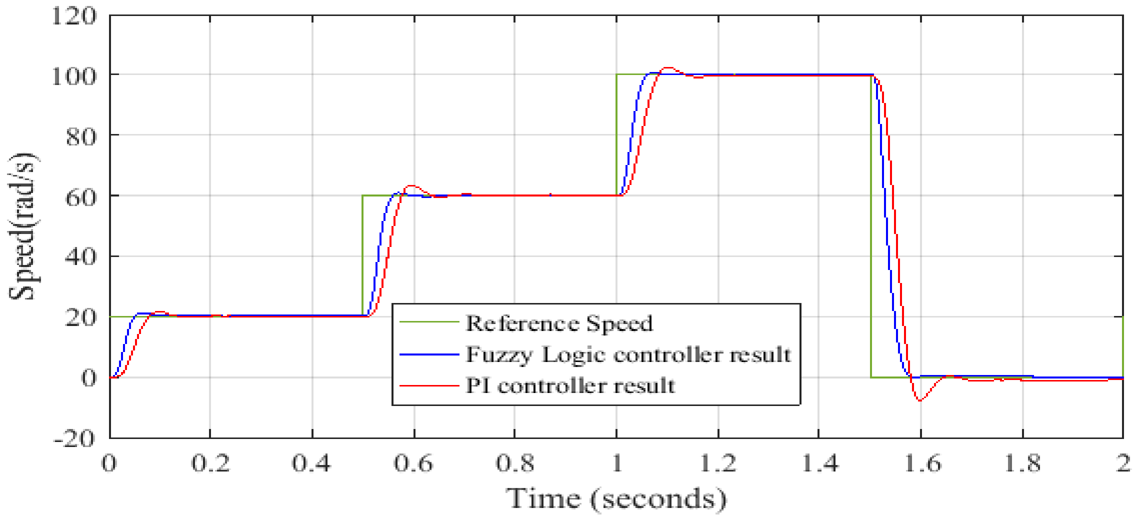

Figure 4.24: Fuzzy Logic and PI speed controller for variable input reference at no-load condition

The result in Figure 4.24 shows the fuzzy logic and PI speed controller when the reference input varied. In the figure the speed controlled by using the fuzzy logic speed controller is better in overshoot, settling time, and rise time than the conventional PI controller as before. Figure 4.25 shows the speed error between the fuzzy-logic and PI speed controller.

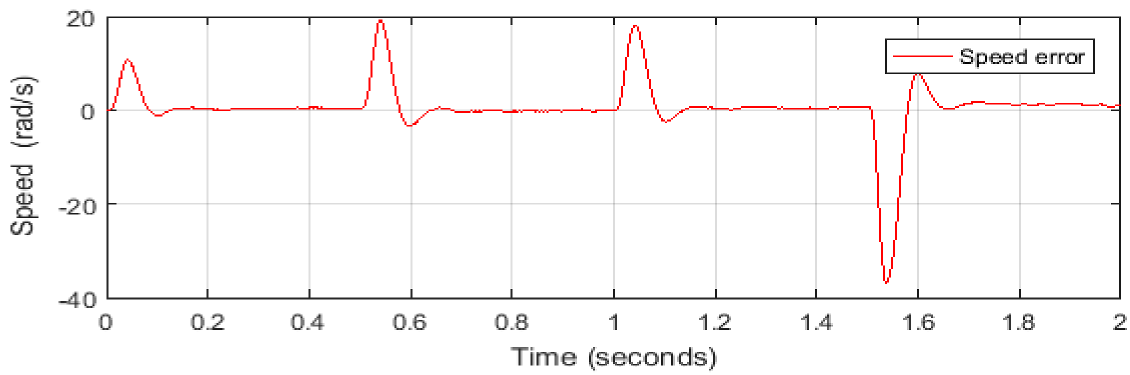

Figure 4. 25:: The difference between Fuzzy Logic and PI speed controller Vs time.

4.1.7. The Effect of External Load on the Speed Controllers of the Induction Motor

All the previous speed control system discussions were conducted at a no-load condition. The results of the speed dynamic performance parameters in the case of PI and fuzzy logic speed controllers are almost similar and competent, just they have small differences in case of constant load conditions. In order to distinguish the two controllers, the system is simulated under the application of sudden load (5Nm) change and constant setpoint condition for both performed control systems in Figure 4.27.

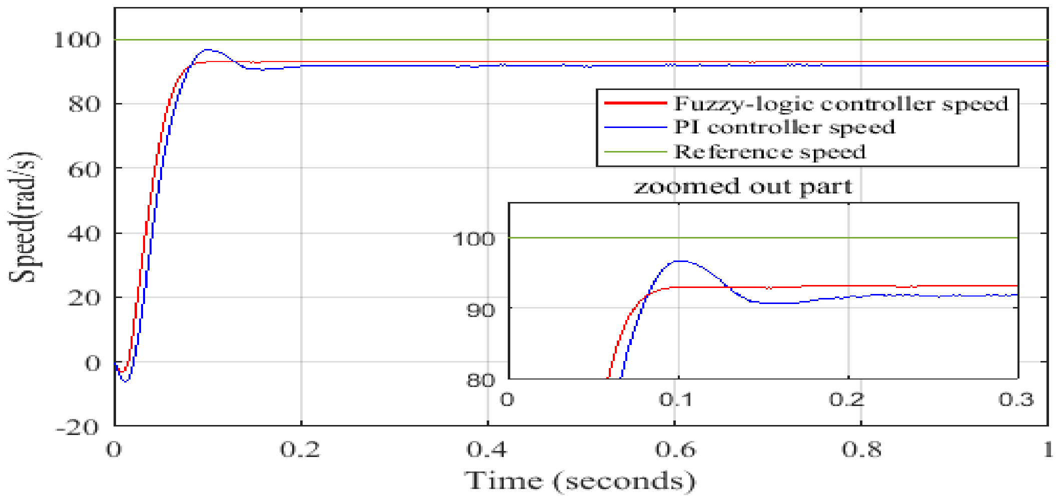

Figure 4. 26: PI and fuzzy logic speed controller vs. time for 100rad/s at (5NM) load condition

Table 4.2: Shows the detailed speed dynamic performance parameters for the controllers' result in a no-load condition.

Performance criteria	Fuzzy logic controller	PI controller
Rise time(sec)	0.0431	0.0447
Settling time(sec)	0.1	0.21
Peak time (sec)	0.092	0.12
Steady- state error (rad/s)	7	8

The general performance parameters result for sudden load change condition is shown in Table 4.2. The result shows that when there is a sudden load change the speed dynamic performance is decreased. Specifically, the settling time, rise time, and peak time values are increased when compared to the system simulated under no-load condition. This shows that when the load is increased the system performance will be decreased. There is no variation in the case of overshoot but there is a steady-state error in the result with the system simulated under no-load condition.

CHAPTER 5

CONCLUSIONS AND RECOMMENDATIONS

5.1. Conclusions

In this thesis, the sensorless speed control of the induction motor based on indirect field-oriented control with fuzzy logic and PI speed control model is designed and simulated through MATLAB software. An induction motor due to its low cost, less maintenance, lower weight, high efficiency, improved ruggedness, and reliability widely used in many areas of the industrial application. In industries, mechanical loads should not only be driven at a constant speed but should also be driven at the desired speed by varying the speed of the motor. Therefore, the need for speed control methods for the induction motor arises. There is a different kind of speed control methods are used for an induction motor, in this thesis the closed-loop PI and fuzzy logic controllers are designed for speed control of indirect vector control of an induction motor drive.

From the obtained simulations result the performance of speed control of the indirect vector control of an induction motor for conventional PI and Fuzzy control has been compared. Accordingly, the PI speed controller has a settling time 0.2sec, 5.851% overshoot, 0.045sec rise time, 0.1sec peak time, and 0% steady-state error for 100 rad/s at no-load condition. On the other hand, the fuzzy logic speed controller has a settling time of 0.085sec, 0.505% overshoot, 0.0386sec rise time, and 0% steady-state error for 100 rad/s at no-load condition. Thus, values show that the fuzzy-logic based speed control of indirect vector control of induction motor gives a better speed response than that of the conventional PI controller at no-load condition. The performance of PI and fuzzy-logic controller evaluated under the application of sudden load (5Nm) change and constant setpoint condition for both performed control systems. The settling time, rise time, and peak time values are increased when compared to the system simulated under no-load condition. This shows that when the load is increased the system performance will be decreased. There is no variation in the case of overshoot but there is a steady-state error in the result with the system simulated under no-load condition. The system also simulated under setpoint change conditions but the dynamic performance in both controllers is similar to the system results using constant setpoint condition.

From the result, the speed is estimated by using open-loop speed estimation. This sensorless speed tracks the actual speed of the motor when the motor runs at the constant speed, changing the reference speed and in the regenerative mode of operation. The neural network estimates the rotor position in the proposed method where the Levenberg-Marquardt backpropagation to train the network for three-layer, ten neurons for the first layer, five neurons for the second layers, and one neuron for output layers with the inputs of the current from the current model and flux from voltage model equations used to provide the estimation of rotor position.

5.2. Recommendations

In this thesis, several ideas can be discussed and analyzed but some work is not included in this thesis due to time limitation and this is included in the recommendation for future work.

The main recommendations for this thesis are summarized as:

1. The motor parameters variation was not considered through the research works. Therefore, study the motor parameters variation at different speeds, remains a remarkable study.
2. This thesis done speed control by using fuzzy logic control can be also extended to other latest control and tuning methods of artificial intelligent like an artificial neural network, Adaptive Neuro-Fuzzy, particle swarm optimization in addition to the fuzzy controller.
3. The thesis can be also extended for hardware implementation using Digital signal processing (DSP).
4. The thesis can also extend to operate the motor in the speed region beyond the rated speed in the field weakening region. A flux-weakening technique is applied when an extension of the motor speed beyond base speed is desired.

Acknowledgements: This research thesis was funded by Adama Science and Technology University under the grant number of **ASTU/SM-R/077/19**, Adama, Ethiopia.

References

[1] Muhammad H. Rashid,, Power Electronics Devices Circuits and Applications, Bangladesh fourth edition, 2014.

[2] A. E.Fitzgerald, Electrical Machine, Cambridge sixth edition, MA March 5, 2006..

[3] Ned Mohan, Advanced electric drives, John Wiley & Sons, Inc., Hoboken, New Jersey second edition, 2014.

[4] BIMAL K Bose, Modern Power Electronics and AC Drives, Pearson Education, 4th Edition, 2004.

[5] Michael Filippich, Digital control of Three phase Introduction Motor, ThesisUniversity of Queensland, Oct 2002.

[6] Mengweili, Differential Algebric Approach to speed and parameter Estimator of Induction, thesis univeresity of Tennessee, 2005.

[7] Stephen j.Chapman, Electric Machinery Fundamentals, Fifth Edition, 2004.

[8] Ashutosh Mishra and Prashant Choudhary, "Speed Control of An Induction Motor By Using Indirect Vector Control Method," *International Journal of Emerging Technology and Advanced Engineering*, vol. 2 No.12, pp. 144-150, December 2012.

[9] Vipul G. Pagrut, Ragini V. Meshram, Bharat N. Gupta, PranaoWalekar, "Internal Model Control Approach to PI Tunning in Vector Control of Induction Motor," *International Journal of Engineering Research & Technology (IJERT)*, vol. 4, no. 06, June-2015.

[10] ALNASIR, Z.A, "Design of Direct Torque Controller of Induction Motor (DTC)," *International Journal of Engineering and Technology (IJET)*, vol. 4, Apr-May 2012.

[11] Farazdaq R.Yasiena*, Mustafa S.Alib, "Performance Comparison between Conventional PI and PI-Like Fuzzy Speed Controller for Three Phase Induction Motor," *American Scientific Research Journal for Engineering, Technology, and Sciences (ASRJETS)*, vol. 42, pp. 148-156, 2018.

[12] M. Jannati*, T. Sutikno**, N.R.N. Idris*, M.J.A. Aziz “, "A Novel Method for Rotor Field-Oriented Control of Single Phase Induction Motor," *International Journal of Electrical and Computer Engineering (IJECE)* , vol. 5 No.2 , April 2016.

[13] P. Nagasekhar Reddy1, P. Linga Reddy2 and J. Amarnath3 , "Sensorless Control of Induction Motor using Simulink by Direct Synthesis Technique," *International Journal of Electrical Engineering* , Vols. 4, Number 1, pp. 23-32, 2011.

[14] https://www.enggcyclopedia.com/wp-content/uploads/2012/09/Electric-motor-structure.png.

[15] M.P. Kazmierkowski, R. Krishnan, F. Blaabjerg, Control in Power Electronics Selected problems, Acadamic press, 2002.

[16] Rik W. De Doncker, and Donald W. Novotny , "The Universal Field Oriented Controller," *IEEE Transactions On Industry Applications,* vol. 30 No.1, 2000.

[17] https://www.researchgate.net/publication/325896460, "Comparison of Field Oriented Control and Direct Torque Control".

[18] R. Gandhi Raj1 and B. Palpandi2 , "Development of Fuzzy Logic-Based Speed Control of Novel Multilevel Inverter-Fed Induction Motor Drive," *IEEE Transactions on Industrial Electronics* , no. No. 4, pp. 745-752, Jul. 2018 .

[19] https://en.wikipedia.org/wiki/Artificial_neural_network. .

[20] F. Blaschke, "The Principle of Field Orientation as Applied to the New Trans- vector Closed Loop Control Systems for Rotating Machines," *Siemens Review,* vol. 39 No.5, pp. 217-220, 2001.

[21] Ashish Chourasia, Vishal Srivastava, Abhishek Choudhary, and Sakshi Praliya, "Comparison studyof Vector Control of Induction Motor Using Rotor Flux Estimation by Two Different Methods," *International Journal of Electronic and Electrical Engineering,* vol. 7 No. 3, pp. 201-206, 2014.

[22] S. Campbell, H. A. Toliyat , DSP-based electromechanical motion control, CRC Press, 2004.

[23] Mircea Popescu, "Induction Motor Modeling for Vector Control Purposes," *Helsinki University of Technology Department of Electrical and Communications Engineering Labratory of Electromechanics*, 2000.

[24] L. Umanand and S. Bhat, "Online estimation of stator resistance of an induction motor for speed control applications," *IEE Proc. Electr. Power Appl.,* vol. 142, p. 97– 103 , Mar. 2001.

[25] P.Zhang, Bin Lu, and T.G. Habetler, "A Remote and Sensorless Stator Winding Resistance Estimation Method for Thermal Protection of Soft-Starter-Connected induction machines," *IEEE Transaction on industrial electronics,* vol. 55 NO.10, pp. 3611-3618, October 2008.

[26] Venu Gopal B T, "Comparison between Direct and Indirect Field Oriented Control of Induction Motor," *International Journal of Engineering Trends and Technology (IJETT),* vol. 43, pp. 364-369, January 2017.

[27] Fitsum Bekele, "Study and Implementation of DSP Based Sensorless Speed Control of Induction Motor," *Addis Ababa Institute of Technology, Addis Ababa, Ethiopia,* April 2011.

[28] Girma Kassa, "Design and Comparative analysis of Genetic algorithm tuned Fractional and Integer order PI controllers with Adaptive neuro fuzzy controller for speed control of indirect vector controlled Induction motor," vol. addis ababa institute of technology, January, 2019.

[29] Seung-Ki Sul", Control of Electric Machine Drive Systems, Institute of Electrical and Electronics Engineers, Inc, December 2010.

[30] Seung-Ki Sul, "Control of Electric Machine Drive Systems," *United States of America, John Wiley & Sons*, Inc, 2011..

[31] Paul C.Krouse, Oleg Wasynczuk, Scott and D.Sudhoff,, Analysis of electric Machinery and drive Systems, United States of America ,John Wiley and sons, 2002.

[32] Tze-Fun Chan and Keli Shi, Applied Intelligent Control of Induction Motor Drives, 2011 First Edition.

[33] Tze-Fun Chan and Keli Shi, Applied Intelligent Control Of Induction Motor Drives, Singapore ,John Wiley & Sons (Asia), 2011.

[34] https://image.slidesharecdn.com/spvm-140605022805-phpapp01/95/sinusoidal-pwm-and-space-vector-modulation-for-two-level-voltage-source-converter-13-638.jpg?cb=1406352751.

[35] Bengi Tolunay, "Space Vector Pulse Width Modulation for Three-Level Converters a LabVIEW Implementation," *Industrial Technology ICIT, Hong Kong,* Februari 2012.

[36] A.S. Gebreegzabher, "Control Scheme Modelling and Analyzing of Three-phase Inverter for Induction Motor Drive Using SVPWM Technique for Three Wheel Electric Vehicles (Bajaj) Application," *Adama Science and Technology University, Adama, Ethiopia* , September,2019.

[37] https://mpoweruk.com/images/inverter.gif.

[38] https://image.slidesharecdn.com/spvm-140605022805-phpapp01/95/sinusoidal-pwm-and-space-vector-modulation-for-two-level-voltage-source-converter-12-638.jpg?cb=1406352751.

[39] A John Wiley and Sons, High Power Converter and Ac drives, publication 2006.

[40] https://image.slidesharecdn.com/spvm-140605022805-phpapp01/95/sinusoidal-pwm-and-space-vector-modulation-for-two-level-voltage-source-converter-19-638.jpg?cb=1406352751.

[41] https://image.slidesharecdn.com/projectreview-1-110814133530phpapp01/95/project-review-13-728.jpg?cb=1313329085.

[42] https://image.slidesharecdn.com/svpwm-150306110056-conversiongate01/95/advanced-techniques-of-pulse-width-modulation-30-638.jpg?cb=1425639761.

[43] C.Lascu, I.Boldea, F.Blaabjerg , "A Modified Direct Torque Control for Induction Motor Sensorless Drive," *IEEE Tran,* Vols. 36, no. 1, pp. 122-130, Jan 2000.

[44] Teshome Hambissa , "Analysis and DSP Implementation of Sensor-less Direct FOC of Three-Phase Induction Motor Using Open-Loop Speed Estimator," *Addis Ababa Institute of Technology ,* May 17 2017.

[45] C.Lascu, I.Boldea, F.Blaabjerg , "A Modified Direct Torque Control for Induction Motor sensorless drive," *IEEE Tran,IA,* vol. 36 no.1, pp. 122-130, Jan 2000 .

[46] GÜNAY MEK , "Sensorless direct field oriented control of induction machine by flux and speed estimation using model reference adaptive system," *the middle east technical university ,* April-2004.

[47] PRANAV PRADIP SONAWANE AND MRS. S. D. JOSHI, "Sensorless speed control of induction motor by artificial neural network," *International Journal of*

Industrial Electronics and Electrical Engineering, ISSN:, vol. 5, no. 2, pp. 2347-6982, Feb. 2017.

[48] Rubai,A., Kotaru, R, "Online Identification and Control of Dc Motror using Learning Adaptation of Neural Networks," *IEEE Trans. On Ind. Aplic*, vol. 36 No:3, 2004.

[49] Roland S.Burns, Advanced control Engineering, Boston, Johannesburg, Butterworth Heinenann(BH), 2001.

[50] Madhavi, and Muley, "Speed Control of Induction Motor using PI and PID Controller," *IOSR Journal of Engineering (IOSRJEN)*, vol. 3, no. 5, pp. 25-30, 2013.

[51] Benudhar, Mohanty, and Swagat, "A Comparative Study on Fuzzy and PI Speed Controllers for Field-Oriented Induction Motor Drive," *Modern Electric Power Systems, Wroclaw, Poland MEPS'10*, 2010.

[52] Saji Chacko1, Dr. Chandrashekhar N.Bhende2 , "modeling and simulation of field oriented control induction motor drive and influence of rotor resistance variations on its performance," *International Journal (ELELIJ)* , Vols. 5, No 1, February 2016.

[53] Amit Mishra and Zaheeruddin, "Design of Speed Controller for Squirrel-cage Induction Motor using Fuzzy logic based Techniques," *International Journal of Computer Applications*, Vols. 58, no. 22, pp. 10-18, November 2012.

[54] Sharda Patwa, "control of starting current in three phase induction motor using fuzzy logic controller," *International Journal of Advanced Technology in Engineering and Science*, Vols. 1, no. 12, pp. 27-32, December 2013.

[55] R. Arulmozhiyal, "Space Vector Pulse Width Modulation Based Speed Control of Induction Motor using Fuzzy PI Controller," *International Journal of Computer and Electrical Engineering*, Vols. 1, No. 1, April 2009.

[56] Chiu S, "Software Tool for Fuzzy Control," *In Industrial application of fuzzy logic and intelligent system ed.J. Yen, R. Langari and L.A.Zadeh, IEEE Press*, pp. 313-400, 2001.

[57] Mostafa A. Hamood, Waleed F. Faris Marwan A. Badran, "Fuzzy Logic Based Speed Control System for Three Phase Induction Motor," *EFTIMIE MURGU*, pp. ISSN 1453 - 7397, January 2013.

[58] Ronal S. Burn, Advanced Control Engineering, B.H.Publishing, Ltd, 2001.

[59] Mugdha Bhandari1, Shivaji Gavade2, Shwetha S H3, "Model Reference Adaptive Technique for Sensorless Speed Control of Induction Motor Using MATLAB\SIMULINK," *International Journal of Emerging Technology in Computer Science & Electronics (IJETCSE) ,* vol. 14, no. 2, April 2015.

[60] F.Z.Peng, T.Fukao , "Robust Speed Identification for Speed Sensorless Vector Control of Induction Motors," *IEEE Tran. IA ,* vol. 30 no. 5, pp. 1234-1239, Oct.1994 .

[61] P.L.Jansen and R.D.Lorenz , "Observer based direct field orientation: Analysis and comparison of alternative methods," *IEEE Tran. IA,* vol. 30 no.4, pp. 945-953, Jul/Aug, 1994 .

Appendixes

Appendix A: MATLAB Simulink model

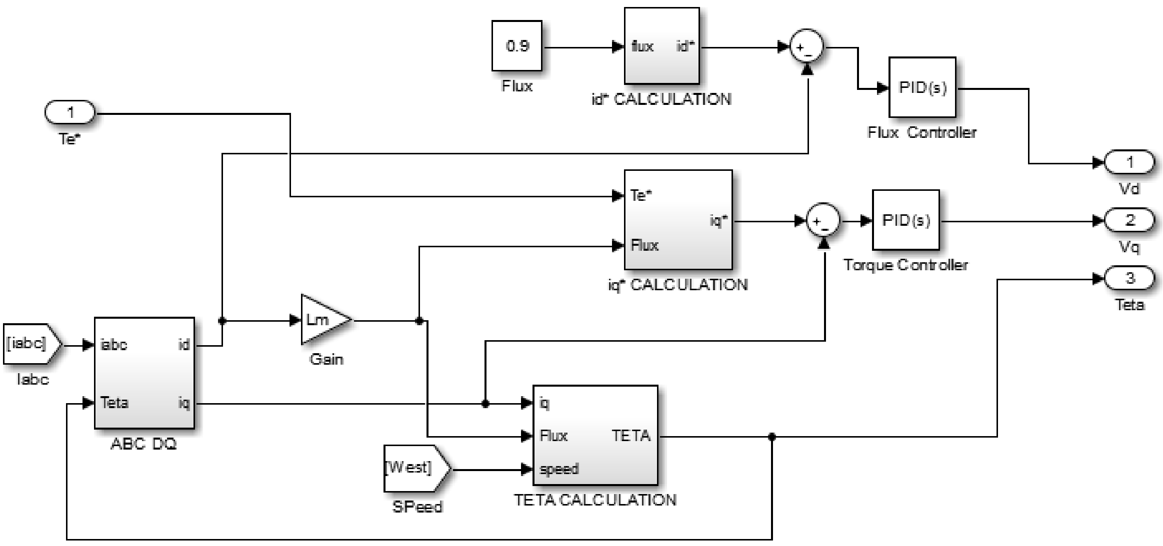

Fig.A.1. MATLAB Simulink subsystem model for indirect field-oriented control.

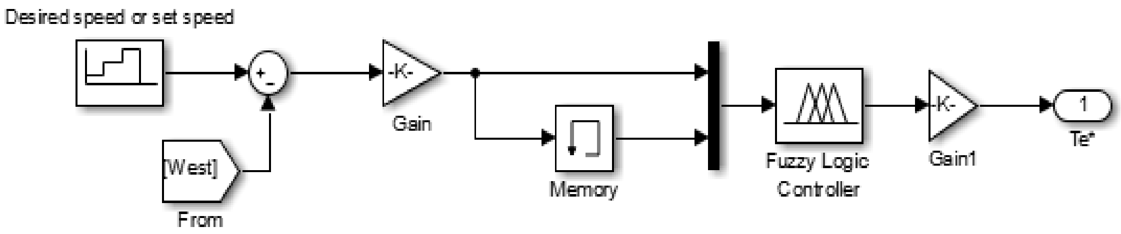

Fig.A.2. MATLAB Simulink subsystem model for fuzzy logic controller

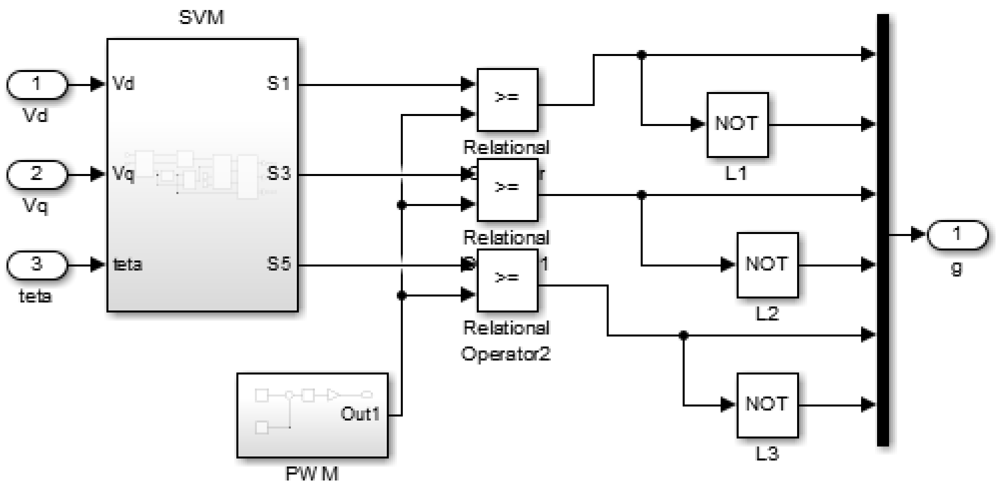

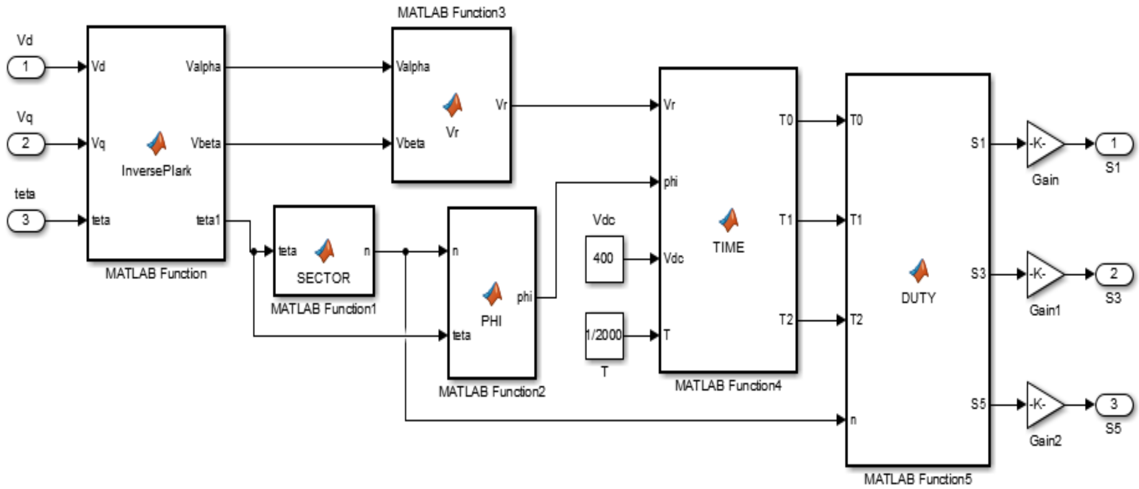

Fig.A.3. MATLAB Simulink subsystem model for space vector modulation.

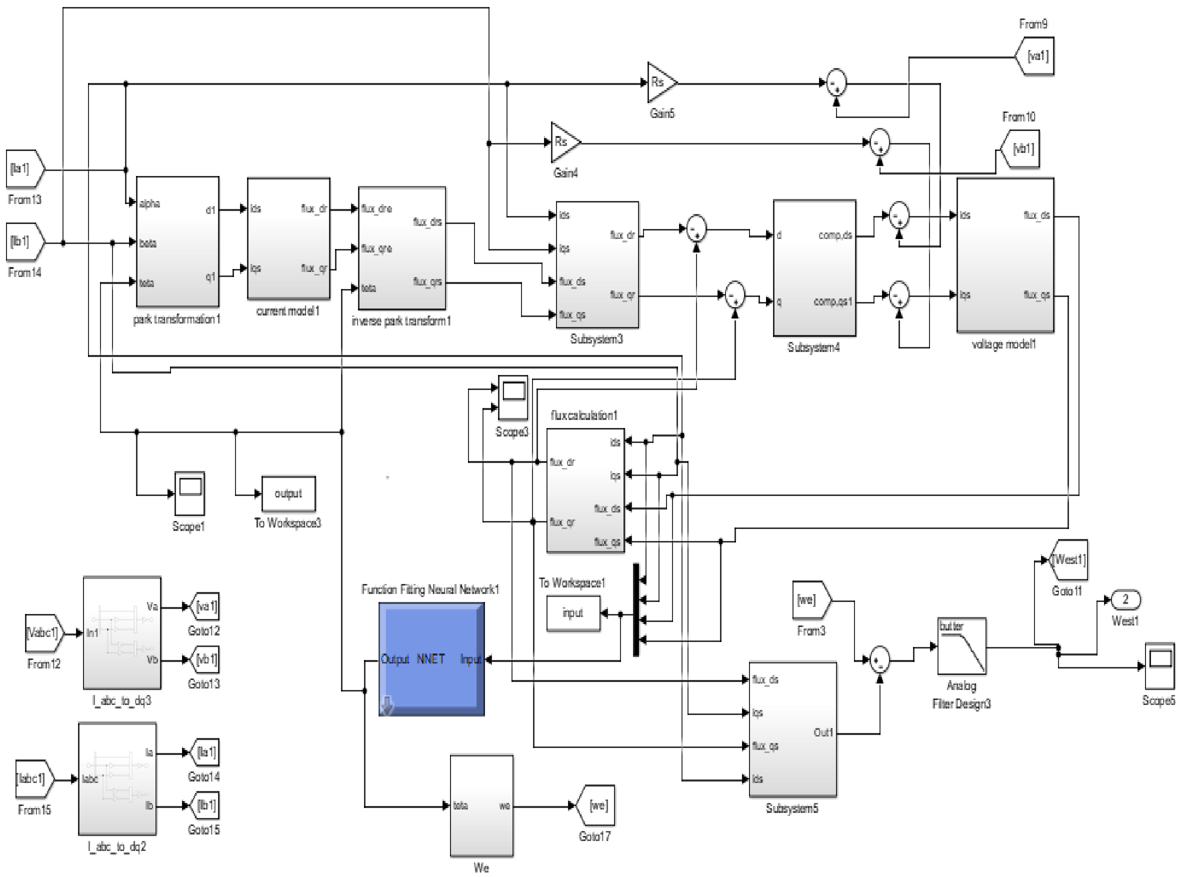

Fig.A.4. MATLAB Simulink subsystem model Flux and speed Estimation

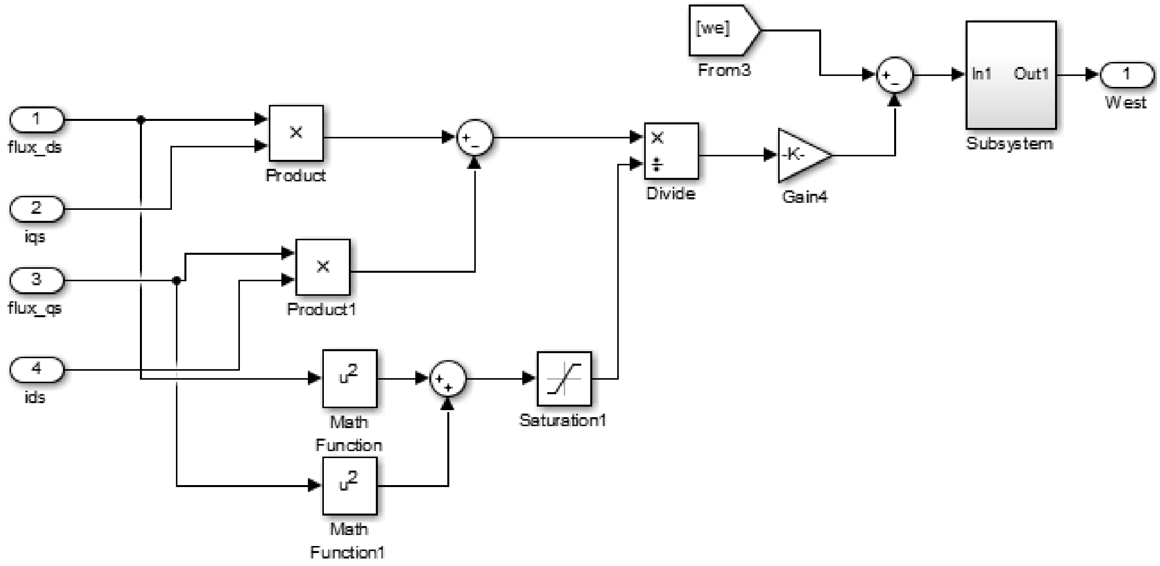

Fig.A.5. MATLAB Simulink subsystem of speed Estimation

Appendix B: MATLAB Code for space vector pulse width modulation

M-file for Determine Valpha, Vbeta, and Angle alpha:

```
function [Valpha, Vbeta, teta1] = Clark (Vd, Vq, teta)

Valpha= Vd*cos(teta)-Vq*sin(teta);

Vbeta= Vd*sin(teta)+Vq*cos(teta);

teta1= atan2(Vbeta, Valpha);
```

M-file for sector selection

```
function n = SECTOR(alpha)s
n=0;
if(alpha>0)&&(alpha<=pi/3)
n=1;
end
if(alpha>pi/3)&&(alpha<=2*pi/3)
n=2;
end
if(alpha>2*pi/3)&&(alpha<=pi)
```

```
n=3;
end
if(alpha<=0)&&(alpha>-1*pi/3)
n=6;
end
if(alpha<=-1*pi/3)&&(alpha>-2*pi/3)
n=5;
end
if(alpha<=-2*pi/3)&&(alpha>-1*pi)
n=4;
end
```

M-file for Determine Vref

```
function Vr = Vr(Valpha, Vbeta)
Vr=0;
Vr=sqrt(Valpha^2+Vbeta^2);
```

M-file for Determine angle

```
function phi = PHI(n, alpha)
phi=0;
if(n==1)
phi=alpha;
end
if(n==2)
phi=alpha-pi/3;
end
if(n==3)
phi=alpha-2*pi/3;
end
if(n==6)
phi=alpha+pi/3;
```

```
end
if(n==5)
phi=alpha+2*pi/3;
end
if(n==4)
phi=alpha+pi;
end
```

M-file for Determine Dwell Time

```
function [T0, T1, T2] = TIME (Vr,phi,Vdc, T)

a=Vr/Vdc;
T1=T*a*sin(pi/3-phi)/sin(pi/3);
T2=T*a*sin(phi)/sin(pi/3);
T0=T-T1-T2;
```

M-file for Determine gate signal and their sequences

```
function [S1, S3, S5] = DUTY (T0, T1, T2, n)

S1=0;
S3=0;
S5=0;
if (n=1)

S1=T1+T2+T0/2;
S3=T2+T0/2;
S5=T0/2;
end
if(n==2)
S1=T1+T0/2;
S3=T1+T2+T0/2;
S5=T0/2;
end
if(n==3)
S1=T0/2;
S3=T1+T2+T0/2;
```

```
S5=T2+T0/2;
end
if(n==4)
S1=T0/2;
S3=T1+T0/2;
S5=T1+T2+T0/2;
end
if(n==5)
S1=T2+T0/2;
S3=T0/2;
S5=T1+T2+T0/2;
end
if(n==6)
S1=T1+T2+T0/2;
S3=T0/2;
S5=T1+T0/2;
end
```

Appendix C: MATLAB Code for Artificial Neural Network

```
x = input'; % input - input data.
y = output'; % output - target data.
% 'trainlm' is usually the fastest.

% Levenberg-Marquardt backpropagation.
trainFcn = 'trainlm';
% Create a fitting network
hiddenLayerSize = [10 5];
net = fitnet(hiddenLayerSize,trainFcn);
% Setup division of data for training, validation, testing
net.divideParam.trainRatio = 80/100;
```

```
net.divideParam.valRatio = 10/100;
net.divideParam.testRatio = 10/100;
net.trainParam.epochs= 1000;
% Train the network
[net,tr] = train(net,x,y);
% Test the network
y = net(x);
e = gsubtract(x,y);
performance = perform(net,x,y)
%To generate the NN on Simulink block
gensim(net)
```

Appendix D: Induction motor parameters and NN training Front

Table D.1: induction motor nameplate

Parameter	Symbol	Unit	Value
Types of rotor	–	–	Squirrel cage
Number of pole pairs	p	–	2
Frequency	F	Hz	50
Stator resistance	R_s	Ω	0.966
Stator inductance	L_s	H	0.00439
Rotor resistance	R_r	Ω	1.45
Rotor inductance	L_r	H	0.00439
Mutual inductance	L_m	H	0.002373
Moment of inertia	J	kgm^2	0.009

Rated voltage	V_r	V	400
Rated speed	ω_r	RPM	1460
Rated power	P_r	KW	2.2
Friction factor	F	N.m.s	0.00061
PWM frequency	Frequency Switching	KHz	2

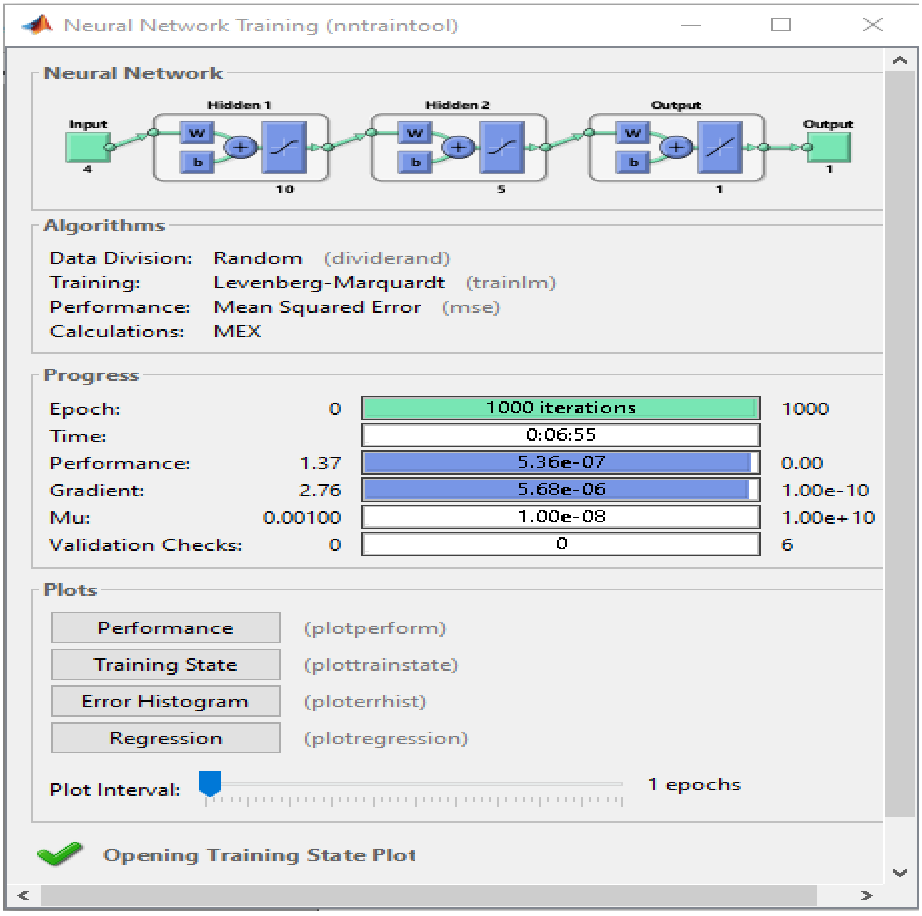

Figure D.2: Neural Network Training Front Page